



Politechnika Poznańska  
Wydział Elektryczny  
Instytut Elektroniki i Telekomunikacji  
ul. Piotrowo 3a, 60-965 Poznań



Maciej Bartkowiak

# Vector-Oriented Methods for Compression of Color Images and Video

Doctoral Dissertation

Advisor: Dr. Marek Domański, professor

---

Poznań, 1999

# Contents

<b>Abstract</b>	<b>5</b>
<b>Streszczenie</b>	<b>6</b>
<b>1 Introduction.</b>	<b>7</b>
1.1 The scope of the dissertation and the thesis. . . . .	7
1.2 Organization and a review of the dissertation. . . . .	8
<b>2 Representation of color images and video.</b>	<b>11</b>
2.1 Introduction. . . . .	11
2.2 Digital color images and video as vector signals. . . . .	12
2.3 Standard color spaces and their purposes. . . . .	14
2.4 Perceptually uniform color spaces. . . . .	18
2.5 Statistical and spectral properties of natural color images and video. .	22
2.5.1 Distribution of color data in natural images. . . . .	22
2.5.2 Dynamic changes of color content in videophone sequences. . .	28
2.5.3 Mutual dependencies between color components. . . . .	29
2.5.4 Energy compaction resulting from color space transformation.	30
2.5.5 Spectral properties of color images. . . . .	31
2.6 Human perception of color images and its implications. . . . .	33
2.7 The quality criteria - objective measures of the color image quality. .	34
<b>3 Review of color image and video compression methods related to vector approach.</b>	<b>38</b>
3.1 Introduction. . . . .	38
3.2 Vector control of component-wise compression. . . . .	40
3.3 Joint color and spatial compression techniques. . . . .	41
3.4 Scalar quantization and vector quantization. . . . .	42
3.5 Color quantization. . . . .	45
3.5.1 Introduction. . . . .	45
3.5.2 Representation fidelity. . . . .	47

3.5.3	The palette design problem. . . . .	48
3.5.4	Palette design through iterative optimization. . . . .	49
3.5.5	Heuristic methods for palette design. . . . .	50
3.5.6	Simplified codebook design. . . . .	52
3.5.7	Improvements of the color quantization technique. . . . .	53
3.6	Lossless and lossy compression of color quantized images. . . . .	53
<b>4</b>	<b>New vector-oriented techniques for color image compression.</b>	<b>59</b>
4.1	Introduction. . . . .	59
4.2	The concept of image coding based on chrominance vector quantization. . . . .	60
4.3	Chrominance quantization algorithms. . . . .	61
4.3.1	Introduction. . . . .	61
4.3.2	Binary splitting algorithms. . . . .	62
4.3.3	Classic solution based on principal component analysis. . . . .	63
4.3.4	An alternative method for determination the maximum of $\Delta E_{pca}$ . . . . .	65
4.3.5	Improvements of the PCA-based splitting. . . . .	67
4.3.6	Simulations. . . . .	70
4.3.7	Experimental results. . . . .	73
4.4	Images of scalar chrominance and their properties. . . . .	77
4.5	Lossless compression of the scalar chrominance. . . . .	81
4.5.1	Introduction. . . . .	81
4.5.2	Proposed compression scheme and its implementation. . . . .	83
4.5.3	Experimental results. . . . .	84
4.6	Lossy compression of images with vector quantized chrominance. . . . .	87
4.6.1	Introduction. . . . .	87
4.6.2	Application to existing image compression standard. . . . .	90
<b>5</b>	<b>Color video compression by the use of scalar chrominance.</b>	<b>92</b>
5.1	Introduction. . . . .	92
5.2	Chrominance vector quantization of video sequences. . . . .	93
5.3	Intraframe transform coding of scalar chrominance. . . . .	94
5.3.1	Introduction. . . . .	94
5.3.2	DCT-based coding. . . . .	95
5.3.3	Coding based on discrete Walsh transform. . . . .	97
5.4	Interframe coding. . . . .	99
<b>6</b>	<b>Conclusions.</b>	<b>103</b>
6.1	Recapitulation. . . . .	103
6.2	Summary of developments and achievements. . . . .	104
6.3	Possible extensions and further work. . . . .	106



# Acknowledgements

First of all, I would like to express my sincere thanks to Prof. Marek Domański for the truly memorable research experience I have had with him, for his invaluable support, and for his infinite patience.

I would like to thank Prof. Hans Georg Musmann and his colleagues in the Institut fuer Theoretische Nachrichtentechnik and Informationsverarbeitung for their kind hospitality in Hannover and for helpful and stimulating discussions.

I would like to thank the Foundation for Polish Science for the material support which allowed me to concentrate on the research.

Also, I owe many thanks to my colleagues, Adam Łuczak and Sławek Maćkowiak, who have helped me to implement some parts of the software, and who provided the library for software simulation of video codecs. To Grzegorz Popek, for careful reading of the manuscript. To all my friends for making my life easier. To my parents and sister, who allways unconditionally loved and supported me through all my endeavors, I love you.

*This work is dedicated to my beloved Mother.*

Maciej Bartkowiak  
Poznań, July 29, 1999.

# Abstract

The dissertation is devoted to color image and video coding. These signals are represented in digital systems on the basis of trichromatic model of the human visual system, and their acquisition and reproduction often exploits such phenomena, like metamerism. Traditional methods for compression of color signals operate on each of the three color components independently, by repeating the same operations and neglecting completely or almost completely the strong mutual statistical dependencies between the components. The existence of such dependencies is demonstrated in this dissertation using color histograms.

The dissertation reviews exploitation of mutual dependencies between color components in efficient coding of color images. This exploitation is done through joint treatment of the color components as vector coordinates in color space and application of vector distance measures. A new vector-oriented technique is proposed for representation of color by the use of dimensionality reducing mapping. Due to the lossy character of further compression, such mapping is realized through vector quantization.

The dissertation discusses the topics of vector quantization of color and chrominance. Experimental verification of a proposed efficient quantization algorithm is demonstrated. Original methods for lossy compression based on predictive coding and transform coding of color images and video with the aid of vector quantized chrominance are presented. High efficiency of the achieved methods proves that using vector-oriented processing allows to exploit better the correlation between color components, especially in compression applications for very low bit rate digital channels, where it is necessary to gain the maximum compression by preserving the acceptable quality.

# Streszczenie

Rozprawa poświęcona jest kodowaniu kolorowych obrazów statycznych i ruchomych (sekcji wizyjnych). Reprezentacje tych sygnałów w systemach cyfrowych są oparte na trójkromatycznym modelu wzroku, a do akwizycji i reprodukcji obrazów powszechnie wykorzystuje się takie zjawiska, jak metameryzm. Tradycyjne metody kompresji kolorowych sygnałów wizyjnych operują niezależnie na każdej składowej barwnej, z całkowitym lub niemal całkowitym powtórzeniem tych samych operacji bez uwzględnienia silnych związków statystycznych pomiędzy składowymi. Istnienie tych związków jest zademonstrowane w rozprawie przy użyciu histogramów koloru.

W rozprawie dokonano przeglądu wykorzystania wzajemnych relacji pomiędzy składowymi barwnymi w efektywnym kodowaniu obrazów kolorowych poprzez łączne traktowanie składowych barwnych jako współrzędne wektora w przestrzeni barw oraz stosowanie wektorowych miar odległości. Zaproponowano nową wektorową technikę reprezentacji koloru przy pomocy odwzorowania redukującego liczbę wymiarów wektora. Ze względu na stratny charakter kompresji takie odwzorowanie jest zrealizowane poprzez kwantyzację wektorową.

Rozprawa omawia zagadnienie kwantowania wektorowego koloru oraz kwantowania wektorowego chrominancji. Przedstawiono badania eksperymentalne zaproponowanego efektywnego algorytmu kwantyzacji. Zaprezentowano oryginalne techniki kompresji stratnej oparte na kodowaniu predykcyjnym i transformatowym kolorowych obrazów i sekwencji reprezentowanych za pomocą skwantowanej chrominancji. Wysoka efektywność otrzymanych metod dowodzi, że zastosowanie wektorowego przetwarzania pozwala pełniej wykorzystać związki korelacyjne pomiędzy składowymi barwnymi, zwłaszcza w zastosowaniach kompresji dla kanałów cyfrowych o bardzo niskiej przepływności, gdzie konieczne jest uzyskanie jak największej kompresji przy zachowaniu zadowalającej jakości.

# Chapter 1

## Introduction.

### 1.1 The scope of the dissertation and the thesis.

The scope of this dissertation is color image and video compression. Among numerous methods developed hitherto, vector-oriented ones are mostly considered. These are defined as such techniques which exploit mutual dependencies between color components. Such dependencies are very important for high and very high compression ratios, whereby each possibility to improve the coding efficiency is vital due to very strong artefacts related to lossy coding. Therefore, very low bit rate coding techniques are developed and their efficiency is experimentally verified.

The main thesis of this dissertation is following:

- It is possible to obtain color image and video compression methods, whereby color is represented in a color space of reduced dimensionality by the use two-dimensional vector quantization of the chrominance components. Such methods exploit mutual dependencies between color components which are demonstrated in natural images. It is possible to achieve high coding efficiency, which makes proposed methods competitive to very low bit rate codecs being standardized.

The main goal of the research is to prove the above thesis. Vector quantization of chrominance is recognized as the core technique which allows to achieve compact representation of color images and video. According to this decision, the work is decomposed into following partial tasks:

1. Investigation of statistical properties of natural color images and videophone sequences.
2. Development of an efficient technique for vector quantization of chrominance.

3. Experimental verification of the efficiency of vector quantization of chrominance.
4. Definition of scalar chrominance.
5. Investigation of the statistical and spectral properties of scalar chrominance signal and investigation of the influence of chrominance codebook on these properties.
6. Proposition of lossless and lossy techniques for compression of scalar chrominance.
7. Experimental verification of the efficiency of scalar chrominance compression.
8. Extension of the representation of still images to image sequences.
9. Proposition of lossy compression techniques for intraframe and interframe coding of video.
10. Experimental verification of the efficiency of video coding based on scalar chrominance.

## 1.2 Organization and a review of the dissertation.

The dissertation is organized into six chapters which can be considered as constituting two basic parts. First part consisting mostly of literature studies presents up to date knowledge regarding color image and video properties and compression techniques with the special focus on vector-oriented approaches. Some author's contributions related to the studies of color image properties are presented in appropriate sections. The second part describes the new vector-oriented techniques developed and by the author. Examples of numerous simulation experiments using test images and videophone sequences are given.

In chapter two, the main issues related to representation of color images and video data in digital systems and its implications are discussed:

- First, historical background of color representation is briefly drawn. Selected standard color spaces used to represent color as a triplet of vector coordinates are discussed. Examples of perceptually uniform color spaces are given together with respective color difference formulas.
- Subsequently, statistical and spectral properties of natural color images and video are discussed. Statistical distribution of color data in natural images is

discussed on the basis of color histograms and experimental examples thereof are presented. Studies on dynamic changes of color distribution between consecutive frames of test videophone sequences are presented. Research on mutual dependencies between color components are reported and their implications to coding of color images are concluded. Spectral properties of color images represented in different color spaces are compared and their consequences are discussed. Selected aspects of human perception of color images are considered. Finally, the purpose of objective error criteria regarding color image and video impairments is discussed as well as the lack of an universal and standardized quality measure.

Chapter three presents those known techniques of color image compression which are related to vector-oriented approach to color coding:

- First, historical background of color image compression is drawn, and a general framework of image compression is outlined.
- Component-wise compression techniques that use vector-oriented control of the coding process are discussed. Known examples of vector-oriented techniques which rely on joint treatment of the color components are presented.
- Subsequently, the definitions of quantization and vector quantization which are vital to this research are brought. The topic of color quantization is then extensively discussed on the basis of numerous approaches known. The problem of lossless and lossy compression of color quantized images is considered and a model of such system is proposed. Examples of practical implementations known from the literature are discussed.

Chapter four deals with the new vector-oriented techniques for coding of color images developed by the author:

- First, the concept of joint representation and compression of the chrominance components using dimensionality reducing mapping is introduced. Subsequently, the technique based on chrominance vector quantization is described.
- Codebook design algorithms for chrominance vector quantization are studied deeply. An approach based on binary splitting scheme is discussed. Classic suboptimum splitting algorithm based on principal component analysis is described. An equivalent, yet alternatively formulated solution derived by the author is presented. Improvements of the principal component analysis algorithm for non-Gaussian data sources are drawn. Simulations of the algorithm using a proposed data distribution model are reported. Finally, experimental results of vector quantization of test images are discussed.

- Subsequently, the definition of scalar chrominance signal is given. General statistical and spectral properties of this signal are discussed. An efficient codebook ordering algorithm is described and experimental results are reported.
- Lossless compression of the scalar chrominance signal is covered in the next section. Implications of specific statistical properties of images with vector quantized chrominance to predictive differential coding are discussed. A compression scheme that exploits correlation between luminance component and scalar chrominance is proposed. Finally, experimental results are presented, whereby the efficiency of the proposed system is compared to standard H.263 very low bit rate video codec.
- Lossy compression of scalar chrominance is dealt with in the next section. Application of transform-based coding is discussed. System enhancements are described which are aimed at improved coding efficiency. A filtering technique for reduction of coding artifacts is proposed. Application of the system to a standard JPEG codec is discussed. Experimental results are presented and conclusions are drawn.

Chapter five extends the color image compression technique based on chrominance vector quantization to video coding at very low bit rates.

- Application of chrominance vector quantization to videophone sequences is discussed first. A general framework of motion-compensated hybrid video coding is outlined.
- Intraframe coding mode is covered in the following section. Basic issues related to DCT-based coding are discussed and the problem of controlling the bit rate is addressed. Experimental results are presented. An alternative compression scheme based on discrete Walsh transform is considered. Coding artifacts of DCT-based and DWT-based compression are demonstrated and compared. An experimental comparison of both schemes to H.263 standard codec operating in intraframe mode is also provided.
- Interframe coding of scalar chrominance is outlined in next section. Comparison of standard inter-frame prediction of the chrominance components to prediction in scalar chrominance domain is demonstrated. Experimental results using standard videophone sequences are presented and conclusions are given.

# Chapter 2

## Representation of color images and video.

### 2.1 Introduction.

It has been recognized early that human perception of color is based on receptors sensitive to electromagnetic waves in at least three overlapping subbands. The *trichromatic theory* developed by Grassmann in the later half of the nineteenth century and based on the works of Maxwell, Young and Helmholtz, assumed simply that three image types were formed by these receptors and transmitted to the brain. The latter was supposed to compare the signal ratios between the three images locally to derive a form of color appearance of particular objects in the perceived scene (Fairchild, 1998). This primitive system could not explain certain visual phenomena, like light and chromatic adaptation, afterimages, excluding co-appearance of certain hues, or some color vision deficiencies. However the trichromatic theory made possible early registration of color images using photosensitive media and a set of three chromatic filters. Color television was one of the first consumer products exploiting the principles of trichromacy (Sharma and Trussel, 1997). The standards for transmission and reproduction of color television signal established by *Federal Communication Commission* (FCC), *Commission Internationale Consultatif Radiodiffusion* (CCIR), *European Broadcast Union* (EBU) and later by *International Telecommunication Union* (ITU-R, 1994a, 1994b) inherit the fundamentals of analogue television together with its simplified models of the human visual system (Parkkinen and Jaaskelainen, 1989; Poynton, 1996).

Although the physiology of color appearance, as well as image perception and recognition have been recently deeply understood as very complex, it is still the trichromatic theory that determines today's technical approach to color image acquisition and reproduction. Also, new kinds of chromatic photoreceptors have been

discovered in human’s retina (Wyszecki and Stiles, 1982), that suggests insufficiency of trichromatic models (Parkkinen and Jaaskelainen, 1989; Trussel and Kulkarni, 1996), however contemporary imaging technologies still use three components to acquire and display color in electronic media.

## 2.2 Digital color images and video as vector signals.

Throughout this dissertation the term *digital image* will be referred to as a representation of some mostly natural scene through a discrete numerical approximation of its two-dimensional, spatially varying spectral radiance. This representation is intended to be efficiently visualized taking into account particular properties and limitations of the human visual system.

Digital image is represented as a finite matrix  $\mathbf{X}$  of size  $N_1 \times N_2$  with its elements  $X_{i,j}$  (where  $i = 0 \dots N_1 - 1$  and  $j = 0 \dots N_2 - 1$ ) describing the values of respective picture elements (*pixels*). This representation assumes that the original continuous image is sampled on a regular orthogonal grid. Alternative sampling schemes are possible, for example a quincunx sampling based on a hexagonal grid is considered as being slightly more efficient (Mersereau and Dudgeon, 1984), however it is out of the scope of this dissertation.

In case of color image, a color must be defined for each pixel, and according to trichromatic model a set of three numbers is needed for this purpose. These numbers define the intensities of three primaries that mixed additively or subtractively match the desired color. On the other hand, the three numbers can be thought of as coordinates of the color in a three-dimensional color space. A color image can be treated as a set of three independent monochrome images or as a two-dimensional discrete vector field (Machuca and Phillips, 1983):

$$\mathbf{X} = [\underline{X}_{i,j}]_{N_1 \times N_2}, \quad (2.1)$$

where each vector  $\underline{X}_{i,j}$  is defined by

$$\underline{X}_{i,j} = \begin{bmatrix} R_{i,j} \\ G_{i,j} \\ B_{i,j} \end{bmatrix}, \text{ or } \begin{bmatrix} Y_{i,j} \\ C_{Bi,j} \\ C_{Ri,j} \end{bmatrix}, \text{ or } \begin{bmatrix} L_{i,j}^* \\ a_{i,j}^* \\ b_{i,j}^* \end{bmatrix}, \text{ etc.} \quad (2.2)$$

depending on the color space assumed, which will be discussed later.

An alternative representation of color in digital images by the use of *quaternions* (or *hypercomplex numbers*) has been proposed fairly recently by Sangwine (1996, 1997). Quaternions, invented by Hamilton (1866) are a 4-space generalization of complex numbers, consisting of one real part and three imaginary parts,  $\mathbf{i}$ ,  $\mathbf{j}$  and  $\mathbf{k}$ . Sangwine proposed to deal with a trichromatic representation of color by placing the three color components into the three imaginary parts, for example:

$$0 + R\mathbf{i} + G\mathbf{j} + B\mathbf{k} \quad (2.3)$$

which is suggested by symmetry of such arrangement. Quaternion algebra offers a convenient mathematical tool to deal with color signal processing.

Similarly to images, digital video is a discrete signal defined in a three-dimensional<sup>1</sup> spatio-temporal domain. Therefore it will be denoted as

$$\mathbf{X} = [\underline{X}_{i,j,n}]_{N_1 \times N_2 \times L}, \quad (2.4)$$

(where  $L$ , is the length of the video sequence). A color video signal needs an appropriate data structure to be represented in a digital system

$$\underline{X}_{i,j,n} = \begin{bmatrix} R_{i,j,n} \\ G_{i,j,n} \\ B_{i,j,n} \end{bmatrix}, \text{ or } \begin{bmatrix} Y_{i,j,n} \\ C_{B_{i,j,n}} \\ C_{R_{i,j,n}} \end{bmatrix}, \text{ etc.} \quad (2.5)$$

For long sequences of high spatio-temporal resolution the physical sizes of such data structures become unmanageable. Usually, except true three-dimensional video processing techniques (for example, three-dimensional subband coding), the three-dimensional nature is simplified by decomposition into spatial and temporal domain and a hybrid processing (for example motion-compensated coding) is performed. In the latter case, a digital video signal is treated as a sequence of digital images called *video frames*. This is an obvious remain of film and related media, where the moving scene is recorded as its in-time sampled representation. Each frame is therefore a time sample from a continuously evolving discrete vector field.

The important difference between spatial sampling and temporal sampling in video sequences is an issue related to antialiasing filtering. Optical imperfections of analog television cameras often account for initial spatial blurring of high-frequency components, however known artifacts appearing on heavily striped objects in TV indicate the bandwidth is not limited enough. In digital images and video, an antialiasing filter is defined for conversion between resolution standards (ITU-R, 1994).

---

<sup>1</sup>In this thesis, as in the theory of multidimensional signals, the term “three-dimensional” refers to signals described by functions of three independent variables and is not related to three-dimensional scenes.

There is no filtering performed in time domain prior to temporal downsampling, however. Therefore it is natural to expect some aliasing artifacts related to rapid motion in the scene content. Only fairly recent investigation (Musmann, 1998) indicated serious problems with efficient coding of video sequences of very low spatial and temporal resolution, related to temporal aliasing phenomena.

## 2.3 Standard color spaces and their purposes.

Commonly known Grassmann’s laws of additive color mixture (1853; Wyszecki and Stiles, 1982) allowed a construction of early colorimetric systems based on the principles of trichromacy. Such a system specifies a color appearance in terms of the amounts of three additive primaries. Two stimuli viewed under the same conditions match each other (*i.e.* they appear the same for an average observer) if they can be described by the same amounts of given primaries, therefore these amounts, together with a definition of the primary set, allow for a unique specification of a given color. Nevertheless, there might be several different spectra, that appear to the observer to be the same color. Such distinct spectra are called *metamers* and they are exploited by most color output systems (*e.g.* CRT monitors, color photography).

The first colorimetric system which became an international standard, established by *Commission Internationale de L’Éclairage* (CIE) in 1931 was based on a set of primaries  $\mathcal{R}$ ,  $\mathcal{G}$  and  $\mathcal{B}$ , associated with monochromatic lights with wavelengths of 700.0, 546.1 and 435.8 nm, respectively. The values of  $R$ ,  $G$ , and  $B$  in equation 2.6 indicate the amounts of the primaries that have to be composed in additive mixture to match the stimuli  $\mathbf{C}$ ,

$$\mathbf{C} \stackrel{\text{vis}}{=} R \mathcal{R} + G \mathcal{G} + B \mathcal{B} , \tag{2.6}$$

where  $\stackrel{\text{vis}}{=}$  denotes visual match. For any radiation of continuous spectrum  $\varphi(\lambda)$  it is possible to calculate the amounts of  $\mathcal{R}$ ,  $\mathcal{G}$  and  $\mathcal{B}$  for its matching stimuli by

computing respective integrals:

$$\begin{aligned}
 R &= \int_{\lambda_{min}}^{\lambda_{max}} \varphi(\lambda) \bar{r}(\lambda) d\lambda \\
 G &= \int_{\lambda_{min}}^{\lambda_{max}} \varphi(\lambda) \bar{g}(\lambda) d\lambda \\
 B &= \int_{\lambda_{min}}^{\lambda_{max}} \varphi(\lambda) \bar{b}(\lambda) d\lambda ,
 \end{aligned} \tag{2.7}$$

where  $\bar{r}(\lambda)$ ,  $\bar{g}(\lambda)$  and  $\bar{b}(\lambda)$  denote the *standard color matching functions* associated with respective primaries. They are determined for an average observer (the CIE *standard colorimetric observer*).

Unfortunately, it might be impossible to match certain spectra by a combination of nonnegative intensities of  $\mathcal{R}$ ,  $\mathcal{G}$  and  $\mathcal{B}$  primaries, since many almost purely monochromatic lights lay outside of the  $\mathcal{R}\mathcal{G}\mathcal{B}$  triangle, which is reflected by negative lobes of the color matching functions for some ranges of wavelength (cf Fig. 2.1).

The CIE XYZ (1931) colorimetric system solves this problem by introduction of a new set of primaries and respective color matching functions  $\bar{x}(\lambda)$ ,  $\bar{y}(\lambda)$  and  $\bar{z}(\lambda)$  (cf Fig. 2.1):

$$\begin{aligned}
 X &= \int_{\lambda_{min}}^{\lambda_{max}} \varphi(\lambda) \bar{x}(\lambda) d\lambda \\
 Y &= \int_{\lambda_{min}}^{\lambda_{max}} \varphi(\lambda) \bar{y}(\lambda) d\lambda \\
 Z &= \int_{\lambda_{min}}^{\lambda_{max}} \varphi(\lambda) \bar{z}(\lambda) d\lambda .
 \end{aligned} \tag{2.8}$$

The transformation from the trichromatic  $R$ ,  $G$  and  $B$  values to the  $X$ ,  $Y$ , and  $Z$  values (2.9) is linear and is determined in such a way to avoid negative values of color matching functions  $\bar{x}(\lambda)$ ,  $\bar{y}(\lambda)$  and  $\bar{z}(\lambda)$  for all wavelengths.

$$\begin{bmatrix} X \\ Y \\ Z \end{bmatrix} = \begin{bmatrix} 0.49000 & 0.31000 & 0.2000 \\ 0.17697 & 0.81240 & 0.01063 \\ 0 & 0.01000 & 0.99000 \end{bmatrix} \begin{bmatrix} R \\ G \\ B \end{bmatrix} \tag{2.9}$$

Additionally, the  $\bar{y}(\lambda)$  is chosen to be coincident with *luminous efficiency function* (Wyszecki and Stiles, 1982). In order to obtain non-negative color matching function for any visible spectrum the  $\bar{x}$ ,  $\bar{y}$  and  $\bar{z}$  primaries had to be chosen to lay outside of the visible gamut. Therefore the primaries are not physically realizable and they are called *imaginary*. The  $XYZ$  system is a reference colorimetric system for many practically applied color spaces.

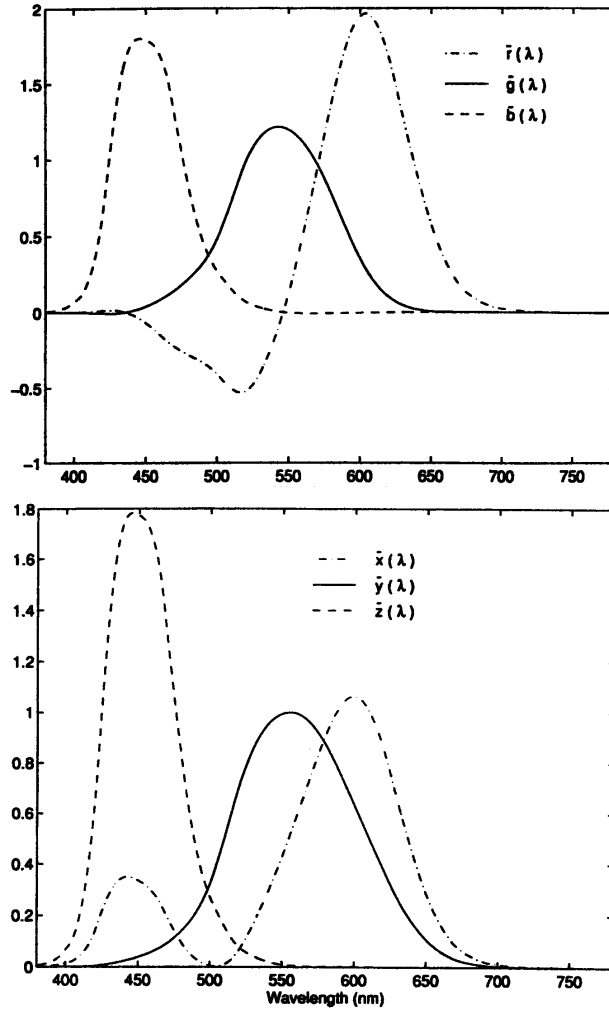


Figure 2.1: The CIE  $\bar{r}(\lambda)$ ,  $\bar{g}(\lambda)$  and  $\bar{b}(\lambda)$  color matching functions (upper plot) and the  $\bar{x}(\lambda)$ ,  $\bar{y}(\lambda)$  and  $\bar{z}(\lambda)$  color matching functions (reproduced after Sharma and Trussel, 1997).

The color spaces defined for various purposes and applications are usually three-dimensional Euclidean spaces with a color specified by the means of three coordinates not to be confused with trichromatic coordinates. The coordinates in these color spaces can be obtained from  $X$ ,  $Y$  and  $Z$  trichromatic values using respective linear

or nonlinear transformations and taking into account the viewing conditions.

Contemporary standards for television broadcasts in North America, Europe and Japan differ slightly and also the reference sets of R, G and B primaries applied are different. The international ITU–R Recommendations BT.601 and BT.709 (1994a, 1994b) specify the set of primaries that are closely representative of common studio monitors used for video and computer graphics. A linear transform between  $R$ ,  $G$  and  $B$  values and  $X$ ,  $Y$  and  $Z$  trichromatic values is given by the equation 2.10.

$$\begin{bmatrix} R \\ G \\ B \end{bmatrix} = \begin{bmatrix} 0.939555 & 0.050173 & 0.010272 \\ 0.017775 & 0.965795 & 0.016430 \\ -0.001622 & -0.004371 & 1.005993 \end{bmatrix} \begin{bmatrix} X \\ Y \\ Z \end{bmatrix} \quad (2.10)$$

The nonlinear  $R'G'B'$  systems specified by video standards to be closely matched to the characteristics of real monitors involve additional *gamma correction* for dual purposes of coding into perceptually uniform space and precompensating the non-linearity of the CRT. For example, the gamma transfer function defined by ITU–R Rec. 709 is given by equation 2.11.

$$R' = \begin{cases} 4.5R, & R < 0.018 \\ 1.099R^{0.45} - 0.099, & R \geq 0.018 \end{cases} \quad (2.11)$$

Similar dependencies are defined for  $G'$  and  $B'$  values. Digital images are also mostly stored in gamma–corrected format in order to avoid the visible effects of quantization.

Additional color spaces for the purpose of transmission of color television signal (defined by television standards) and compression of color images (recommended in compression standards) separate the *lump* from the *chroma* information, where the both terms are rather loosely defined. The  $Y$ ,  $(B - Y)$  and  $(R - Y)$  components (the two latter being also called *differential chrominance*) are obtained from gamma–corrected  $R'$ ,  $G'$  and  $B'$  values as shown in equation 2.12.

$$\begin{bmatrix} Y \\ B - Y \\ R - Y \end{bmatrix} = \begin{bmatrix} 0.299 & 0.587 & 0.114 \\ -0.299 & -0.587 & 0.886 \\ 0.701 & -0.587 & -0.114 \end{bmatrix} \begin{bmatrix} R' \\ G' \\ B' \end{bmatrix} \quad (2.12)$$

Various scale factors are applied to  $(R - Y)$  and  $(B - Y)$  components, depending on application. For component analog video transmission the  $(B - Y)$  and  $(R - Y)$  components are denoted as  $U$  and  $V$  and they are scaled by  $\frac{0.5}{0.886}$  and  $\frac{0.5}{0.701}$ , respectively (Poynton, 1996). On the other hand, for digital video and digital image coding applications, a color representation with  $Y$ ,  $C_B$  and  $C_R$  notation is applied (ITU–R, 1994a). The  $Y$ ,  $C_B$  and  $C_R$  signals are represented as eight–bit integer numbers,

where  $Y$  has a range of 219 and an offset of 16, and  $C_B$  and  $C_R$  span over  $\pm 112$  range with an offset of 128. This coding reserves the extremes of the range for signal processing headroom and footroom.

The perceptual (but not perceptually uniform)  $IHS$  color space (Nibblack, 1986; Pratt 1991) commonly used in machine vision application has its coordinates aimed at corresponding with subjectively perceived basic color attributes: “intensity”, “hue” and “saturation”. A rectangular to polar coordinates transformation (see equation 2.13) is involved in calculation of the chrominance coordinates in so called *Maxwell plane* which is passing through the corners of maximum pure red, green and blue in linear  $RGB$  space.

$$\begin{aligned} \begin{bmatrix} I \\ v_1 \\ v_2 \end{bmatrix} &= \begin{bmatrix} 1/3 & 1/3 & 1/3 \\ 1 & -1/2 & -1/2 \\ 0 & -\sqrt{3}/2 & \sqrt{3}/2 \end{bmatrix} \begin{bmatrix} R \\ G \\ B \end{bmatrix}, \\ H &= \begin{cases} \arctan v_2/v_1 & \text{if } v_2 \geq 0 \\ \pi + \arctan v_2/v_1 & \text{if } v_2 < 0 \end{cases} \\ S &= \sqrt{v_1^2 + v_2^2} \end{aligned} \tag{2.13}$$

There exist several formulations for similar color spaces denoted as  $HSV$ ,  $LHS$ ,  $HSB$ , *etc.* which differ basically by various definitions of “lightness” or “brightness” (which are of similar meaning) and appropriate formulas to calculate the  $S$  coordinate, often in less straightforward way the  $IHS$  space is based on. According to Poynton (1996), the use of all these color spaces should be abandoned, since their definition of “intensity” conflicts badly with the properties of color vision. On the other hand, if a proper “intensity” measure is chosen (*i.e.* according to BT.601), the  $IHS$  space is not perceptually orthogonal and any modification of luminance can cause perceptual shifts in hue and saturation. Moreover, a distance measure in this space is not relevant since it is invalid to perform arithmetic mixtures of colors expressed in polar coordinates. For example, smoothing an edge between areas of saturated “green” and saturated “magenta” results in intermediate colors (*e.g.* saturated “yellow”) located on an arc in the color space spanned between these two colors.

## 2.4 Perceptually uniform color spaces.

The basic purpose of perceptually uniform color spaces is to provide a tool for quantifying perceived color differences. It is natural to consider the distance between colors in three-dimensional color space as being related to perceived difference between these colors. The problem is that neither standard CIE tristimulus spaces

nor color spaces commonly used in image coding and computer vision applications provide a reliable correspondence between these two. That is, a certain distance between two points in a perceptually non-uniform color space produces an unnoticeable perceived color difference, while the same distance in another location of the space may be perceived as significant color shift. To estimate such nonuniformity, ellipsoids perceived as uniformly colored are determined in various ranges of the color space and their diameters are compared. For example, the perceptual nonuniformity of the  $XYZ$  color space is as big as 80:1 (Wyszecki and Stiles, 1982; Poynton, 1996).

One of the most widely used and probably historically first uniform color space is one built on the basis of color-order system proposed by Munsell in the early part of the twentieth century. The *Munsell Book of Color* contains a full gamut of visible colors ordered in equal increments along three dimensions (“value”, “hue” and “chroma”) corresponding to three perceptual attributes.

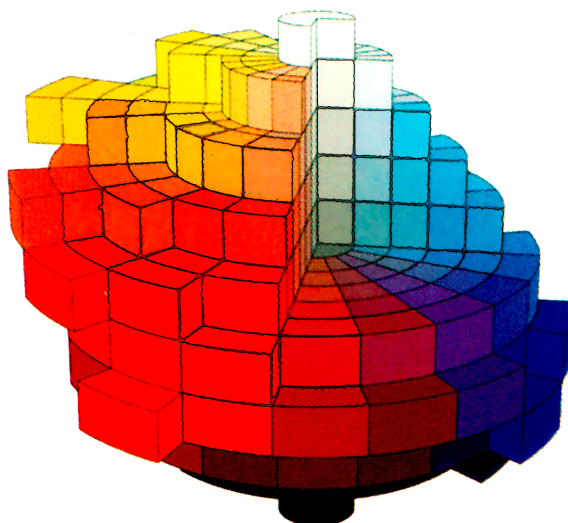


Figure 2.2: Spatial organization of the Munsell color-order system.

Quantifying a difference between two color samples requires taking into account their specification in polar coordinates. An appropriate formula (2.14) proposed and further improved by Godlove (1951) express a visual color difference as Euclidean distance,

$$\Delta E_{God} = \sqrt{2 C_1 C_2 \left[ 1 - \cos (H_1 - H_2) \right] + (C_1 - C_2)^2 + 16 (V_1 - V_2)^2}, \quad (2.14)$$

where  $V_1$  and  $V_2$ ,  $H_1$  and  $H_2$ ,  $C_1$  and  $C_2$  denote respective numerical values of “value”, “hue” and “chroma” of both samples being compared. The magnitude of  $\Delta E_{God}$  is

expressed in units related to *just noticeable color difference* defined by the National Bureau of Standards,

$$1 [\Delta E_{God}] = 1.2 [\text{j.n.d.}] . \quad (2.15)$$

Miyahara *et al* (1988, 1994) proposed a transformation (2.16) to obtain Munsell attributes of a color given its trichromatic representation.

$$\begin{aligned} M_1 &= f(1.02 X) - f(Y) \\ M_2 &= 0.4 (f(0.847 Z) - f(Y)) , \\ \text{where } f(\mu) &= \frac{18.51 \mu}{\mu + 17.58 \left( 1 + \frac{5.416 \mu}{\mu + 30.07} \right)} , \\ S_1 &= (8.981 + 0.916 \cos \Theta) M_1 \\ S_2 &= (8.120 + 2.973 \cos \Theta) M_2 , \\ \text{where } \Theta &= \arctan \frac{M_2}{M_1} , \\ H &= \arctan \frac{S_2}{S_1} \\ V &= f(Y) \\ C &= \sqrt{S_1^2 + S_2^2} . \end{aligned} \quad (2.16)$$

This transformation allowed for precise inspection of the distribution of quantized  $R'$ ,  $G'$  and  $B'$  color components in Munsell space by Gan *et al.* (1991). It has also been applied to perceptual image segmentation for image coding applications by Horita and Miyahara (1991).

Before the above transformation was known, perceptually uniform color spaces were obtainable from trichromatic representation by very complicated, often table-based formulas. In 1976 CIE recommended two near-uniform color spaces,  $L^*a^*b^*$  and  $L^*u^*v^*$  to promote an industrial standard color difference formula with acceptably low computational requirements. Due to its slightly better accuracy and some practical advantages over  $L^*u^*v^*$  (Fairchild, 1998), the  $L^*a^*b^*$  color space achieved higher popularity in image processing applications. The  $L^*$ ,  $a^*$  and  $b^*$  coordinates are related to the  $X$ ,  $Y$  and  $Z$  trichromatic values through a set of nonlinear trans-

formations:

$$\begin{aligned}
L^* &= 116 f\left(\frac{Y}{Y_n}\right) - 16 \\
a^* &= 500 \left[ f\left(\frac{X}{X_n}\right) - f\left(\frac{Y}{Y_n}\right) \right] \\
b^* &= 200 \left[ f\left(\frac{Y}{Y_n}\right) - f\left(\frac{Z}{Z_n}\right) \right],
\end{aligned} \tag{2.17}$$

$$\text{where } f(\mu) = \begin{cases} \sqrt[3]{\mu} & \mu > 0.008856 \\ 7.787 \mu + \frac{16}{116} & \mu < 0.008856 \end{cases}$$

Here,  $Y_n$ ,  $X_n$  and  $Z_n$  are the  $XYZ$  trichromatic values representing the reference white light. The value of  $L^*$  corresponds to the perceived lightness, whereas  $a^*$  and  $b^*$  correspond to “green–red” and “blue–yellow” balance, respectively. The Euclidean distance between two color stimuli specified through respective coordinates  $L_1^*$ ,  $a_1^*$ ,  $b_1^*$  and  $L_2^*$ ,  $a_2^*$ ,  $b_2^*$ ,

$$\Delta E_{a^*b^*} = \sqrt{\left(L_1^* - L_2^*\right)^2 + \left(a_1^* - a_2^*\right)^2 + \left(b_1^* - b_2^*\right)^2}, \tag{2.18}$$

express the color difference, whereby (Sharma and Trussel, 1997)

$$2.3 [\Delta E_{a^*b^*}] = 1 [\text{j.n.d.}] . \tag{2.19}$$

Both  $L^*a^*b^*$  and  $L^*u^*v^*$  spaces exhibit perceptual nonuniformity reduced to as low as 6:1. Therefore they are much better suited for measuring color differences in applications such as objective distortion measure, to be discussed in section 2.7.

Application of the  $L^*a^*b^*$  to color image processing has been investigated by several researchers. For example, Van Dyck and Rajala (1991) examined the influence of color space selected for image representation on the visibility of coding errors of lossy subband coding. The general observation is that the visual differences between images compressed at high bit rates in various color spaces are subtle. For high compression ratios however, subband coding in  $L^*a^*b^*$  offers less noticeable artifacts as compared to  $XYZ$ ,  $RGB$  and  $YIQ$  space. Charrier *et al.* (1997) compared the performance of color image coding using block–based vector quantization with compression ratios ranging from 5:1 to 30:1. Coding was performed independently on three components of images represented in numerous color spaces and reconstructed images were asserted subjectively using rigorous statistical verification.  $L^*a^*b^*$  was indicated as one providing better visual quality than  $L^*u^*v^*$ ,  $LHS$ ,  $XYZ$ ,  $RGB$  and other spaces.

## 2.5 Statistical and spectral properties of natural color images and video.

### 2.5.1 Distribution of color data in natural images.

Statistical properties of color images were studied by several researchers. Pirsh and Stenger (1976), Limb and Rubinstein (1972, 1977) and Wan and Kuo (1996) studied the statistical distribution of single color components in various color spaces. Similar results have been obtained by the author (Bartkowiak, 1995), which prove that representation of color using luminance–chrominance system is beneficial from the compression point of view due to reduced dynamic range of chrominance components, and narrower probability density function as compared to  $RGB$  space (cf Figs 2.4, 2.5 and 2.6). First of all, the range of possible values of both the chrominance components is bounded by the extreme values of the  $R$ ,  $G$  and  $B$  components (cf Fig 2.3)

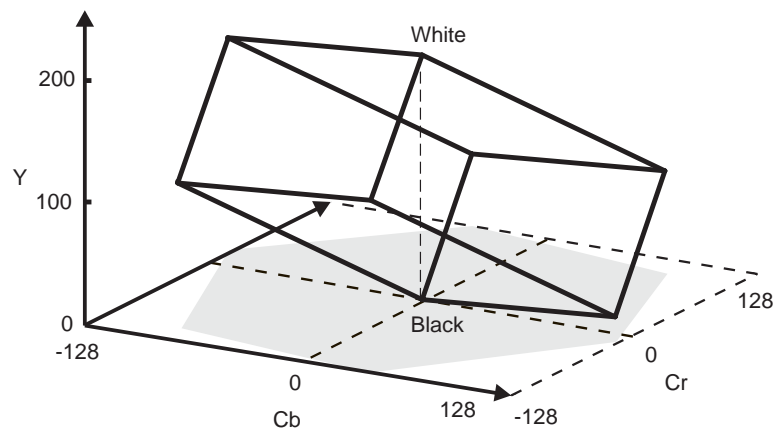


Figure 2.3: The range of possible  $(C_B, C_R)$  pairs related to limited range of  $R$ ,  $G$  and  $B$  components. Here, this area is shown as a projection of the  $RGB$  cube onto the chrominance plane.

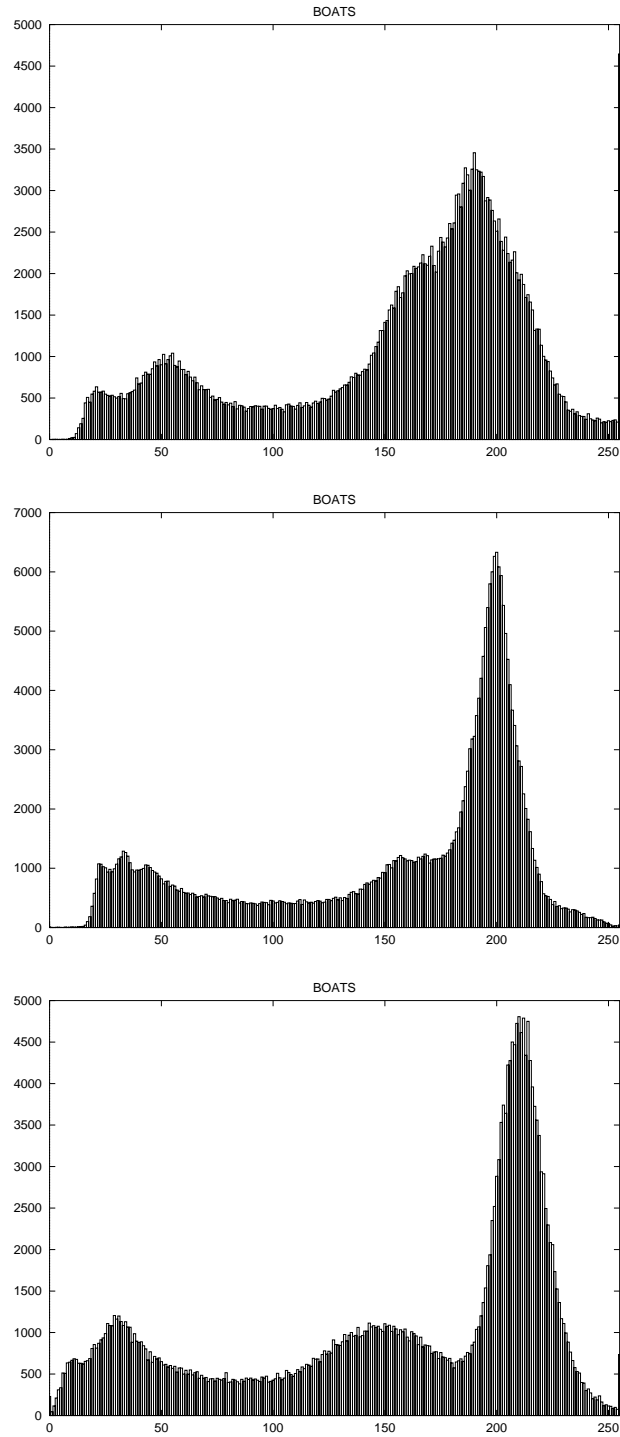


Figure 2.4: Example of distribution of color components in natural image: histogram of  $R'$  component (upper plot),  $G'$  component (middle plot) and  $B'$  component (lower plot) of the test image BOATS (cf Photo 2).

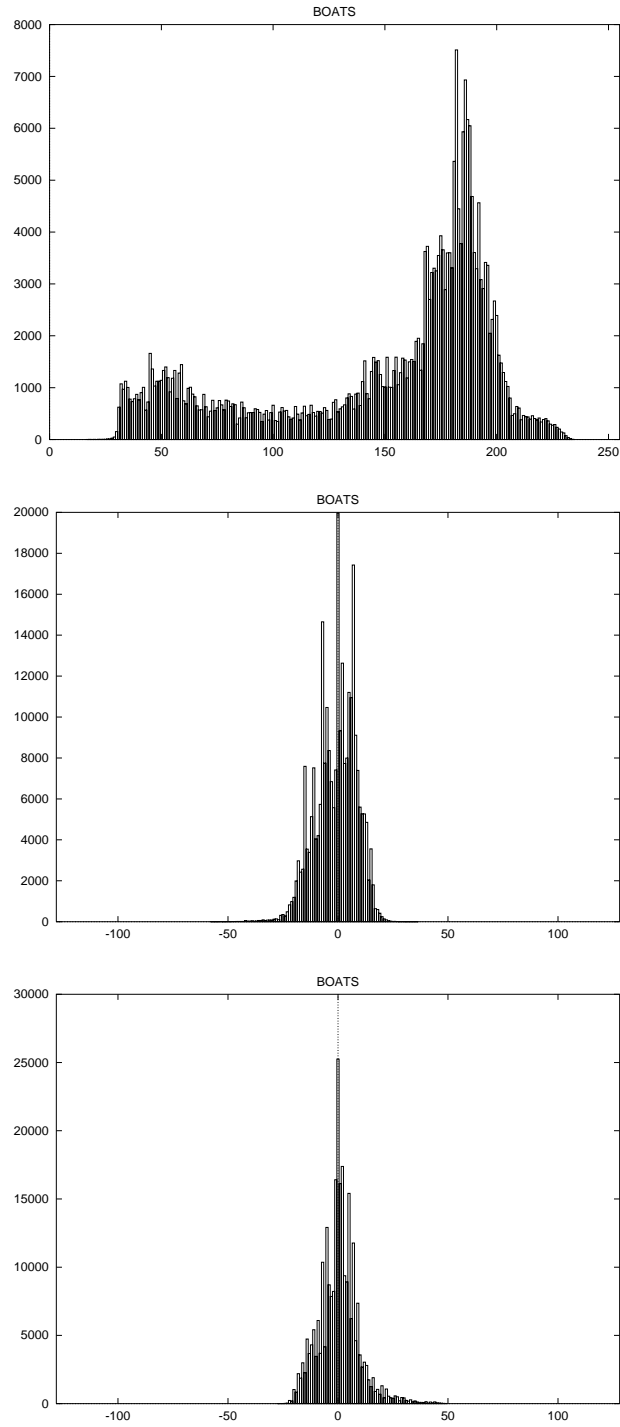


Figure 2.5: Example of distribution of color components in natural image: histogram of  $Y$  component (upper plot),  $C_B$  component (middle plot) and  $C_R$  component (lower plot) of the test image BOATS.

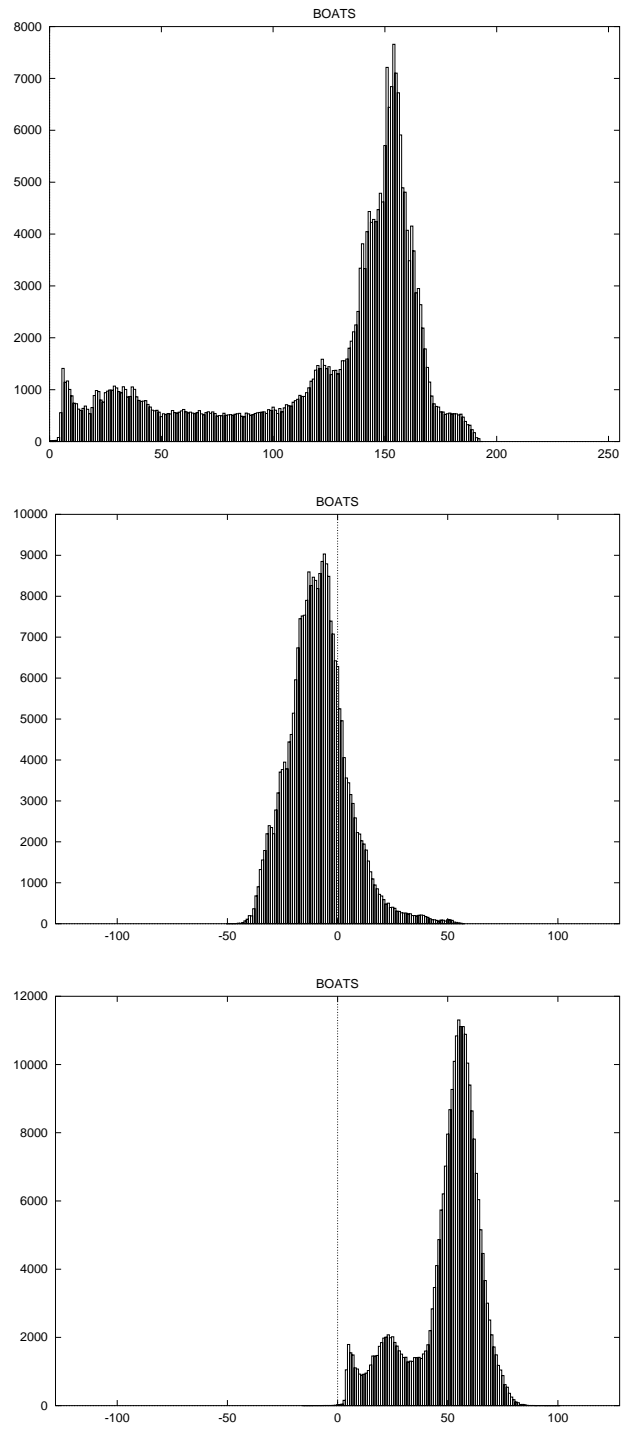


Figure 2.6: Example of distribution of color components in natural image: histogram of  $L^*$  component (upper plot),  $a^*$  component (middle plot) and  $b^*$  component (lower plot) of the test image BOATS.

The luminance–chrominance representation reveals sparseness of color data distribution in natural scene images. Bartkowiak and Domański (1995b) demonstrated such sparseness by the use of two–dimensional histograms of the chrominance data (cf Fig 2.7). The chrominance vectors are mostly concentrated near the origin of the chrominance plane because weakly saturated colors dominate in natural scene images. Several centers of local concentration of data distribution in the color space can be observed. These histogram peaks correspond to the colors of various objects present in the scene (Burton and Moorhead, 1987; Brelstaff and Troscianko, 1992).

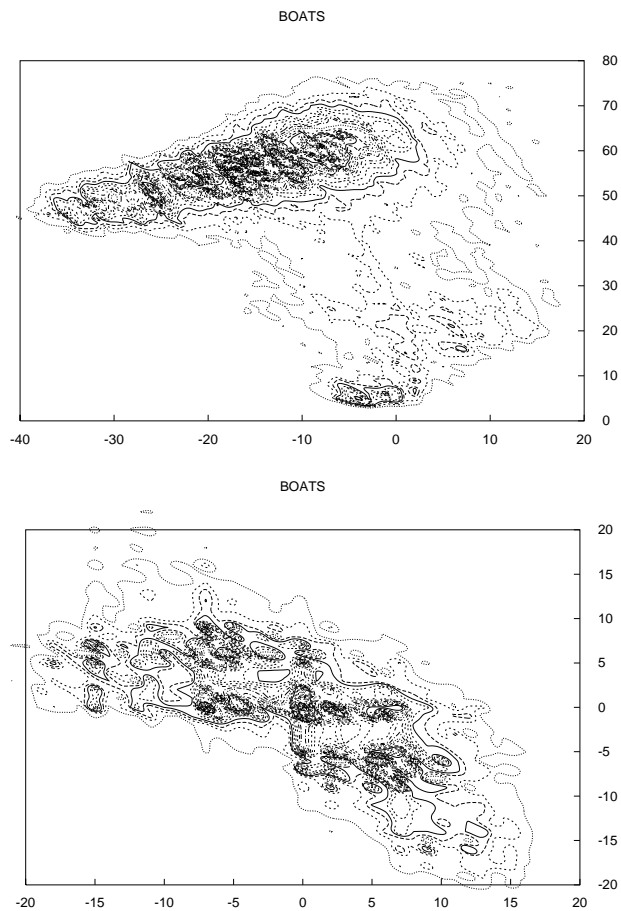


Figure 2.7: Example of color distribution sparseness in natural image depending on the color space used: color histogram of the test image BOATS drawn as a contour plot in the  $a^*b^*$  plane of the CIE  $L^*a^*b^*$  space (upper plot), and  $C_B C_R$  plane (lower plot).

Similar results are obtained for color frames drawn from test videophone sequences (Bartkowiak and Domański, 1995b and 1999a). Since such images typically represent indoor scenes, the local concentration of chrominance data is even more apparent here. Indoor scenes, in contradistinction to outdoor ones, typically contain more artificial objects, fabrics, *etc.* which usually exhibit uniformly colored

surfaces. The latter account for higher the probability of many spatially adjacent pixels having very similar color values. This phenomenon is particularly observed in the chrominance plane, because the  $C_B$  and  $C_R$  (or  $a^*$  and  $b^*$ ) components are virtually independent from the varying lighting conditions.

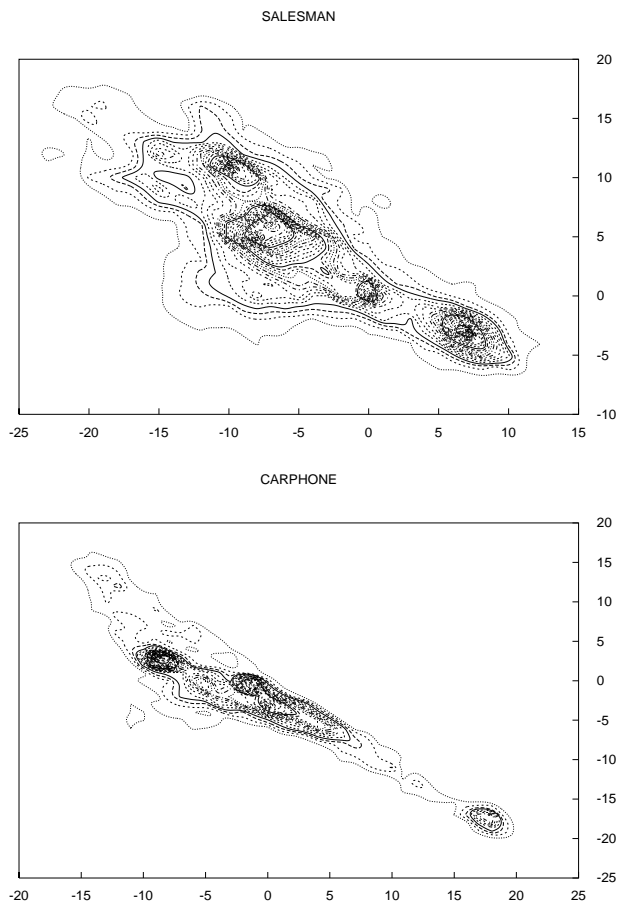


Figure 2.8: Chrominance histogram of single frames drawn from the test images SALESMAN (upper plot) and CARPHONE (lower plot) drawn as a contour plot in the  $C_B C_R$  plane. Original color images shown in color plates (Photo 7 and 6).

Such sparse distribution of chrominance can be modeled by a multimodal distribution, whereby each of its modes (a local maximum of the two-dimensional probability function) corresponds to a chrominance value characteristic to certain object in the scene.

The distribution sparseness of the color data suggests that the set of colors present in a particular image can be easily approximated with a small set of representatives. Such a representation may be obtained by the means of vector quantization, which is covered in section 3.5.

## 2.5.2 Dynamic changes of color content in videophone sequences.

Temporal dependencies in the color data distribution throughout consecutive frames of the test videophone sequences have been studied by Bartkowiak and Domański (1995b). This research demonstrated that the respective locations of histogram maxima are usually relatively stable in time (cf. Fig 2.9). The respective

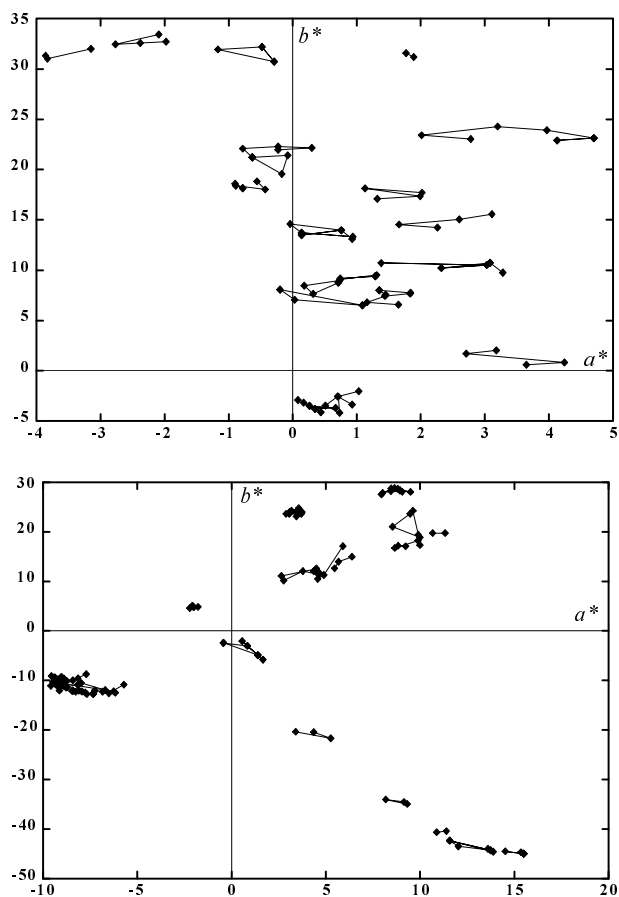


Figure 2.9: Temporal evolution of the most dominant histogram peaks over consecutive 10 frames. Left plot: SALESMAN sequence, right plot: CLAIRE sequence. Here, respective trajectories of the histogram peaks are drawn in the chrominance plane of the  $L^*a^*b^*$  color space.

colors change only slightly from frame to frame. This observation is valid unless there is a dramatic change in the scene content (so called “scene cut”). The explanation of the observed slight changes in the chrominance histograms from frame to frame is that object covering or exposure which are related to their mutual displacements reduce and increase these regions in the histogram which correspond to moving objects. Whereas the motion of content and the camera imposes also

changes of illumination, the latter have very low impact on the chrominance distribution.

### 2.5.3 Mutual dependencies between color components.

Statistical co-occurrence of certain values of the color components in natural images (as discussed in section 2.5.1 and reflected by histogram sparseness) suggests that there is a strong correlation between these components. Experiments show that this correlation depends on the color space used.

Abel, Bhaskaran and Lee (1992) determined the cross correlation between color components of natural images in *RGB* and luminance–chrominance color spaces. The results were also compared to correlation between three components of Karhunen–Loeve transform of the images. The general conclusion is that while offering significant energy compaction, the luminance–chrominance representation still exhibits strong correlation between luminance and both the chrominance components as compared to Karhunen–Loeve transform. In general, the inter-component redundancy may be expressed as a difference between separate and joint entropies, for example

$$\mathcal{R}_{YC_B C_R} = \left[ \mathcal{H}(Y) + \mathcal{H}(C_B) + \mathcal{H}(C_R) \right] - \mathcal{H}(Y, C_B, C_R) , \quad (2.20)$$

where  $\mathcal{R}_{YC_B C_R}$  denotes the redundancy resulting from statistical dependence between  $Y$  component and  $C_B$  and  $C_R$  components,  $\mathcal{H}(Y)$ ,  $\mathcal{H}(C_B)$  and  $\mathcal{H}(C_R)$  denote the entropies of the  $Y$ ,  $C_B$  and  $C_R$  components, respectively.  $\mathcal{H}(Y, C_B, C_R)$  is the second order joint entropy, defined by Pirsh and Stenger (1976) as

$$\mathcal{H}(Y, C_B, C_R) = \mathcal{H}(Y) + \mathcal{H}(C_B|Y) + \mathcal{H}(C_R|Y, C_B) . \quad (2.21)$$

For example, it has been demonstrated, that for typical natural scene images the average redundancy resulting from separate representation of the luminance and single chrominance components using 6-bit accuracy is equal to 0.668 bpp and 0.585 bpp, respectively. On the other hand, the average value of redundancy resulting from separate coding of all the three color components is as big as 2.174 bpp. These values have been averaged over 6 standard test images.

Similarly to joint entropy (2.21) defined are the joint entropies reflecting statistical dependencies between first-order prediction error of the chrominance components and the luminance,  $\mathcal{H}(Y, \Delta C_B)$ ,  $\mathcal{H}(Y, \Delta C_R)$ ,  $\mathcal{H}(Y, \Delta C_B, \Delta C_R)$ , *etc.* In contradistinction to formula 2.20, the above definitions allow to measure the inter-component redundancy considering also correlation between neighboring pixels. Such values

reported by Pirsh and Stenger show significant dependencies. For example, the extension of redundancy definition to first-order prediction errors reveals additional coding gain of 0.258 bpp and 0.277 bpp that can be achieved by joint encoding of single chrominance components together with the luminance. On the other hand, joint encoding of the  $(Y, \Delta C_B, \Delta C_R)$  triple offers additional average coding gain as big as 0.74 bpp. These results motivate the research aimed at developing efficient vector-oriented coding techniques.

#### 2.5.4 Energy compaction resulting from color space transformation.

Since the dynamic range and the probability density function are strongly related to the signal energy, a phenomenon called *energy compaction* is associated with transformation of the image data from *RGB* to a luminance–chrominance space. As proposed by Pratt (1971), the degree of energy compaction can be measured as:

$$\eta_1 = \frac{r_{11}^2}{\text{tr}\{\tilde{\mathbf{R}}_X\}}, \quad \eta_2 = \frac{r_{22}^2}{\text{tr}\{\tilde{\mathbf{R}}_X\}}, \quad \eta_3 = \frac{r_{33}^2}{\text{tr}\{\tilde{\mathbf{R}}_X\}}, \quad (2.22)$$

where  $r_{nm}^2; n,m=1\dots 3$  denote the elements of the covariance matrix  $\tilde{\mathbf{R}}_X$  of image  $\mathbf{X}$ , defined as

$$\tilde{\mathbf{R}}_X = \frac{1}{N_1 N_2} \sum_{i=0}^{N_1-1} \sum_{j=0}^{N_2-1} (\underline{X}_{i,j} - \underline{\bar{X}}) (\underline{X}_{i,j} - \underline{\bar{X}})^T \quad \text{and} \quad \underline{\bar{X}} = \frac{1}{N_1 N_2} \sum_{i,j} \underline{X}_{i,j}, \quad (2.23)$$

$T$  denotes a vector transpose and  $\text{tr}\{\tilde{\mathbf{R}}_X\}$  is a trace of the matrix  $\tilde{\mathbf{R}}_X$ ,

$$\text{tr}\{\tilde{\mathbf{R}}_X\} = \sum_{k=1}^3 r_{kk}^2. \quad (2.24)$$

Limb and Rubinstein (1972, 1977) compared the efficacy in energy compaction offered by the Karhunen–Loeve transformation to the efficacy of various color transformations of the analog *RGB* signal. For typical images, standard *YIQ* space exhibits only slightly weaker energy compaction as compared to KLT, whereby 78%–85% of the signal energy is concentrated in the luminance component, while KLT displays 85%–93% energy compaction. Abel, Bhaskaran and Lee (1992) report similar results, *i.e.* 83%–85% of image energy concentrated in the luminance as compared to 90%–95% compaction achieved using KLT.

## 2.5.5 Spectral properties of color images.

Fourier spectra of natural color images have been studied by many researchers (*e.g.* Abel, Bhaskaran and Lee, 1992). A common approach is to calculate the two-dimensional discrete Fourier transform of each of the color components independently. Such analysis results in three complex-valued images showing the spectra of respective components.

The common general observation is that the magnitude spectra (and consequently the power spectra) are almost identical comparing the  $R$ ,  $G$  and  $B$  color components. On the other hand, in the luminance-chrominance representation the bulk of the fine detail high frequencies is concentrated in the luminance component (as shown in the example Fig. 2.11). In fact, the  $YC_B C_R$  color space is optimized in order to achieve such desirable reduction of signal bandwidth of the chrominance components (Limb and Rubinstein, 1977; Poynton, 1996). This bandwidth reduction is commonly exploited both in analog and digital television:

- in analog systems the chrominance signals are transmitted using much narrower a bandwidth,
- in digital systems the chrominance components are represented with reduced spatial resolution with respect to the luminance, which is achieved through subsampling.

The subsampling of chrominance components applied in digital TV and video coding uses one of the standardized (ITU-R, 1994a) schemes, which uniformly reduce

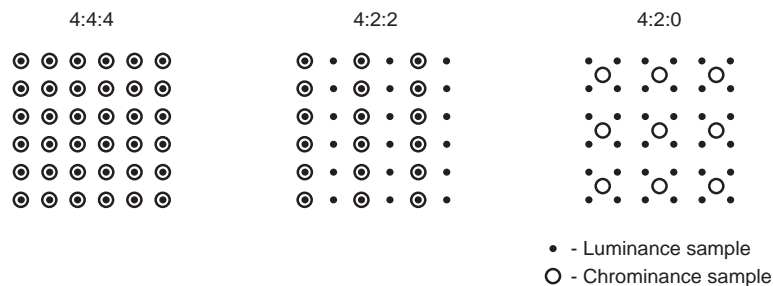


Figure 2.10: Basic chrominance subsampling schemes.

the spatial resolution of the chrominance on the basis of a regular grid (cf Fig. 2.10). Murching and Woods (1994) argue that such fixed subsampling causes blurring particularly visible at the edges. An adaptive subsampling scheme is proposed, whereby the local density of chrominance samples is controlled by the luminance activity measured as a variance value within small window.

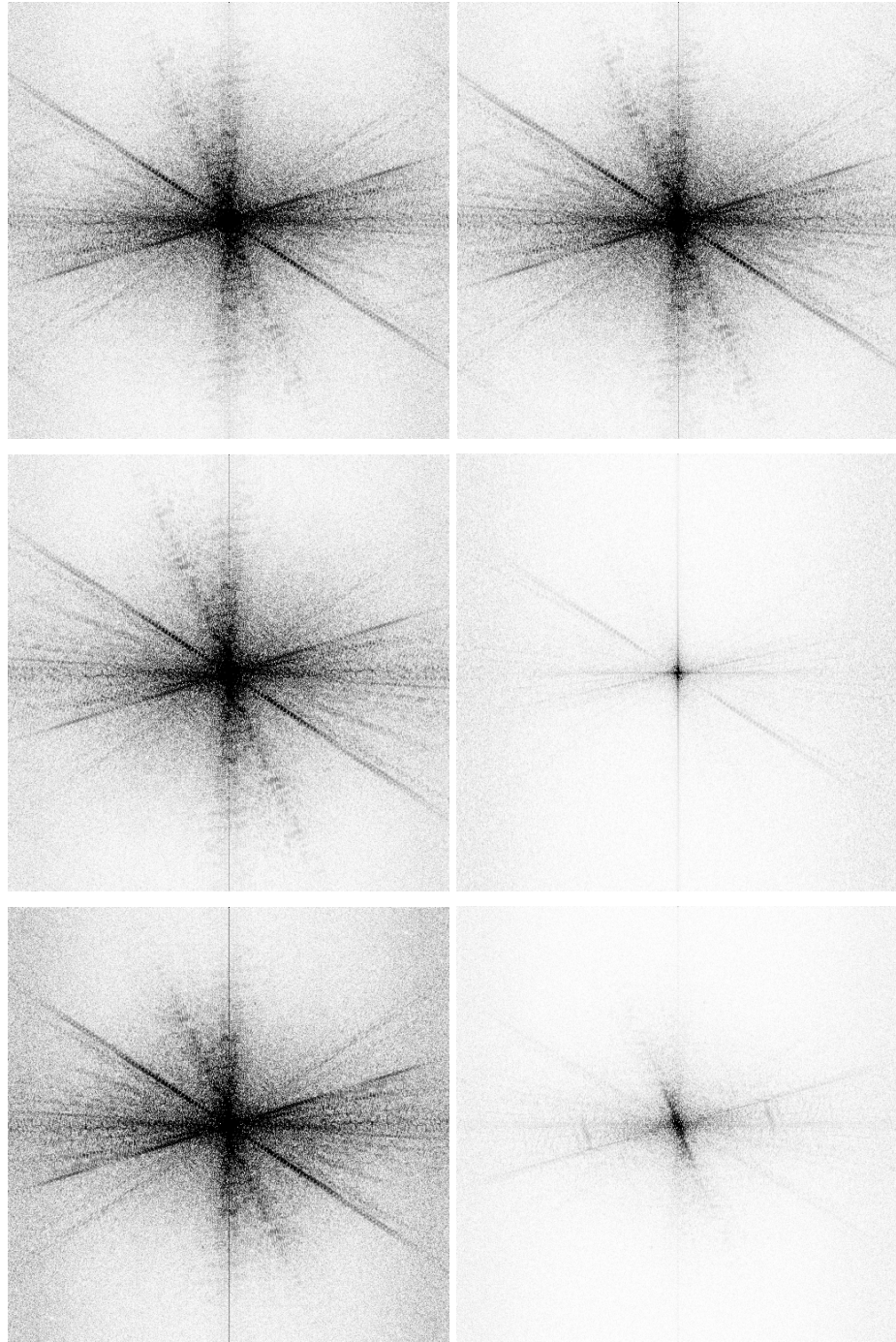


Figure 2.11: The magnitude of the Fourier spectra of  $R$ ,  $G$  and  $B$  component (left column, downwards) and the  $Y$ ,  $C_B$  and  $C_R$  component (right column, downwards) of the test image BOATS.

The irregular subsampling scheme proposed does not require additional information regarding the sample position pattern to be transmitted. On the other hand

as shown by Murching and Woods, while preserving the average sample rate this scheme offers significant increase of the objective quality (average PSNR increase of about 5dB, however even 24dB increase is observed in extreme cases) as well as better visual appearance of the subsampled images.

## 2.6 Human perception of color images and its implications.

Whereas many aspects of human vision related to perception of color alone are partially explained and modeled, it is not being studied in equal degree, how complex images are perceived (Wyszecki and Stiles, 1982; Sharma and Trussel, 1997; Sharma *et al*, 1998). Only the basic properties related to perceptibility of simple color patterns have been studied and measured.

Van Nes and Bouman (1967) studied the sensitivity of the human eye to isochromatic luminance gratings of various spatial frequencies, while Mullen (1985) measured such sensitivity to isoluminant chromatic patterns. Pennenbaker and Mitchell (1993) compared respective plots (cf Fig. 2.12) and concluded that human visual system suffered from poor response to spatial details in colored areas of constant luminance compared to its response to identical details in luminance in the absence of color.

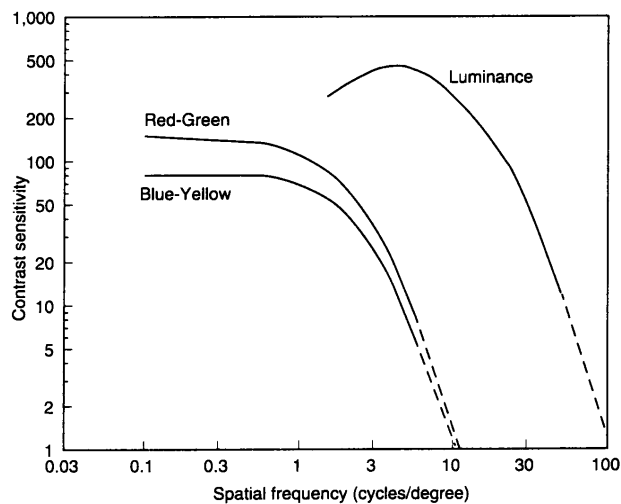


Figure 2.12: Sensitivity of the eye to luminance and chrominance intensity changes (after Pennenbaker and Mitchell (1993)).

On this basis digital image and video codecs are more lossy with respect to the chrominance details as compared to luminance details, which is reflected by alloca-

tion of most of the bitstream to the luminance component. For example, Watson (1994) proposed quantization tables for DCT-based coding that were perceptually optimized taking into account human sensibility to coding artifacts occurring independently in  $Y$ ,  $C_B$  and  $C_R$  components.

De Valois and Switkes (1983) investigated, how sensitivity to chromatic gratings change in the presence of luminance patterns and *vice versa*. The conclusion is that chromatic variation is masked by luminance patterns only slightly and only if they exhibit similar frequency content. On the other hand, luminance patterns are easily masked by chromatic changes of similar frequency. These results suggest that compression strategy aimed at highest possible quality of luminance at the cost of low quality of chrominance resulted from very lossy coding of the latter is invalid from the perception point of view.

Author's own observations confirm the common opinion that whereas the ability of the human eye to perceive purely chromatic changes quickly decreases with growing their frequency, the sensitivity to color fidelity alone is very high and strongly depends on the context. For example, even slight erroneous coloration of image in the areas representing human skin results in strong negative impressions.

## 2.7 The quality criteria - objective measures of the color image quality.

The purpose of image quality measure is to quantify the difference between two images. The basic application of such comparison is evaluating and comparing various techniques for image enhancement (whereby the input image and the enhanced image are both compared to the original image) and lossy compression (whereby the reconstructed image is compared to the original one). Typically, given lossy image compression technique is called *more efficient* if it offers higher quality of the reconstructed images at the same compression ratio or higher compression ratio at the same quality as compared to the concurrent technique.

Quantifying the difference between the original image and its distorted version resulting from lossy encoding and subsequent reconstruction (decoding) involves calculation of the distance between image data represented in some model space. This model space should reflect human perception of visual impairments, since it is desirable that the objective distortion measure corresponds to some extent to the human perceived discrepancies between the two images compared. As this perception is very hard to model (ANSI, 1995; cf also Miyahara, 1988; van den Branden Lambrecht and Farrel, 1996), simplified models are used, the most ubiquitous being

pixelwise image differences.

*Normalized mean squared error* (NMSE) is the commonly used pixelwise distortion measure, whereby the error magnitude at each pixel is determined using the energy of the error between corresponding pixels in the original and the distorted image, respectively, and the total error is expressed as normalized the sum of errors at each point,

$$\text{NMSE} \stackrel{\text{def}}{=} \frac{\sum_{i,j} \|\underline{X}_{i,j} - \hat{\underline{X}}_{i,j}\|^2}{N_1 N_2 \sup \|\underline{X}\|^2}, \quad (2.25)$$

where  $\|\underline{X}_{i,j} - \hat{\underline{X}}_{i,j}\|$  is the norm calculated in the color space of the difference vector between the pixel of the original image,  $\underline{X}_{i,j}$  and the distorted image,  $\hat{\underline{X}}_{i,j}$ .  $\sup \|\underline{X}\|$  is the maximum possible magnitude of the original image pixels which is directly related to the dynamic range. The value of NMSE is often used to calculate the peak signal to noise ratio (PSNR). On the basis of perception laws discovered by Weber and Fechner, the logarithmic scale is used,

$$\text{PSNR} \stackrel{\text{def}}{=} -10 \log(\text{NMSE}) \quad [\text{dB}]. \quad (2.26)$$

Whereas direct calculation of the PSNR rating for monochrome images is straightforward, for color images it has to be defined

- what is the norm used in formula 2.25,
- what is the color space used,
- what is the dynamic range of color components.

Due to the lack of normalization or common agreement regarding the above, it is ubiquitous to calculate the PSNR for each of the color component independently using the input color space the data is represented in. Such calculated PSNR ratings do not correspond to perceived magnitude of color difference. For more reliable quality assessment, calculation of the PSNR may be performed in the perceptually uniform color space. For example, Bartkowiak and Domański (1998a) used the formula 2.14 to calculate the color error in Munsell color space obtained from  $YC_B C_R$  components through the transformation 2.16. This quality measure has been employed to compare the performance of a standard JPEG codec (ITU-T, 1992; IJG, Undated) and the wavelet-based codec implemented by Davis *et al* (1997) (cf Fig. 2.13 and Photos 1–4). Such comparison confirms that it is not possible to reliably evaluate two lossy coding techniques which display different kind of distortions in the reconstructed pictures. Similar distortion measure was used by Bartkowiak and

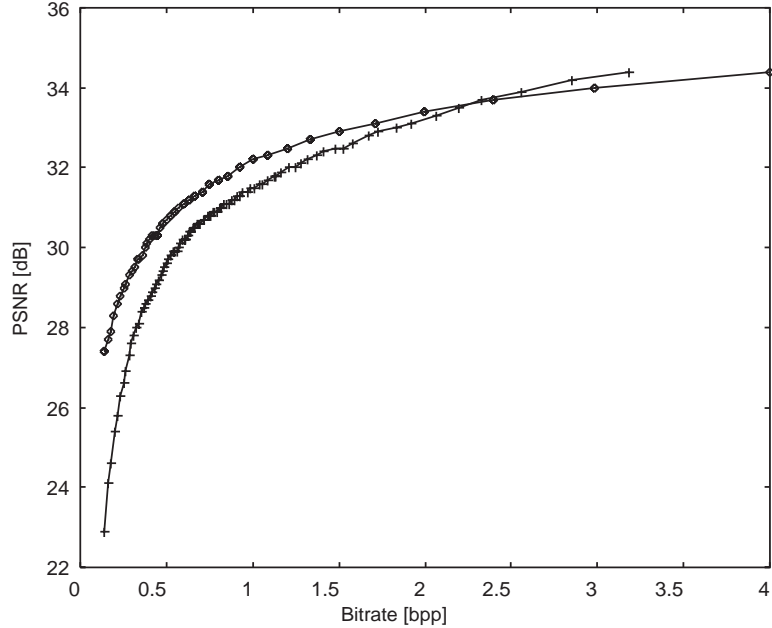


Figure 2.13: Comparison of the quality of image BOATS reconstructed from component-wise JPEG (+) and wavelet (◇) encoding of its  $Y$ ,  $C_B$  and  $C_R$  components at various bit rates. Here, the value of PSNR is calculated in Munsell color space according to formula 2.14.

Domański (1995a) to evaluate color image restoration performed by vector median filters (cf *e.g.* Astola *et al.*, 1990) operating in various standard color spaces.

Among several alternative pixelwise distortion measures proposed to better reflect human perceived discrepancies, the variance of the difference image advocated by Eskiçlioglu and Fisher (1994)

$$\sigma_{\text{DI}}^2 = \frac{1}{N_1 N_2} \sum_{i,j} \left[ \|\underline{X}_{i,j} - \hat{\underline{X}}_{i,j}\| - \frac{1}{N_1 N_2} \sum_{i,j} \|\underline{X}_{i,j} - \hat{\underline{X}}_{i,j}\| \right]^2 \quad (2.27)$$

takes into account contrast adaptation phenomenon (Wyszecki and Stiles, 1982, Fairchild, 1998). On the other hand, due to local averaging properties related to perception of local coloration in the image (Chaddha, Tan and Meng, 1994; Tremeau *et al.*, 1994; Fairchild, 1998), mean error (ME) and local squared error (LSE) are considered as more relevant to quantify coding artifacts:

$$\text{ME} = \frac{1}{N_1 N_2} \sum_{i,j} (\underline{X}_{i,j} - \hat{\underline{X}}_{i,j}) \quad (2.28)$$

Color Plate 1:  
Original images and color distortions related to lossy coding.



**Photo 1 and 2:** Original standard color images: LENA  $512 \times 512$  (left) and BOATS  $512 \times 512$  (right).



**Photo 3 and 4:** Reconstructed image BOATS after JPEG compression to 0.33 bpp, whereby PSNR = 24.4 dB (left) and wavelet compression to 0.18 bpp, whereby PSNR = 24.3 dB (right). PSNR values based on mean squared error calculated in Munsell color space.

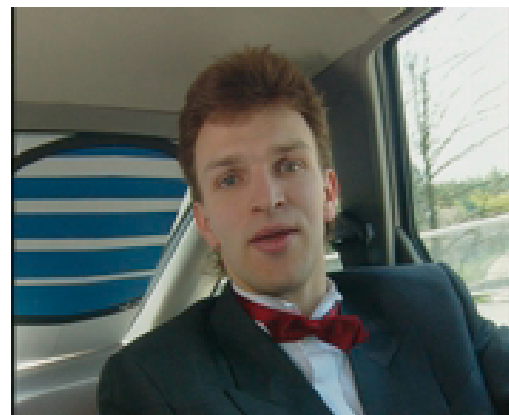


**Photo 5 and 6:** Original first frames drawn from the standard videophone sequences: CLAIRE (left) of CIF ( $352 \times 288$ ) resolution and CARPHONE (right) of QCIF ( $174 \times 144$ ) resolution.

$$\text{LSE} = \sum_{k=i-M/2}^{i+M/2} \sum_{l=j-M/2}^{j+M/2} \|\underline{X}_{i,j} - \hat{\underline{X}}_{i,j}\|^2 \quad (2.29)$$

Here, the value of  $M$  determines the size of some local neighborhood which should be dependent on the viewing angle. Maximum error ( $E_{\max}$ ),

$$E_{\max} = \max_{i,j} \|\underline{X}_{i,j} - \hat{\underline{X}}_{i,j}\| \quad (2.30)$$

is an error measure which respects the psychophysiological effect of asserting the general image quality on the basis of most distorted part of the image (Miyahara, 1988). Przelaskowski (1998) reviews and compares many of the pixelwise error measures. The general observation is that none of the above pixelwise distortion measure exhibit a satisfactory correspondence with subjective assessments.

In general, an objective comparison of different lossy compression techniques is very difficult due to the various spatio-colorimetric distortions caused by different types of information being removed by these techniques, varying viewing environment, image content, aesthetic considerations and even the viewer experience. Numerous advanced distortion measures proposed hitherto attempt to address these aspects. For example, Kotani *et al.* (1991, 1993) proposed a picture quality scale based on the image difference calculated in Munsell color space. Such difference image is subsequently shaped in frequency domain using a spatial frequency response of the eye (determined for an average observer), a set of distortion functions is applied which model the eye nonlinearities, and an appropriately trained neural net is employed for final quantification of the global distortion. Van den Branden Lambrecht and Farnell (1996) use an opponent color space developed by Poirson and Wandell (1993; also Fairchild, 1998), a perceptual decomposition of the image spectrum and noise spectrum using a bank of Gabor filters and a masking curve developed by Legge and Foley (1980). Domański (1998) reviews various advanced distortion measures developed hitherto.

Application of the above advanced distortion measures requires standardization of the method itself and the parameters of the models used. Unfortunately, due to the lack thereof and the lack of publically available implementations it is not possible to use such distortion measures in this dissertation. On the other hand, subjective evaluation of the techniques to be proposed in chapters 4 and 5 may always be done on the basis of several examples shown on color plates.

# Chapter 3

## Review of color image and video compression methods related to vector approach.

### 3.1 Introduction.

A variety of image compression schemes has been proposed hitherto. These methods are usually primarily developed for monochrome images. Typical compression schemes may be considered as consisting of two or three stages:

1. Image modeling stage is a formation of certain image description that can be efficiently represented by a finite set of parameters (Netravali and Haskell, 1988).

For example a set of transform coefficients in transform/wavelet coding (*e.g.* Clarke, 1985; Vetterli and Kovačević, 1995; Woods and O'Neil, 1986), set of geometrical affine mappings in fractal coding (Jacquin, 1992), set of shape/texture description in region/object-based coding (*e.g.* Kunt, Ikonopoulou and Kocher, 1985; Musmann, Hötter and Ostermann, 1989) or a set of motion vectors in interframe video coding (*e.g.* Bhaskaran and Konstantinides, 1995; Tekalp, 1995; Torres, 1996) may be used.

2. In model approximation stage the image representation is simplified by rounding or even discarding selected parameters with regard to their low importance.

Scalar or vector quantization (to be discussed later) is applied for this purpose (*e.g.* Jayant and Noll, 1984; Gersho and Gray, 1991). Of course, no quantization can be involved in lossless compression, since the encoded model must be

exact in order to allow ideal reconstruction of the original image.

3. Entropy coding that exploits statistical redundancy in the data stream is finally employed.

*Run-length coding* (Meyr, Rosdolsky and Huang, 1974) and its mutations encode streams of repeated symbols using more compact representation that includes the number of repetitions. Dictionary-based *Huffman coder* (Huffman, 1952) and *arithmetic coder* (Pasco, 1976; Rissanen, 1976; Witten *et al*, 1987) represent more frequent symbols using bit streams with smaller number of bits than less frequent symbols. This requires prior estimation and transmission of the the code table or symbol statistics. On the contrary, *Ziv-Lempel coding* (Ziv and Lempel, 1977 and 1978) does not require earlier calculation nor transmission of the optimal code table. Arithmetic coder assigns variable-length bitstreams to variable-length groups of symbols, while Ziv-Lempel coding consists in application of constant-length symbols only. The latter algorithm has been corrected and improved by Welch (1984), which is known as *LZW algorithm*.

Clarke (1995), Skarbek (1993, 1998) and Domański (1998) review and compare the various image representation and compression methods.

Color image compression requires addressing the problem of efficient dealing with color. Historically first, this problem was approached by independent processing of the three color components, namely  $R$ ,  $G$  and  $B$  (*e.g.* Carbrej, 1960), which were later replaced by more appropriate luminance–chrominance representation (*e.g.* Pratt, 1971; Limb and Rubinstein, 1974; Limb, Rubinstein and Thompson, 1977; Yamaguchi, 1984). Due to its simplicity, such scenario gained great popularity which is reflected by the amount of published papers on separate coding as well as contemporary compression standards (JPEG, MPEG-1, MPEG-2, H.261, H.263, *etc.*). However, as discussed in section 2.5.3 color images and video generally do not contain three times as much information as their greyscale counterparts and separate representation of individual color components leads to significant redundancy. Therefore, if the color components are coded separately, similar information is coded several times and lots of the processing efforts is redundant. It is natural to expect a certain loss of efficiency as a result of separate coding of similar information occurring in several components.

Modern color image compression methods (Bartkowiak and Domański, 1998a; Domański, 1998) attempt to respect the above inter–component dependencies in order to increase the coding efficiency. This may be realized in several ways taking into account the vector nature of color signal, as discussed in section 2.2:

- by vector control of component–wise coding,
- by joint processing of the color components,
- by dimensionality reducing mapping and encoding a scalar representation of the color signal.

All the above methods will be referred to as *vector-oriented methods*. Experimental results show, that in contradistinction to independent component–wise coding, whereby the mutual dependencies between color components are an obstacle in achieving highest efficiency, these dependencies are beneficial in vector–oriented compression methods.

### 3.2 Vector control of component–wise compression.

Most of the adaptive image compression techniques utilize the local spatial information to adapt their control procedures to the local activity of the image contents. Thus, it is possible to obtain better efficiency by allocating more bits to these regions which require more exact representation, while flat and smooth regions can be treated more roughly. This is a common scenario of many compression techniques developed primarily for monochrome images (Jayant and Noll, 1984; Clarke, 1985). Since for most natural color images the edges and similar patterns occur at approximately the same location in each component (Maragos, Mersereau and Schafer, 1984), it is reasonable to estimate the spatial activity using jointly the information from three channels.

Usually, the gradient operator is used for estimation of the local activity:

$$\nabla \mathbf{X} = [\nabla_i \underline{X}_{i,j}, \nabla_j \underline{X}_{i,j}] \quad (3.1)$$

where

$$\begin{aligned} \nabla_i \underline{X}_{i,j} &= \underline{X}_{i+1,j} - \underline{X}_{i,j} & \text{or} & & \nabla_i \underline{X}_{i,j} &= \frac{\underline{X}_{i+1,j} - \underline{X}_{i-1,j}}{2}, \\ \nabla_j \underline{X}_{i,j} &= \underline{X}_{i,j+1} - \underline{X}_{i,j} & \text{or} & & \nabla_j \underline{X}_{i,j} &= \frac{\underline{X}_{i,j+1} - \underline{X}_{i,j-1}}{2} \end{aligned} \quad (3.2)$$

denote a discrete estimate of horizontal and vertical gradient calculated component–wise).

The conceptual difference between component–wise and vector control is related to the way the gradient is applied. While component–wise approach controls the compression parameters of each color component independently, using the respective

components of the gradient matrix  $\nabla\mathbf{X}$ , the vector approach uses some norm of the matrix to control the three channels simultaneously. Experimental results discussed hereafter show, that adaptive control of coding parameters benefits from the vector approach since the estimation of spatial activity is more precise when using whole information about color changes at a given pixel position.

A block-based compression technique employing vector quantization algorithms to code groups of pixels forming multi-dimensional vectors is able to exploit many correlation dependencies between pixels within each block. A special case of such scenario, called *address-vector quantization* exhibits local smoothness and also continuity of edges across block boundaries. Thanks to local stationarity, some combinations of neighboring blocks can be predicted with high probability (Feng and Nasrabadi, 1988). An extension of this technique to the case of color images has been proposed by its authors (Feng and Nasrabadi, 1989). Application of an algorithm for joint prediction of the blocks of three-component vectors on the basis of an assumed 3-dimensional statistical model of inter-block coincidence leads to bit rates as low as 0.5 to 0.6 bpp with SNR=28 to 31 dB, which is at least twice as better compression ratio in comparison to traditional vector quantization.

A combination of subband compression and vector quantization techniques that gives a class of algorithms for efficient compression of image subbands under given bit rate constraints. Such scenario proposed by Senoo and Girod (1992) has been extended by Li and Jain (1996) by the application of an *activity map* in order to control the suppression of upper subbands. Various local spatial activity estimation methods within different color spaces have been investigated. Bit rates of 0.28 to 0.6 bpp have been reported as yielding good visual quality of reconstructed color images.

### 3.3 Joint color and spatial compression techniques.

The concept of joint color and spatial compression is a natural extension of the idea behind vector control of component-wise processing. Basically, it consists in joint treatment of the vector component by application of Euclidean distance whenever color difference has to be calculated. In case of quantization this leads to replacement of the scalar quantization with vector quantization in color space (which shall be discussed in next section). A good motivation for the application of vector methods is that the natural mutual dependency between color components is exploited by them, whereas, due to unremovable cross-component redundancy, it is an obstacle in efficient coding of separate color components.

It is possible to introduce vector-oriented mechanisms into even very simple com-

pression schemes, *e.g.* differential pulse code modulation (DPCM). Introduction of quantization to coding of the prediction error within DPCM scheme leads to a class of lossy compression techniques. Maragos, Mersereau and Schafer (1984) proposed a multichannel prediction together with joint (*i.e.* vector) quantization of the three color components of the prediction error. High quality reconstructed color images were obtained at a rate of 1 bpp, while the separate encoding of  $R$ ,  $G$  and  $B$  color component independently led to 3 bpp bit rate at the comparable quality of reconstructed images.

Block truncation coding developed by Delp and Mitchell (1979) is a block-based method, where each block is compressed by preserving only the very first statistical moments of the data. Several extensions have been proposed for coding of color images with the vector approach consisting in joint treatment of the color data (Yang *et al*, 1994). If each block of  $4 \times 4$  pixels is coded by two representative colors, an average compression ratio of about 1:14 can be achieved with very good quality of reconstructed images.

Compression techniques based on several variations of vector quantization (to be discussed in next section) employing codevectors of joint spatial and color information have been successfully used in various applications (Boucher and Goldberg, 1984; Barrilleaux *et al*, 1987; Oehler *et al*, 1991; Wang and Chang 1992). Experimental results show that simultaneous treatment of spatial and color information within square pixel blocks of variable or fixed size  $2 \times 2$  to  $4 \times 4$  leads to superior performance over the results of traditional component-wise compression at the same bit rates from the range 0.5–2 bpp, since the MSE measure is minimized in a multispectral sense. The increase of computational costs in the joint spatial and color codebook design is not very high though, thanks to much faster convergence of typical LBG algorithm applied here.

A vector extension of fractal-based coding (Jacquin, 1992) has been proposed by Zhang and Po (1995). The approach extends the class of 3-dimensional affine transforms traditionally employed in compression of monochrome images to a 5-dimensional affine transform class in order to exploit the possible similarity in 5-dimensional space. The results show that there is a compression ratio improvement of about 1.5 times over that achieved when color components are coded separately. Using an Euclidean distance measure and variable block size, bit rates below 1 bpp have been achieved with good image quality and PSNR of about 31 dB.

### 3.4 Scalar quantization and vector quantization.

*Quantization* (a mapping from an input space  $\mathbb{R}$ , or its discrete subset, to a finite set  $\{X_n\}$ , as defined in equation 3.3) of the original signal value is necessary

to reduce its entropy from infinity to finite value in order to make possible the finite state representation in digital system.

$$\begin{aligned} \mathcal{Q} : \mathbb{R} &\mapsto \{X_n\}, \\ \forall_{X \in \mathbb{R}} \quad \mathcal{Q}(X) &= X_k, \quad \text{such that } k = \arg \min_n |X - X_n| \end{aligned} \quad (3.3)$$

For scalar valued signal it is possible to determine the optimal quantizer that minimizes assumed error criterion. Usually, for non-uniformly distributed signals, quantizers that respect signal distribution are optimal in contradistinction to *uniform quantizers*. For example, mean squared error is minimized by optimal *Max-Lloyd quantizer* which is explicitly specified for two and three-level quantizers, or obtained from iterative Max-Lloyd algorithm for higher number of levels (Max, 1960, Lloyd, 1982).

Quantization is an essential part of any lossy compression scheme. Direct quantization of the signal value corresponds to introduction of *quantization error* with amplitude proportional to the quantizer step size (the distance between consecutive representation values,  $|X_{k+1} - X_k|$  or  $|X_k - X_{k-1}|$ ). In case of images, quantization error leads to visible artifacts called *false contouring* or *banding*, where smooth local changes of the value are converted to abrupt steps with visible edges between them. Other possibilities commonly exploited in practical image compression involve quantization of the image data in alternative representation, *e.g.* in frequency domain.

Vector signals can be quantized component-wise with application of independently optimized quantizers to each of the components or with no optimization at all. Such quantization can be considered as a mapping from continuous space  $\mathbb{R}^N$  into a vector space, that is a Cartesian product of  $N$  sets corresponding to particular scalar quantizers, also referred to as *marginal quantizers*, for example

$$\mathcal{Q} : \mathbb{R}_+^3 \mapsto \{R_n\} \times \{G_n\} \times \{B_n\}, \quad (3.4a)$$

$$\forall_{\begin{bmatrix} R \\ G \\ B \end{bmatrix} \in \mathbb{R}_+^3} \quad \mathcal{Q} \left( \begin{bmatrix} R \\ G \\ B \end{bmatrix} \right) = \begin{bmatrix} R_l \\ G_m \\ B_k \end{bmatrix},$$

such that

$$\begin{aligned} l &= \arg \min_n |R - R_n|, \\ m &= \arg \min_n |G - G_n|, \\ k &= \arg \min_n |B - B_n|. \end{aligned} \quad (3.4b)$$

From 3.4 it is evident, that such quantization is not optimal, since the Cartesian product  $\{R_n\} \times \{G_n\} \times \{B_n\}$  generates an excessive set of states with much of them possibly never used, especially if the statistical distributions of individual components are far from uniform.

A contrary, *vector quantization* scenario involves a design of jointly optimized set of representative vectors  $\{\underline{X}_n\}$ , called *codebook*. The basic difference between vector and component-wise (*i.e.* scalar) quantization is that minimization of the distance is performed in vector space, as shown in the example 3.5.

$$\mathcal{VQ} : \mathbb{R}^3 \mapsto \{\underline{X}_n\}, \quad \text{where } \underline{X}_n = \begin{bmatrix} R_n \\ G_n \\ B_n \end{bmatrix}, \quad (3.5a)$$

$$\forall \begin{bmatrix} R \\ G \\ B \end{bmatrix} \in \mathbb{R}^3 \quad \mathcal{VQ} \left( \begin{bmatrix} R \\ G \\ B \end{bmatrix} \right) = \begin{bmatrix} R_k \\ G_k \\ B_k \end{bmatrix}$$

$$\text{such that } k = \arg \min_n \left\| \begin{bmatrix} R \\ G \\ B \end{bmatrix} - \begin{bmatrix} R_n \\ G_n \\ B_n \end{bmatrix} \right\| \quad (3.5b)$$

Here,  $\|\cdot\|$  denotes a vector norm.

Vector generalization of the iterative Max-Lloyd quantizer design algorithm has been proposed by Linde, Buzo and Gray (1980) (the *LBG-algorithm*), which is identical to the *K-means clustering algorithm* (MacQueen, 1967). This algorithm is in fact designed to improve given initial codebook by iterative mapping of the data vectors to the nearest codebook entries and recalculation of the entries as the centroids of the clusters of data just mapped. By repetitions of these two steps the codebook slowly converges to a local minimum of the multidimensional error function (cf. Fig. 3.1). As opposed to its scalar counterpart, LBG algorithm does not guarantee to obtain a codebook for the minimum-distortion quantizer. Therefore, and because it does guarantee to improve any codebook it starts with, the choice of initial codebook is crucial.

Many efficient lossy compression schemes are based on the principles of vector quantization, where the codevectors in the codebook are formed from groups of pixel values organized into blocks rather than color components of single pixels (Jayant and Noll, 1984; Gersho and Gray, 1992). Since the design of an optimal codebook

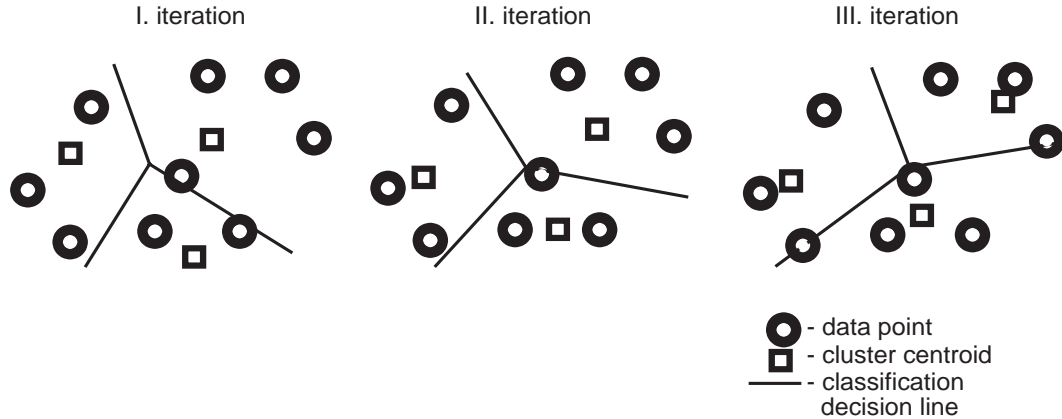


Figure 3.1: Three consecutive iterations of the LBG algorithm.

in highly-dimensional space is very difficult and computationally intractable, simplified heuristic algorithms are often applied.

In practical real-time applications vector quantization is also not feasible due to high computational requirements related to codebook design. For example, digital cameras perform component-wise quantization of the color image being acquired, using perceptually optimized scalar quantizers for red, green and blue component signals encoded as  $R'$ ,  $G'$  and  $B'$ , respectively (Poynton, 1996). This perceptual optimization consists in application of gamma correction, as discussed in section 2.3.

## 3.5 Color quantization.

### 3.5.1 Introduction.

As stated in previous section, direct quantization of the signal value can be regarded as a simplest compression, where the index  $k$  of representation level,  $X_k$  (or vector,  $\underline{X}_k$ ) is stored instead of the quantized value itself. Be it component-wise or vector quantization, the great advantage of this compression scheme is related to low complexity of the decoding process which can be easily implemented in hardware. The circuitry required for decoding of the actual signal value on the fly consists of simple look-up table containing the values of each representation level (or vector). This simplicity accounts for the great popularity gained by *color quantization* (Jain and Pratt, 1972) in low-cost computer imaging systems. Video adapters installed in personal computers and workstations employ a color palette of arbitrarily limited size (usually a power of two, but not greater than 256) to represent a color of individual pixels with indices of respective palette elements. Thanks to the size of the

palette reduced to *e.g.* 256 the amount of memory needed is reduced to one third, assuming resolution of the output digital-to-analog converters of eight bit per color component.

Color quantization is a necessary procedure to prepare an image of high color resolution to be displayed with a limited palette of colors. It is often considered as an instance of vector quantization performed in color space, according to the example 3.5. Basically, it consists of two stages:

1. *palette design* in which the palette colors are determined,
2. *pixel mapping*, in which each input pixel in the original image is assigned one of the colors in the palette.

In the framework of vector quantization, the colors in the palette can be considered as codes in a codebook, and the pixel mapping as the image pixel coding.

Since natural images typically contain a large number of distinguishable colors, displaying such images with a limited palette is difficult. Therefore the visual quality of images quantized to a smaller number of colors depends critically on the way the limited set of colors is chosen. There are two alternatively used classes of color palettes:

1. A *standard palette* is a comprehensive set of colors, typically obtained as combinations of the three (perceptually) uniformly quantized color components. This kind of palette is sometimes provided and forced by the displaying system for all displayed images, and is called in computer terminology a system palette or a common (or shared) colormap. The advantage of using a standard palette is the possibility of simultaneous displaying several images, albeit with compromised quality. On the other hand, lots of the palette colors are “wasted” since they do not appear in the particular image. Therefore, the actual colors of the image are represented very roughly, so the visual and objective quality is low. Some efforts have been done by McFall *et al* (1989), Venable *et al* (1990) and Kolpatzik and Bouman (1995) towards the proposal of universal palette for displaying various classes of images. In order to virtually increase the available gamut of tones and shades some *multilevel halftoning* techniques are usually applied together with standard palettes (*e.g.* Gentile, Walowit and Allebach, 1990).
2. A *custom palette* is an optimized palette designed individually for the particular image, to minimize the approximation error, defined in some arbitrary terms. The advantage of using the custom palette is the possibility to design it as well as possible using one of the well developed techniques (Orchard and

Bouman, 1991). The obvious drawback is the limitation of most display hardware devices which are able to use simultaneously only one color palette. The latter is called in computer terminology a *private colormap*. In such devices only one image can be displayed correctly using its individual palette among several others presented on the screen. Iverson and Riskin (1993) developed an efficient technique for combining palettes of two or more images in order to make this limitation less annoying. Proposed algorithm performs pairwise nearest neighbor matching between elements of two or more palettes in order to quickly combine the palettes for simultaneous display of several images with only slight distortion of their original colors.

### 3.5.2 Representation fidelity.

In the image resulting from color quantization, each color from the palette approximates a whole set of slightly different colors from the original image. To optimally perform this approximation, in general, the visual difference between quantized and the original image should be minimized. Pixelwise minimization of the Euclidean distance measure leads to minimum objective distortion in terms of total squared error. Such optimization rule does not lead to visual optimum however, since it does not take into account the spatial neighborhood of the pixel being considered, which is crucial for perception of color differences (Gentile, Walowit and Allebach, 1990; Tremeau *et al*, 1994; Chaddha, Tan and Meng, 1994; Verevka and Buchanan, 1995; Kim *et al* 1996). Therefore, alternative pixel mapping criteria are often applied. Usually, they take into account the spatial activity in local region of perceptual adjacent pixels. For example, Liu and Chang (1995) proposed an application of morphological operators to detect and avoid potential false contours.

Approximation  $\hat{X}_{i,j} \simeq \underline{X}_{i,j}$  of the actual colors of pixels within the image,  $\mathbf{X}$ , using colors from the limited palette  $\mathbb{P}$  of size  $|\mathbb{P}|$ ,

$$\forall_{i,j} \quad \hat{X}_{i,j} = \underline{X}_{k(i,j)} , \tag{3.6}$$

where  $k(i,j) = \arg \min_{n=1 \dots |\mathbb{P}|} \varepsilon(\underline{X}_{i,j}, \underline{X}_n) ,$

leads usually to degradation of visual quality, regardless of the optimization criterion used, where the latter is reflected by the choice of the cost function,  $\varepsilon(\ )$ . The most important visual errors result from having too small a palette are following:

- *False contouring (banding)* appears in smooth areas represented with too few intermediate tones or shades. It is caused by the highly correlated nature of the error which results from these large regions being approximated with a single color. The sharp and irregular boundaries of the artifact objects with

constant color are particularly easily perceived in large areas of little content variation in the original image.

- *Color shifts* appear in the areas of pixels with similar approximation error. If the mean error within such a region is not equal to zero, the shift is perceived thanks to the averaging properties of human eye, as well as its high sensitivity to the hue variations.
- *Vanishing colors* are a problem in case of images containing some very small objects of unique color. Due to the very little influence they have on the error measures usually applied by the adaptive palette generation algorithms, it is unlikely they appear in resulting palette. In consequence, the sparse/infrequent colors are very distorted by the approximation using quite different color from the palette.

From the objective viewpoint, the magnitude of the color approximation errors heavily depends on the following properties of the system:

- the number of palette elements,
- the choice of the colors in the palette,
- the applied pixel mapping technique.

The color quantization algorithms described in next sections produce color palettes and yield at quantized images of quality depending on the optimization criteria applied, their sophistication, and finally, the given color image. In general, basic and simplified methods (such as *popularity algorithm*, *median cut*, *octree*) result in relatively poor palettes in terms of PSNR as well as perceived visual quality while the highly-optimized, un-compromised techniques (such as *binary splitting*, *optimal principal multilevel quantization*, *genetic K-means algorithm*, *neural network-based techniques*) offer visually much more pleasant results. In case of small palettes, all color quantized images suffer from false contouring at smooth regions.

### 3.5.3 The palette design problem.

The task of finding an objectively optimal set of representative colors may be formulated as a large scale clustering problem (as proposed by Wan *et al* (1988), Orchard and Bouman (1991), and Wu (1992)). The goal is to find an optimal partition of the set of all colors encountered in a given image  $\mathbf{X}$  into a constrained number of subsets in respect to the predefined error criterion. The centroids of thus defined data clusters form the codebook entries which are optimal in terms of minimal quantization error. As the error measure, mean squared error is commonly used here. It

is known that the problem of finding the global minimum of MSE is NP-complete. Consequently, any computationally efficient solution to color quantization will be sub-optimal (Wu, 1992).

The existing adaptive techniques to design a color palette can be divided into three categories:

1. The methods based on *iterative optimization* start from a given initial set of colors and try to refine the codebook in respect to the global quantization error criterion.
2. The *heuristic methods*, instead of finding local minima by numerous iterations, try to produce acceptable solution very rapidly.
3. Finally, there is a group of very simple algorithms which can be classified as improved scalar quantization based rather than vector quantization.

### 3.5.4 Palette design through iterative optimization.

The iterative LBG algorithm has been successfully applied by Heckbert (1982), Orchard and Bouman (1991), and Pei and Cheng (1995) for final refinement of color palettes designed using their own techniques, despite of being very intensive computationally, due to its exhaustive checking of every data vector against every codebook element for the closest match. A fuzzy extension of the LBG algorithm consists in relaxing the strict classification rule within the centroid recalculation step of the original algorithm. Each data point may be a fuzzy member of several clusters with the membership relation taking a continuous value between 0 and 1. Kok, Chan and Leung (1993) proved experimentally, that, thanks to better dealing with the false classification, this fuzziness yields better convergence and, when applied to the palette design problem, it results in visually better color quantized images with color shifts strongly reduced.

The *genetic K-means clustering* proposed by Scheunders (1996) is a hybrid approach, combining the LBG algorithm together with a Genetic Algorithm (Goldberg, 1989, Davis 1991) as an attempt to avoid its convergence to a local optimum only. This technique operates on a set of palette colors represented as a string of their components. There is an iterative palette refinement sequence which consists of the three stages typical for a genetic approach, namely regeneration, crossover and mutation followed by LBG optimization. Experimental results show that numerous repetitions of such sequence lead to an optimal (in terms of MSE) set of palette colors, virtually independent from the initial color set. A similar technique has recently been proposed by Freisleben and Shrader (1997).

Palette design algorithms exploiting the optimization properties of *neural networks* have been proposed by Verevka and Buchanan (1995), and Réndon *et al* (1997). These techniques employ so called self-organizing *topological maps* invented by Kohonen (1982, 1988). In both approaches, an initial palette is created by taking samples from the original image with predefined intervals. Subsequently, a network training process is applied which consists of an iterative adjustment of the winning “neuron” representing a palette entry. This corresponds to refinement of the palette. Some original simplifications have been proposed for speeding-up this time consuming process. The resulting distribution of the palette colors in the color space follows almost faithfully the color distribution of given input image. The obtained palette is ordered, which is of great importance when further compression of the quantized image (as discussed in section 3.6) is considered.

### 3.5.5 Heuristic methods for palette design.

Most of the proposed heuristic algorithms are based on the statistical analysis of the color distribution of image pixels within the color space. These methods can be classified as *divisive* and *agglomerative*. The divisive methods iteratively subdivide the 3-dimensional color space into cells according to various criteria to determine which cell to partition further and where exactly place the partitioning surface. The agglomerative methods analyze the set of colors present in the image and apply a *hierarchical clustering* by iteratively merging the data clusters according to various rules.

The *popularity algorithm* of Heckbert (1982) uses the color histogram of original image to select the  $K$  most frequently occurring colors. Braudaway (1987) improved the popularity algorithm by artificially reducing the histogram values in a region surrounding each color already chosen as a palette entry, in order to avoid concentrating too many entries about one histogram peak.

In the *median cut algorithm* (Heckbert, 1982) the initial palette is constructed by assigning to each entry an approximately equal number of pixels from the image. The color space is recursively split into rectangular boxes. At each step, the box with the largest number of pixels is divided into two smaller ones, perpendicularly to the axis with the largest data spread, through the median of the color distribution within the box. A modification of the median cut algorithm, proposed by Xiang and Joy (1993) places the partitioning plane through the algebraic mean of the color data projected onto the direction of splitting.

The *variance minimization algorithm* of Wan, Wong and Prusinkiewicz (1988) adaptively assigns more clusters to the regions with large quantization errors, which corresponds to the data variance. This approach employs a greedy rule of maximum reduction of the quantization error at each step of such bipartition. The color space

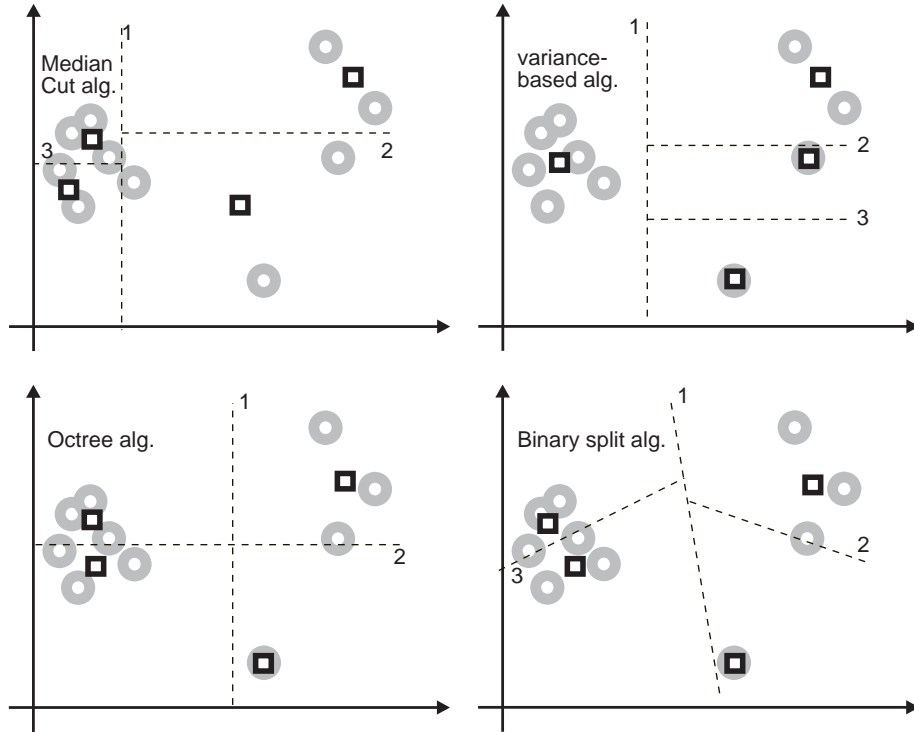


Figure 3.2: A two-dimensional example of the heuristic techniques (median cut, variance minimization, binary splitting and octree) employed to design a 4-element palette through partitioning of the color space in various ways.

is iteratively divided into rectangular boxes until  $K$  clusters are generated. The partition strategy is based on the minimization of the sum of variances of the data in the resulting subboxes. In the final partition, different boxes may contain quite different numbers of data points, but the contribution of each box to the quantization error is approximately equal.

In the *binary splitting algorithm* proposed by Orchard and Bouman (1991), and subsequently improved by Balasubramanian, Allebach and Bouman (1994) the data cluster to be splitted in given step is divided along the direction of maximum color data variation around its centroid by a hyperplane which passes through the centroid. Unlike the other splitting techniques, this approach leads to general polytopal regions. This technique is extensively studied in next chapter.

Wu (1992) formulated a generalization of the splitting-based algorithms called *optimal principal multilevel quantization*, in which the chosen cluster is divided into several smaller ones by a set of planes perpendicular to the direction of the principal eigenvector. The positions of these division planes is optimized by a dynamic programming algorithm, which tends to minimize the resulting error by preserving the statistical moments of the data projected onto the direction of splitting.

The *greedy tree growing* technique (Liu and Chang, 1994, 1995) splits the color space into rectangular boxes. The decision of which region to divide at each step is based on the exhaustive trial-and-error analysis of the total quantization error reduction resulting from particular division. For simplicity, the splitting is performed along one of the axes of the color space. The plane perpendicular to the axis for which the error reduction is largest is selected as the bipartition plane.

The *octree* algorithm (Gervautz and Purgathofer, 1990, Ashdown, 1994) builds a color histogram of the image data in the form of a tree data structure, where each node has eight child nodes. Subsequently, the similar pixel colors are grouped and replaced with their average. The node merging process starts from the deepest level in the tree hierarchy and is iterated as long as the desired number of leaf nodes is obtained. This strategy leads to minimization of the maximum quantization error. A similar *agglomerative clustering* algorithm of Xiang and Joy (1994) merges the nodes between different branches of the tree thus minimizing the increase of the quantization error resulting from each reduction of the color gamut associated with the merging process.

### 3.5.6 Simplified codebook design.

Simplified methods attempt to exploit within scalar quantization the statistical dependency and dimensionality of image data in a way similar to that used in vector quantization. Unlike in the case of simple independent component-wise quantization, the resulting palette contains the combinations of those quantized components that are only that represent a nonzero number of original image pixels.

In *sequential scalar quantization* algorithm proposed by Balasubramanian, Bouman and Allebach (1994, 1995) the 3-dimensional histogram of the color data is sequentially scanned in terms of marginal analysis. The scalar color components are individually quantized in a sequence, with the quantization of each component utilizing conditional information from the quantization of previous component. The Lloyd-Max algorithm is used for the optimal 1-dimensional quantization strategy. The final palette colors are calculated as centroids of data clusters from regions of support of the input distribution.

The very similar *dependent scalar quantization* algorithm of Pei and Cheng (1995) applies binary moment-preserving thresholding to consecutive data bands during the scan of marginal image color distribution. This is preceded by an automatic bit allocation for each data component.

### 3.5.7 Improvements of the color quantization technique.

Several modifications of the palette design procedures have been also proposed in order to take into account the spatial dependencies between neighboring image pixels (Orchard and Bouman, 1991; Balasubramanian, Allebach and Bouman, 1994; Chaddha, Tan and Meng, 1994; Tremeau *et al.*, 1994; Kim *et al.*, 1996). Usually, these modifications are related to the use of subjectively weighted error measure.

$$\text{WTSE} = \sum_{i,j} w(i,j) \|\underline{X}_{i,j} - \hat{\underline{X}}_{i,j}\|^2 \quad (3.7)$$

The weighting factor  $w(i,j)$  is a function of local spatial activity of the image contents, for example the local luminance gradient smoothed by convolution with a smoothing kernel, a maximum value of horizontal and vertical gradient within  $8 \times 8$  pixel block, a sum of the absolute deviation of the color from the mean color within  $8 \times 8$  pixel neighborhood, or a maximum of coefficient-weighted difference between input color and local mean color within  $4 \times 4$  pixel neighborhood.

Moreover, at the pixel mapping stage, appropriate *color halftoning* techniques can induce the perception of the presence of colors that lie between those that are actually present in the image printed or displayed with a limited palette. They rely on the viewer making a local spatial average over patterns of alternating colors. Thus, these techniques sacrifice spatial resolution for tonal resolution, which however may lead to visible texture artifacts. Color halftoning is usually implemented as *dithering* or *error diffusion* algorithms. *Stochastic dithering* and *ordered dithering* are performed by adding respectively random or pseudo-random dither signal to each color component of the image pixels prior to finding their best match in the palette. In error diffusion techniques, the quantization error (the difference between original pixel color and the substituted one) is distributed to neighboring pixels which have not yet been quantized.

## 3.6 Lossless and lossy compression of color quantized images.

Color quantization results in reduction of the original image data. Whereas color quantized images are usually stored in such compressed form, further data reduction is possible. In color quantized images, neighboring pixel are often represented by the same color value, due to reduced entropy and visual similarities between the pixels in original image. Often, especially for low number of palette entries, whole groups of spatially neighboring pixels are approximated with one color from the palette. Information about such regions can be easily compressed using run-length codes

followed by entropy coding. This technique is proposed by the PNG group (1996) together with adaptation of the direction of image linear scanning in order to exploit the repetitions of long data sequences in rows or columns. The compression ratios offered range from 1:2 for natural scene images to 1:8 for drawings, depending on the complexity of the image.

Even higher compression ratios can be achieved with more sophisticated lossless techniques, for example, by the use of two-dimensional prediction together with entropy coding. Gormish (1995) proposed *plane-based coding* with the aid of standard JBIG (ITU-T, 1993a) compression algorithms. The idea is to split the numerical indices to palette elements representing particular pixels into several sets. Separation of the indice values into individual bit planes or into color planes have both been tested prior to binary predictive coding using JBIG. The improvement of the bit rates reduced by 30 to 40 per cent of the standard Lempel-Ziv compression is possible. Another scheme, proposed by Yovanof and Sullivan (1992) employs lossless JPEG (ITU-T, 1992) coder. For each pixel, the best one of 8 various predictors is chosen to exploit the correlation with neighboring pixels. Either Huffman coding or arithmetic coding can be used as the entropy coding of the prediction error. This technique significantly outperforms simple lossless prediction-based compression. Bartkowiak and Domański (1994) proposed an approach that exploits high variance of lightness in color images as compared to other color attributes. Only in cases where the intensity difference does not define the palette entry uniquely, also the difference in chromatic attributes is taken into account. Therefore, one-, two- and three-dimensional symbols are used in Huffman code for differential predictive coding of quantized color. IHS coordinate system has been chosen here. Moreover, a special heuristic algorithm for palette ordering is employed to optimize the efficiency of prediction. Compression ratios of 1:2 to 1:4 are achieved for medical images.

Lossless coding offers relatively low compression ratios in comparison to lossy techniques. Therefore, the latter still remain very attractive research objectives. One way of formulating a lossy compression technique is to introduce some possibility of lower accuracy into lossless scheme as a cost of more efficient representation. For example, a lossy extension of the LZW algorithm has been proposed by Chiang and Po (1997) by introduction of some uncertainty into the process of matching symbol strings. Adaptive thresholding that takes into account masking properties of human visual system is involved and yields minimum visible distortions within given compression constraints. Typically, 25% to 50% improvement is offered in compression efficiency at the PSNR range of 33 to 40 dB and good quality of decompressed images. The great usefulness of this technique is related to its compatibility with the standard LZW decompression.

Another possibility of lossy compression of color quantized images arises from the fact, that many general image compression scenarios can be adopted here. In general, two approaches are possible:

1. A three-channel class of techniques involves color dequantization, *i.e.* each pixel is represented by the three quantized color components from the palette. Such an image is compressed using one of the techniques developed for color images, treating each channel either independently (separate coding) or jointly (vector-oriented coding). After decompression, in order to restore its indexed representation and make it suitable to display with a limited palette, the reconstructed colors should be requantized, because they are no longer the elements of the original palette. A mapping to the old palette may be performed as well as to a new palette designed for the reconstructed image. Both approaches introduce additional errors which accumulate with the first quantization errors and coding artifacts. Due to the mapping stage, decompression is computationally intensive and makes the technique unattractive in practical applications.
2. Instead of treating the color quantized image as a normal color image, the problem of its compression can be reduced to one dimension – the compression may be performed in one-dimensional space of the palette indices. In this case, the indices representing palette colors for adjacent pixels form a pseudo-grayscale image which is compressed using some lossy technique developed for monochrome images. The main advantage of this approach is that it guarantees that the reconstructed image will contain strictly the same set of colors and there is no need to perform requantization.

In order to study the second approach of the above, the mapping from the 3-dimensional color space to the 1-dimensional index space (cf Fig. 3.3) should be discussed. In fact, since the quantized color represents most of the scene content,



Figure 3.3: Compression of color quantized images as processing of image after dimensionality reducing mapping.

this mapping may be thought of as a transformation of the color components in such a way that almost all information content is contained in one channel and the remaining channels can be discarded as they only represent some neglectable residual. In other words, the vector values representing the color of image pixels are represented by scalar values, possibly according to the direction of dominant signal

variation in color space.

Typical color space transformations map from three-dimensional input space to another three-dimensional output space. Here, only the dominant channel is to be encoded, therefore the two remaining vector components are not calculated at all. In other words, the mapping associated with color quantization and a particular order the codebook entries are labeled in, is treated as a *dimensionality reducing mapping*, denoted as  $\mathcal{S} : \mathbb{R}_+^3 \mapsto \mathbb{R}_+$ . In practice, the mapping is only defined for the set of colors  $\mathbb{X}$  present in the image,  $\mathbf{X}$ . These colors are represented by the elements of a finite set  $\mathcal{S}$ , namely the set of indices which label the palette entries:

$$\forall \begin{bmatrix} R \\ G \\ B \end{bmatrix} \in \mathbb{X} \quad \exists S \in \{\mathcal{S} \subset \mathbb{R}\} \quad \mathcal{S} \left( \begin{bmatrix} R \\ G \\ B \end{bmatrix} \right) = \mathcal{S} \left( \mathcal{VQ} \left( \begin{bmatrix} R \\ G \\ B \end{bmatrix} \right) \right) = S. \quad (3.8)$$

Due to the quantization, it is not possible to reconstruct the original image  $\mathbf{X}$ , however there exist a unique inverse mapping  $\hat{\mathcal{S}}^{-1}$ , that is simply a palette look-up, which makes reconstruction of the image after decompression possible. Therefore, any general image compression technique may be employed in the scheme outlined in Fig. 3.3, provided the values of reconstructed image pixels do not differ significantly from the input values. The basic issue to be addressed is the possible decrease of coding efficiency resulting from transformation 3.8, as well as the sensitivity of the inverse mapping  $\hat{\mathcal{S}}^{-1}(S)$  to coding errors affecting the value of  $S$ .

Zaccarin and Liu (1991) showed that the indices of palettized images are highly correlated with the adjacent indices if the color palette is appropriately arranged, *i.e.* if consecutive indices are assigned to visually similar colors and distant indices represent colors that are visually different. In such a case, possibly few high frequency artifacts are introduced into the pseudo-greyscale image within areas where its color counterpart is visually smooth. Several heuristic algorithms have been proposed for ordering of the palette colors together with various compression techniques. Experiments with different palette ordering algorithms show, however, that compression of the pseudo-greyscale image must deal with the problems resulting from the nonlinear transformation related to the mapping from 3-dimensional color space to 1-dimensional index space. In particular, the pseudo-greyscale image possesses some undesirable properties. Numerous impulses and abrupt changes within its content result from the fact that the smooth change of color components within original image may not appear along the chain of ordered palette entries. On the other hand, blurring introduced by various compression techniques may lead to severe color artifacts, because a value intermediate between two color indices does not necessarily correspond to intermediate color. Therefore some color correction

scheme must be applied.

Zaccarin and Liu (1991, 1993) proposed a transform-based compression method which exploits the fact that color variation is locally less important than luminance variation. Aiming at block-based transform coding, the image is divided into square blocks of 8 x 8 pixels and for each block its local subset of colors is ordered according to the luminance values. Such ordering is quite appropriate since usually luminance axis is the one of the greatest spread of color distribution. The ordering optimized using *traveling salesperson problem* algorithms (Lawler, 1985) and using farthest insertion rule have been also considered. The blocks of indices are coded using DCT-based approach similar to that used in JPEG standard. After decompression the pseudo-greyscale image is distorted, so the actual color is chosen from the local subset of palette colors as a color which gives minimum luminance distortion. The local lists of allowed colors within each block are stacked and losslessly encoded using JBIG compression. Bit rates about 1 to 1.5 bpp are reported as yielding good image quality, comparable with the standard 3-channel JPEG coding.

A similar hybrid compression technique proposed by Chen, Petersen and Bender (1993), is also based on the DCT and JBIG scheme, but divides the palette colors into groups of visually similar colors by means of K-dimensional clustering in perceptually uniform color space. The colors within groups are ordered according to their luminance. At the decoding stage, the distorted color is mapped to its closest member within the group. In contrast to the spatial partitioning this approach leads to intra-group errors. This means, that the maximum distortion is constrained within each chrominance group, not within a spatial square block. Similar bit rates are reported in comparison of this technique to the previously discussed one. Tremblay and Zaccarin (1994) modified this approach by application of segmentation-based rather than color-difference-based partitioning of the set of colors and a variable-size block-based correction scheme. Experimental results show that the performance can be improved in this way both in terms of visual quality and MSE ratings. Bit rates of about 1.3 bpp are achievable for typical color images.

Overloop *et al* (1997) proposed a more sophisticated compression technique by the use of transform coding of variable-shape objects. In this approach the image is segmented using the luminance component and the luminance is coded for shape-adaptive transform base functions and Huffman entropy coder. The reconstruction of color information from the decoded luminance is possible thanks to the lists of allowed colors which are determined for each region and compressed using JBIG. Experimental results show visually better reconstructed images in comparison to JPEG coding despite slightly worse MSE ratings at moderate to high compression ratios. In particular, the annoying blocking artifacts are completely eliminated.

Waldemar and Ramstad (1994) proposed a subband coding method to compress the pseudo-greyscale image of palette indices, because of its good performance in traditional compression of monochrome images without causing visible patterns of blocking artifacts (Woods, 1991). A global palette sorting algorithm has been applied here, however, a block based color correction scheme, similar to that one used in previously discussed approaches appeared to be necessary to avoid severe color errors caused by coding artifacts. An original palette ordering algorithm with the aim of maximizing the pixel-to-pixel correlation has been tested together with a simple luminance ordering. Experimental results show better visual quality of reconstructed images in comparison to JPEG coding of the pseudo-greyscale image. The MSE ratings are also clearly better at bit rates of 0.8 to 3.3 bpp for test images such as LENA.

Even considering some successful results discussed above, the color image coding based on color quantization developed hitherto displays several drawbacks:

- In a three dimensional color space, automatic design of a custom color palette which is at least nearly optimum for a given image is not an easy task (Orchard and Bouman, 1991; Wu 1992). Resulting quantized images for reasonable small palettes often suffer from visible color degradation, as discussed in 3.5.
- Further processing, and especially compression of such color quantized images requires proper palette ordering, as discussed in 3.6 which is very difficult. The heuristic algorithms proposed by Zaccarin and Liu (1991), Chen, Peterson and Bender (1993) and Waldemar and Ramstad (1994) are only hit-and-miss solution and exhibit several flaws.
- Lossy compression of color quantized images is prone to severe distortions and sophisticated techniques are needed to recover from them (Zaccarin and Liu 1991; Chen, Peterson and Bender 1993; Overloop, Philips, Torfs and Lemahieu 1997).
- It is not possible to exploit human's lower sensitivity of spatial details in coloration as compared to the sensitivity to identical intensity details, as discussed in 2.6.

# Chapter 4

## New vector-oriented techniques for color image compression.

### 4.1 Introduction.

In this chapter the original color image compression techniques developed by the author will be presented. These techniques are generally based on processing of *scalar chrominance* which is a new concept related to vector quantization of the chrominance components of color image. Such processing exploits a similar dimensionality reducing mapping, as discussed in 3.6, albeit a less radical one, *i.e.* a mapping from two-dimensional chrominance space to one-dimensional space of scalar values,  $\mathcal{S} : \mathbb{R}^2 \mapsto \mathbb{R}_+$ . Application of a hybrid approach, where the luminance component does not take part in vector quantization and is compressed entirely independently from the chrominance components has been chosen after preliminary experiments which revealed its basic advantages:

- It is a compressed representation similar to palette representation, however the codebook can be kept much smaller because many possible colors are obtainable as combinations of the codebook entries with individual luminance values.
- Scalar representation of chrominance may have lower spatial resolution than luminance.
- Codebook design is less complex than classic palette design because codebook for scalar chrominance is designed in a two-dimensional chrominance space. Also optimization of its ordering for further compression is a much simpler task.

The aim of color image compression with chrominance vector quantization is to enhance the traditional color image coding, especially at low bit rates, where

processing is performed in luminance–chrominance (usually  $YC_B C_R$ ) color space. Author’s own experiments show that typically most of the bitstream (*i.e.* 85% to even 90%) is devoted to the luminance component, leaving very small number of bits (*i.e.* 10% to 15% of the bitstream) for encoding of the chrominance components. Consequently, significant distortions are observed in reconstructed images. The proposed techniques for coding of the chrominance may be combined with various techniques of luminance coding. A modification of the standard JPEG compression is shown as an example of such combined approach.

## 4.2 The concept of image coding based on chrominance vector quantization.

The basic idea behind chrominance vector quantization is to replace the two independent channels of the chrominance encoding and decoding by one channel which encodes a scalar signal. This scalar signal results from conversion of the chrominance vector signal by a dimensionality reducing mapping,  $\mathcal{S}$ . This mapping replaces each input chrominance pair by its scalar representation:

$$\forall \begin{bmatrix} C_B \\ C_R \end{bmatrix} \in \mathbb{C} \quad \exists S \in \mathcal{S} \quad \mathcal{S} \left( \begin{bmatrix} C_B \\ C_R \end{bmatrix} \right) = S \quad (4.1)$$

Here,  $\mathbb{C}$  denotes the set of all chrominance vectors observed in a given image,  $\mathcal{S}$  is a set of scalar values used to represent chrominance vectors. This representation is lossy, since the mapping is not fully reversible. In order to minimize the approximation error, a two–dimensional vector quantization in the chrominance plane with adaptively designed codebook is applied.

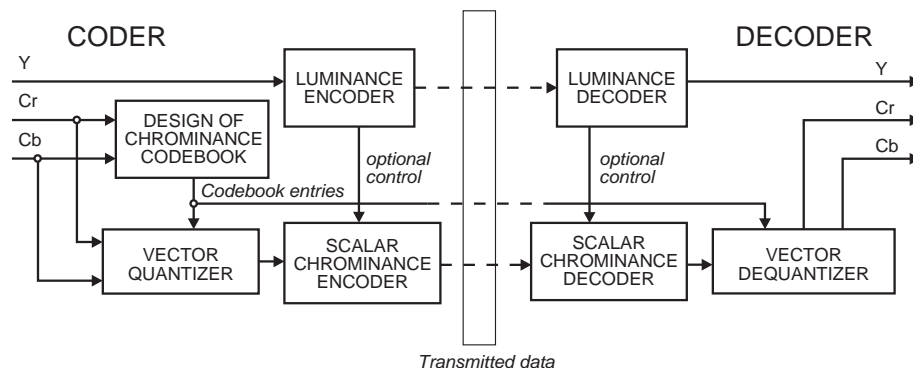


Figure 4.1: General color image compression scheme based on chrominance vector quantization.

A color image resulting from such transformation is represented by two numerical values instead of three: its original luminance value and a scalar value resulting from transformation 4.1, which will be further referred to as *scalar chrominance*. These two components can be compressed (cf Fig. 4.1) either separately or jointly, exploiting their mutual correlation in the later case.

Reconstruction of the output image after decoding of the luminance and the scalar chrominance involves vector dequantization. For this purpose, the codebook entries have to be transmitted (or stored). As the scalar chrominance value may be reconstructed with some error due to lossy compression, the reconstructed color image is distorted. The aim is to keep the total distortion of the whole system (*i.e.* the accumulated distortion of vector quantization and lossy compression) as low as possible.

In order to achieve a reasonable efficiency of the above described system, three practical problems have to be solved here, which will be addressed in next three sections:

1. An appropriate vector quantizer has to be designed, *i.e.* there must be determined a codebook and a quantization principle which result in quantization errors being acceptably low by small number of codebook elements.
2. An appropriate mapping of the codebook elements to the space of scalar values must be determined, which is equivalent to codebook ordering.
3. A compression method appropriate for the scalar chrominance signal must be developed.

## 4.3 Chrominance quantization algorithms.

### 4.3.1 Introduction.

For compression purposes, a codebook can be automatically designed, similarly as it is done by other vector quantization techniques. Numerous algorithms have been proposed to design codebooks in color spaces (as discussed in 3.5). Approaches based on iterative optimization, like the LBG algorithm or Equitz's PNN algorithm (both discussed in 3.5) suffer from high computational costs. However, for low number of codebook entries they do not offer substantially lower quantization error compared to hierarchical clustering (Wu, 1992; Huang and Harris, 1993; Chan and Ma, 1994; Pei and Cheng, 1995). Such techniques, especially based on binary splitting rule are proposed in application to chrominance vector quantization. The rationale behind the choice of splitting-based techniques is also that they usually

very well cope with a multi-modal distribution characteristic for chrominance data, *i.e.* they are able to robustly separate into different clusters those data vectors which belong to different centers of concentration in the multidimensional space.

### 4.3.2 Binary splitting algorithms.

A binary splitting algorithm is an iterative algorithm that attempts to minimize the error of vector quantization in the chrominance plane according to a strategy of a *maximum descent* (or *steepest descent*) class (Riskin and Gray, 1991; Chan and Ma, 1991). The codebook increases by one element at each iteration. Given the input signal statistics by the means of chrominance histogram, the chrominance plane is hierarchically partitioned into disjoint regions, and the data cluster contained in each region is represented by one codebook entry in the vector quantization process to follow. At each iteration, one cluster of the chrominance vectors is split and a respective codebook entry is replaced by two new entries representing the two new clusters (as shown in the Fig. 4.2).

The coordinates of these new entries are determined in such a way that minimizes

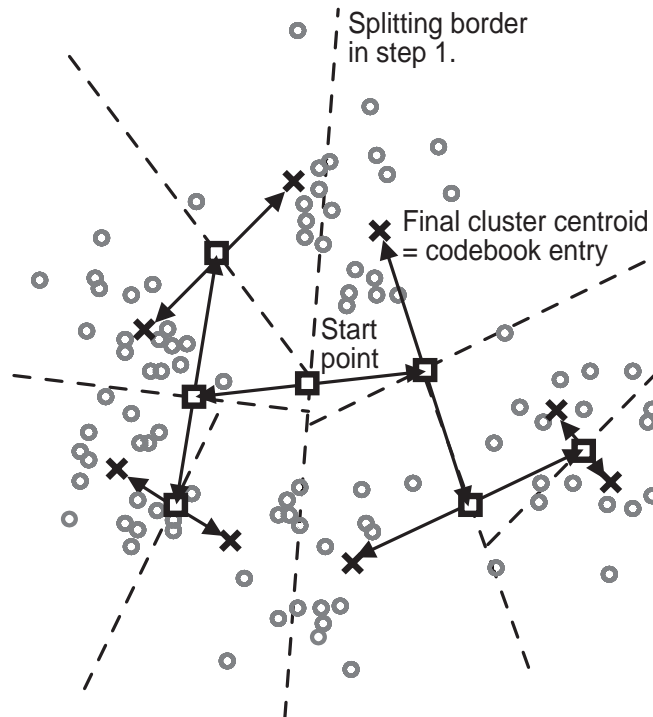


Figure 4.2: Codebook design by the binary splitting algorithm.

the quantization error of data within respective cluster. For example, minimum

squared error is minimized if the codebook entry is calculated as a centroid (an arithmetic average vector)  $\underline{\bar{X}}_i$  of the data cluster  $\mathbb{C}_i$ ,

$$\underline{\bar{X}}_i = \begin{bmatrix} \overline{C_{Bi}} \\ \overline{C_{Ri}} \end{bmatrix} = \frac{1}{|\mathbb{C}_i|} \sum_{\underline{X}_n \in \mathbb{C}_i} \underline{X}_n, \quad (4.2)$$

where  $|\mathbb{C}_i|$  denotes the number of vectors forming the cluster  $\mathbb{C}_i$ . Using the arithmetic average vector offers such important advantage that the mean error of the data cluster represented by this vector is zeroed. Consequently, no color shift is observed in the quantized image assuming perceptual uniformity of the color space used. At each step, the region related to the largest error of its representation is selected for splitting.

### 4.3.3 Classic solution based on principal component analysis.

Classic approach (Orchard and Bouman, 1991) is to split the region in question along a straight line passing through the centroid  $\underline{\bar{X}}_i$  at certain angle  $\varphi$  (shown in Fig. 4.3). The data cluster  $\mathbb{C}_i$  is split into the two new clusters (denoted as  $\mathbb{C}_{2i}$  and  $\mathbb{C}_{2i+1}$ ) according to the rule 4.3,

$$\begin{aligned} \mathbb{C}_{2i} &= \left\{ \underline{X}_n \in \mathbb{C}_i : (C_{Bn} - \overline{C_{Bi}}) \cos(\varphi) \leq (C_{Rn} - \overline{C_{Ri}}) \sin(\varphi) \right\}, \\ \mathbb{C}_{2i+1} &= \left\{ \underline{X}_n \in \mathbb{C}_i : (C_{Bn} - \overline{C_{Bi}}) \cos(\varphi) > (C_{Rn} - \overline{C_{Ri}}) \sin(\varphi) \right\}. \end{aligned} \quad (4.3)$$

Two new centroids  $\underline{\bar{X}}_{2i}$  and  $\underline{\bar{X}}_{2i+1}$  of the clusters  $\mathbb{C}_{2i}$  and  $\mathbb{C}_{2i+1}$ , calculated according to the rule 4.2, replace the centroid  $\underline{\bar{X}}_i$  in the codebook. The greedy strategy is to minimize the final quantization error as rapidly as possible by maximizing the gain  $\Delta E$  which results from the codebook increase by one element.

$$\Delta E = \sum_{\underline{X}_n \in \mathbb{C}_i} \|\underline{X}_n - \underline{\bar{X}}_i\|^2 - \left( \sum_{\underline{X}_n \in \mathbb{C}_{2i}} \|\underline{X}_n - \underline{\bar{X}}_{2i}\|^2 + \sum_{\underline{X}_n \in \mathbb{C}_{2i+1}} \|\underline{X}_n - \underline{\bar{X}}_{2i+1}\|^2 \right) \quad (4.4)$$

Figure 4.3 shows the value of  $\Delta E$  as a function of the angle  $\varphi$  for an example distribution of vectors. No explicit method has been invented so far to determine the optimal angle  $\varphi$  which maximizes the value of  $\Delta E$  for an arbitrary data distribution within the cluster. For large clusters of Gaussian distribution, *principal component analysis* (PCA) invented by Hotelling (1939) is proved to be optimal (Orchard and Bouman, 1991; Wu, 1992). In such case the optimum direction is determined as a direction of a line (represented by its normal vector  $\underline{M} = [\cos(\varphi) \quad \sin(\varphi)]^T$ ) such that the total squared error of the data projected onto this line is maximized:

$$\Delta E_{\text{pca}} = \sum_{\underline{X}_n \in \mathbb{C}_i} \left[ (\underline{X}_n - \underline{\bar{X}}_i)^T \cdot \underline{M} \right]^2, \quad (4.5)$$

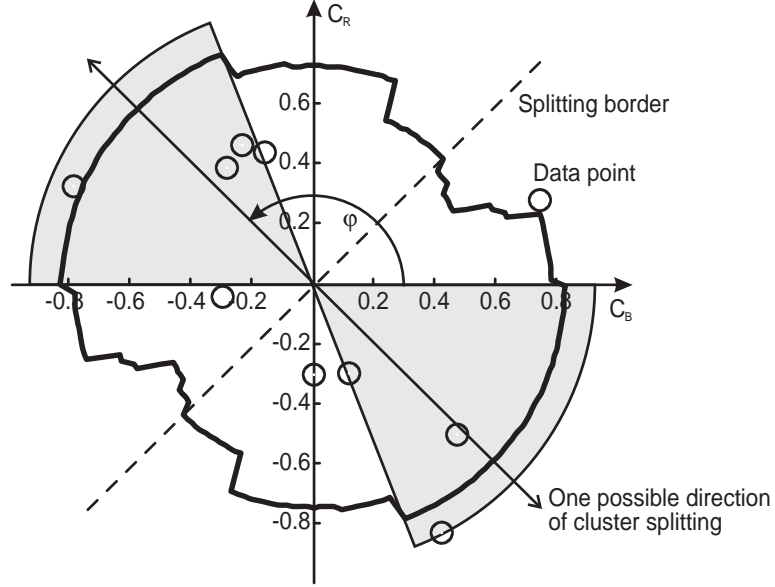


Figure 4.3: The value of gain  $\Delta E$  (solid thick line) determined empirically for the example set of data points shown, as a function of the angle  $\varphi$  at which the cluster is split. The grayed area covers the range of angles resulting with highest gain. The division border determined using PCA is shown as dashed line.

where  $T$  denotes vector transpose and  $\cdot$  is a scalar product. The formula of  $\Delta E_{\text{pca}}$  can be expressed as

$$\Delta E_{\text{pca}} = \underline{M}^T \cdot \tilde{\mathbf{R}}_i \cdot \underline{M} , \quad (4.6a)$$

where

$$\tilde{\mathbf{R}}_i = \sum_{\underline{X}_n \in \mathbb{C}_i} (\underline{X}_n - \bar{\underline{X}}_i) \cdot (\underline{X}_n - \bar{\underline{X}}_i)^T \quad (4.6b)$$

is the covariance matrix of the data in cluster  $\mathbb{C}_i$ . The solution is the eigenvector corresponding to the largest eigenvalue of  $\tilde{\mathbf{R}}_i$ . The respective characteristic equation

$$\det(\tilde{\mathbf{R}}_i - \lambda_i \cdot \mathbf{I}) = 0 , \quad (4.7)$$

expands hereby into second-order equation

$$\begin{aligned}
& \lambda_i^2 - \lambda_i \left[ \sum_{\underline{X}_n \in \mathbb{C}_i} (C_{Bn} - \overline{C_{Bi}})^2 + \sum_{\underline{X}_n \in \mathbb{C}_i} (C_{Rn} - \overline{C_{Ri}})^2 \right] \\
& - \left[ \sum_{\underline{X}_n \in \mathbb{C}_i} (C_{Bn} - \overline{C_{Bi}})(C_{Rn} - \overline{C_{Ri}}) \right]^2 \\
& - \left[ \sum_{\underline{X}_n \in \mathbb{C}_i} (C_{Bn} - \overline{C_{Bi}})^2 \right] \left[ \sum_{\underline{X}_n \in \mathbb{C}_i} (C_{Rn} - \overline{C_{Ri}})^2 \right] = 0 .
\end{aligned} \tag{4.8}$$

The principal vector corresponds to the larger of the two eigenvalues,  $\lambda_1$  and  $\lambda_2$ . It is necessary to numerically solve the above equation in order to determine these values. The necessary calculations require 3  $|\mathbb{C}_i|$  multiplications and 2  $|\mathbb{C}_i|$  summations, where  $|\mathbb{C}_i|$  denotes the number of vectors forming the cluster  $\mathbb{C}_i$ .

#### 4.3.4 An alternative method for determination the maximum of $\Delta E_{\text{pca}}$ .

A compact alternative formula allowing for calculation of the direction of splitting in a two-dimensional case which results in maximum of  $\Delta E_{\text{pca}}$  has been derived by the author. Since equation 4.5 can be expressed as

$$\Delta E_{\text{pca}} = \sum_{\underline{X}_n \in \mathbb{C}_i} \|\underline{X}_n - \overline{X}_i\|^2 \cos^2(\alpha_n) , \tag{4.9}$$

it is easy to determine the direction of splitting (represented by the angle  $\varphi$ ) as such that maximizes the above function. Here, we use a cluster-centered relative chrominance vector  $\underline{X}'_n = \underline{X}_n - \overline{X}_i$  with its components further referred to as  $C'_{Bn}$  and  $C'_{Rn}$ .  $\|\underline{X}'_n\| \cos(\alpha_n)$  is a distance between this vector and its projection onto the splitting border being searched (cf Fig. 4.4).

Let  $\arg \{\underline{X}'_n\} = \arctan(C'_{Rn}/C'_{Bn})$  be an angle between the chrominance vector  $\underline{X}'_n$  and the  $\overrightarrow{OC'_B}$  axis. Then

$$\|\underline{X}'_n\| \sin(\arg \{\underline{X}'_n\}) = C'_{Rn} , \quad \|\underline{X}'_n\| \cos(\arg \{\underline{X}'_n\}) = C'_{Bn} . \tag{4.10a}$$

Now, in order to determine the optimal direction  $\varphi$ , we rearrange:

$$\begin{aligned}
\Delta E_{\text{pca}}(\varphi) &= \sum_{\underline{X}_n \in \mathbb{C}_i} \|\underline{X}'_n\|^2 \cos^2(\arg \{\underline{X}'_n\} - \varphi) = \\
&= \frac{1}{2} \sum_{\underline{X}_n \in \mathbb{C}_i} \|\underline{X}'_n\|^2 + \frac{1}{2} \sum_{\underline{X}_n \in \mathbb{C}_i} \|\underline{X}'_n\|^2 \cos(2 \arg \{\underline{X}'_n\} - 2\varphi) .
\end{aligned} \tag{4.10b}$$

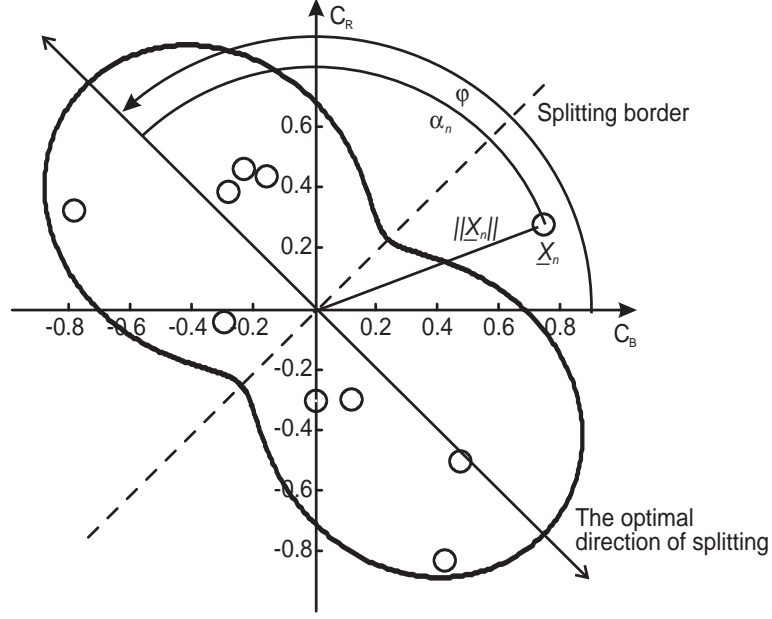


Figure 4.4: The value of  $\Delta E$  (solid thick line) determined according to formula 4.9 and plotted in polar coordinates as a function of the angle of splitting.

We notice, that  $\frac{1}{2} \sum_{\underline{X}_n \in \mathbb{C}_i} \|\underline{X}'_n\|^2$  is constant.

Moreover, since  $\cos(x-y) = \cos(x)\cos(y) + \sin(x)\sin(y)$  and  $\cos(2x) = \cos^2(x) - \sin^2(x)$ , and  $\sin(2x) = 2\sin(x)\cos(x)$  we can expand the second term:

$$\begin{aligned}
& \sum_{\underline{X}_n \in \mathbb{C}_i} \|\underline{X}'_n\|^2 \cos(2 \arg \{\underline{X}'_n\} - 2\varphi) = \\
& = \cos(2\varphi) \sum_{\underline{X}_n \in \mathbb{C}_i} \|\underline{X}'_n\|^2 \cos(2 \arg \{\underline{X}'_n\}) + \\
& + \sin(2\varphi) \sum_{\underline{X}_n \in \mathbb{C}_i} \|\underline{X}'_n\|^2 \sin(2 \arg \{\underline{X}'_n\}) = \\
& = \cos(2\varphi) \sum_{\underline{X}_n \in \mathbb{C}_i} \|\underline{X}'_n\|^2 \left[ \cos^2(\arg \{\underline{X}'_n\}) - \sin^2(\arg \{\underline{X}'_n\}) \right] + \\
& + 2 \sin(2\varphi) \sum_{\underline{X}_n \in \mathbb{C}_i} \|\underline{X}'_n\|^2 \cos(\arg \{\underline{X}'_n\}) \sin(\arg \{\underline{X}'_n\}) = \\
& = \cos(2\varphi) \sum_{\underline{X}_n \in \mathbb{C}_i} (C'_{Bn}{}^2 - C'_{Rn}{}^2) + 2 \sin(2\varphi) \sum_{\underline{X}_n \in \mathbb{C}_i} C'_{Bn} C'_{Rn}
\end{aligned} \tag{4.10c}$$

The expression obtained in 4.10c is a simple function of the variable  $\varphi$ , whose maximum is reached at

$$\varphi_{\text{pca}} = \arg \max_{\varphi} \Delta E_{\text{pca}} = \frac{1}{2} \arctan \left( \frac{2 \sum_{\underline{x}_n \in \mathbb{C}_i} C'_{Bn} C'_{Rn}}{\sum_{\underline{x}_n \in \mathbb{C}_i} C'^2_{Bn} - \sum_{\underline{x}_n \in \mathbb{C}_i} C'^2_{Rn}} \right). \quad (4.11)$$

The equivalence of the solution 4.8 and 4.11 is related to equivalence of 4.5 and 4.9. The experimental results confirm also that the resulting splits are identical. Similarly to 4.8 the proposed above formula requires only 3  $|\mathbb{C}_i|$  multiplications and 2  $|\mathbb{C}_i|$  summations.

### 4.3.5 Improvements of the PCA–based splitting.

In case of non–Gaussian data distribution (*e.g.* for real scene images) the PCA scenario is not optimal. First of all, as stated in 4.3.3, the optimum criterion 4.5 is valid only for large clusters of Gaussian data distribution, *i.e.* for such data clusters which exhibit high symmetry in the data space. Otherwise, a disadvantageous distribution of the data vectors leads to the optimal splitting direction being badly missed, as shown in Fig. 4.5. Moreover, since the two new clusters ( $\mathbb{C}_{2i}$  and  $\mathbb{C}_{2i+1}$ ) may not contain equal number of data vectors, their centroids ( $\overline{\underline{x}}_{2i}$  and  $\overline{\underline{x}}_{2i+1}$ ) do not necessarily lie in equal distance to  $\overline{\underline{x}}_i$ . Consequently, the position of the splitting border obtained from PCA does not minimize the mean squared error.

In fact, the optimal position of the splitting border should be normal to the interval joining the points  $\overline{\underline{x}}_{2i \text{ opt}}$  and  $\overline{\underline{x}}_{2i+1 \text{ opt}}$  which are the centroids of optimal clusters being searched,  $\mathbb{C}_{2i \text{ opt}}$  and  $\mathbb{C}_{2i+1 \text{ opt}}$ , respectively. As these centroids are determined implicitly by the position of the optimal splitting border, it is difficult to solve the above dependence.

Braquelaire and Brun (1997) prove that the optimal position of the splitting border lies between the centroid  $\overline{\underline{x}}_i$  and the median–cut point defined by the condition  $|\mathbb{C}_{2i}| = |\mathbb{C}_{2i+1}|$ . This optimum can be found by an exhaustive search within the above range.

A simpler solution proposed by the author is to deduce the optimal position of the splitting border. By calculating the angle  $\varphi_{\text{act}}$  of a straight line passing through

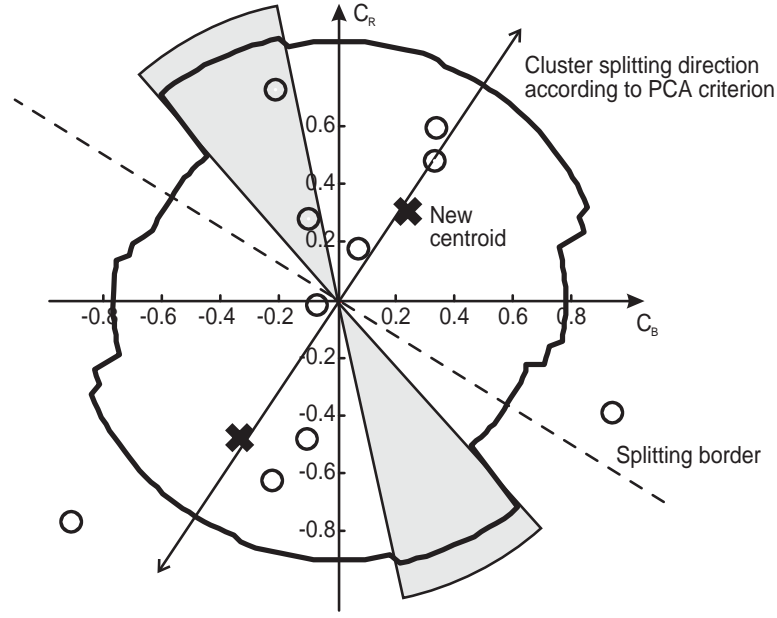


Figure 4.5: An example of splitting direction derived from principal component analysis which does not result in maximum splitting gain,  $\Delta E_{\text{gre}}$ . Here, the grayed area shows the range of optimal splitting directions.

$\bar{\underline{X}}_{2i}$  and  $\bar{\underline{X}}_{2i+1}$ ,

$$\varphi_{\text{act}} = \arctan \frac{\sum_{\underline{X}_n \in \mathbb{C}_{2i}} C'_{Rn} - \sum_{\underline{X}_n \in \mathbb{C}_{2i+1}} C'_{Rn}}{\sum_{\underline{X}_n \in \mathbb{C}_{2i}} C'_{Bn} - \sum_{\underline{X}_n \in \mathbb{C}_{2i+1}} C'_{Bn}}, \quad (4.12)$$

the inaccuracy in determining the  $\varphi_{\text{opt}}$  may be estimated as the difference between the splitting angle  $\varphi_{\text{pca}}$  and  $\varphi_{\text{act}}$ . Moreover, the asymmetry of cluster splitting which results from unequal number of data vectors classified to  $\mathbb{C}_{2i}$  and  $\mathbb{C}_{2i+1}$  may be expressed as

$$\begin{aligned} \|\Delta \bar{\underline{X}}_i\| &= \frac{1}{|\mathbb{C}_{2i}|} \sum_{\underline{X}_n \in \mathbb{C}_{2i}} \left| (\underline{X}_n - \bar{\underline{X}}_i)^T \cdot \underline{M} \right| - \frac{1}{|\mathbb{C}_{2i+1}|} \sum_{\underline{X}_n \in \mathbb{C}_{2i+1}} \left| (\underline{X}_n - \bar{\underline{X}}_i)^T \cdot \underline{M} \right| \\ &= \frac{1}{|\mathbb{C}_{2i}|} \sum_{\underline{X}_n \in \mathbb{C}_{2i}} |C'_{Bn} \cos(\varphi) + C'_{Rn} \sin(\varphi)| \\ &\quad - \frac{1}{|\mathbb{C}_{2i+1}|} \sum_{\underline{X}_n \in \mathbb{C}_{2i+1}} |C'_{Bn} \cos(\varphi) + C'_{Rn} \sin(\varphi)|. \end{aligned} \quad (4.13)$$

The two above values detect, how much obtained splitting differs from such splitting that fulfills the nearest neighbor quantization rule. The latter guarantees minimum value of mean squared error (Gersho and Gray, 1992). Experimental results show that for sufficiently large clusters (as in case of designing codebooks for natural scene images) it is possible to determine the optimal position of the splitting border by iterative rotation and shifting its initial position obtained from PCA by the respective above values followed by subsequent recalculation of the clusters  $C_{2i}$  and  $C_{2i+1}$ . In fact, this procedure is equivalent to iterative repositioning of the splitting border in such a way to be normal to the current interval joining points  $\bar{X}_{2i}$  and  $\bar{X}_{2i+1}$ . Figure 4.6 illustrates one step of such optimization which can be also thought of

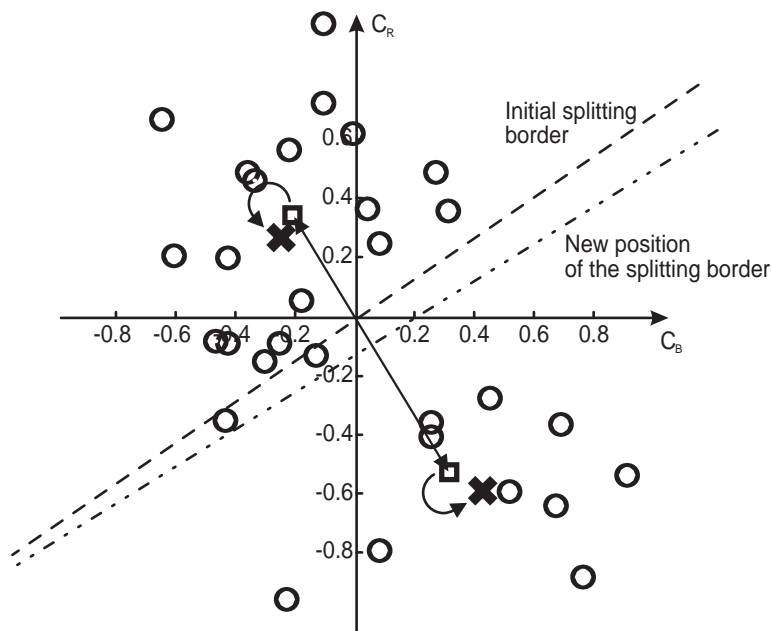


Figure 4.6: An example of splitting improvement by repositioning of the initial splitting border (dashed line). Due to different classification of the data vectors, the centroids of initial clusters (denoted as “ $\square$ ”) are shifted to new positions (denoted as “ $\times$ ”).

as an alternatively formulated two-means LBG algorithm. The main advantage of such formulation over LBG is its lower computational cost related to solving a linear equation for each data vector as opposed to comparing two squared differences between each vector and the centroids of both clusters.

### 4.3.6 Simulations.

The performance of the algorithm based on binary splitting is tested experimentally. In order to avoid the necessity of performing the tests on a very large pool of images, artificially generated random data sets are used. These sets are drawn from multimodal distribution in order to mimic the distribution of chrominance data in natural images, as concluded in section 2.5.1.

For the purpose of these simulations it is assumed that the data distribution within the image exhibits  $K$  centers of local concentration. Each pixel belongs to one of  $K$  objects in the scene. As the objects are not colored uniformly, the color of each pixel is a result of random variation with variance  $\sigma_2$  around the local mean  $\underline{\mu}_k$ . The conditional probability density function of the pixel color  $\underline{X}$  is given as

$$f_{\underline{X}}(\underline{x}|\underline{\mu}) = \frac{1}{\sigma_2\sqrt{2\pi}} e^{-\frac{\|\underline{x}-\underline{\mu}\|^2}{2\sigma_2^2}}, \quad (4.14)$$

and  $\underline{\mu}$  is a random vector with a discrete probability distribution:

$$P\left\{\underline{\mu} = \underline{\mu}_k, \quad k = 1 \dots K\right\} = \frac{e^{-\frac{\|\underline{\mu}_k\|^2}{2\sigma_1^2}}}{\sum_{k=1}^K e^{-\frac{\|\underline{\mu}_k\|^2}{2\sigma_1^2}}}. \quad (4.15)$$

The use of distribution models based on Gaussian distribution is motivated by the difficulty to determine the real general nature of data distribution in natural images, given the variety of forms and objects present in such scenes. On the other hand, the observation of histograms of test natural images suggests an appropriateness of such model. Furthermore, as shall be demonstrated, the results of simulations using artificial data sets are very similar to those obtained from experiments with real images.

The artificially generated random data samples drawn from the distribution 4.14 (cf Fig. 4.7) are used as the input data of the codebook design algorithm based on binary splitting. The mean squared error has been determined as a function of number of codebook entries. Each experiment uses a data set consisting of  $N = 1000$  data vectors and is repeated 10 times. The obtained plots are therefore averaged over 10 curves each. Two series of simulations are performed in order to demonstrate, how the quantization error depends on the basic properties of the multimodal distribution, namely how much the data vector values are concentrated around local means, which is reflected by the  $\sigma_2/\sigma_1$  ratio, and, what is the number of those means,  $K$ .

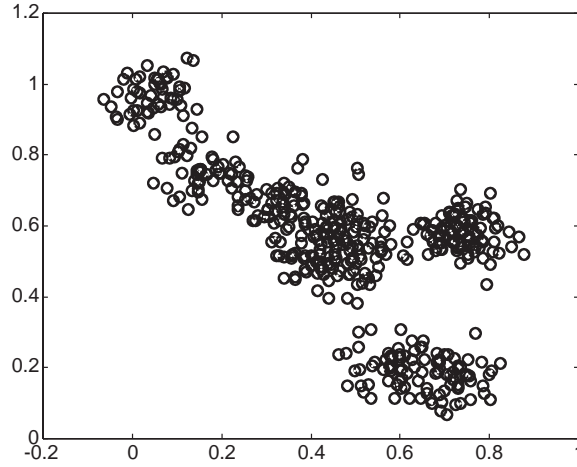


Figure 4.7: An example of data sample of multimodal Gaussian distribution. Here,  $K = 5$ ,  $\sigma_1 = 1.0$ ,  $\sigma_2 = 0.05$ .

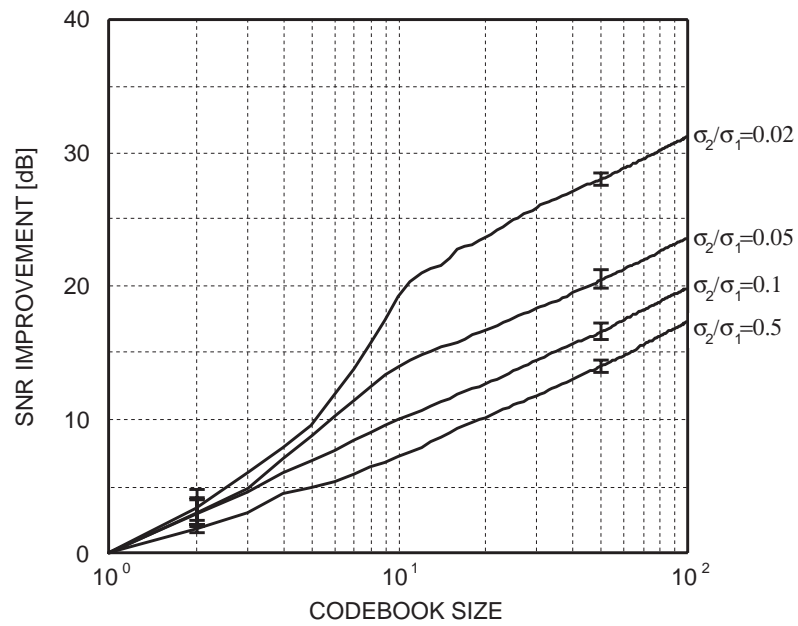


Figure 4.8: Relative improvement of the quality of quantized data set as a function of growing the number of codebook entries for data sets of multimodal Gaussian distribution with  $K = 10$  means and varying  $\sigma_2/\sigma_1$  ratio.

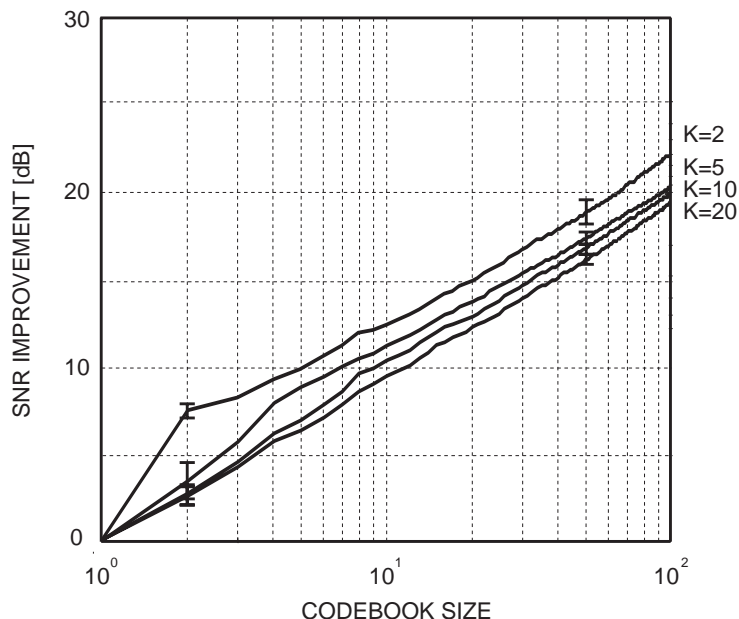


Figure 4.9: Relative improvement of the quality of quantized data set as a function of growing the number of codebook entries for data sets of multimodal Gaussian distribution with  $\sigma_2/\sigma_1$  ratio of 0.1 and varying number of local means,  $K$ .

The mean squared errors decreases continuously with growing number of codebook entries. This constant decrease in loglog scale suggests there is an approximately exponential relation between the quantization error and the number of representative vectors in the codebook which is a property observed for scalar quantizers (Gersho and Gray, 1992) and which weakly supports claims of near optimality of the vector quantizer based on binary splitting rule.

Two characteristic phases can be observed in the graphs plotted. The speed of error decrease is higher at the beginning, as long as the number of codebook entries is smaller than the number of distinct regions of data concentration in the chrominance plane (this figure corresponds to the number of local means as long as the regions mostly do not overlap). For highly concentrated distributions (very low  $\sigma_2/\sigma_1$  ratio) a breakpoint can be observed on the SNR curves. This breakpoint shows the moment in the curve, where data clusters are separated by the codebook design algorithm, *i.e.* each cluster is assigned one codebook entry. Further increase of the codebook size reduces the error less rapidly.

Simulation have also been performed in order to examine the importance of border replacement stage as an improvement of splitting after each step of the PCA

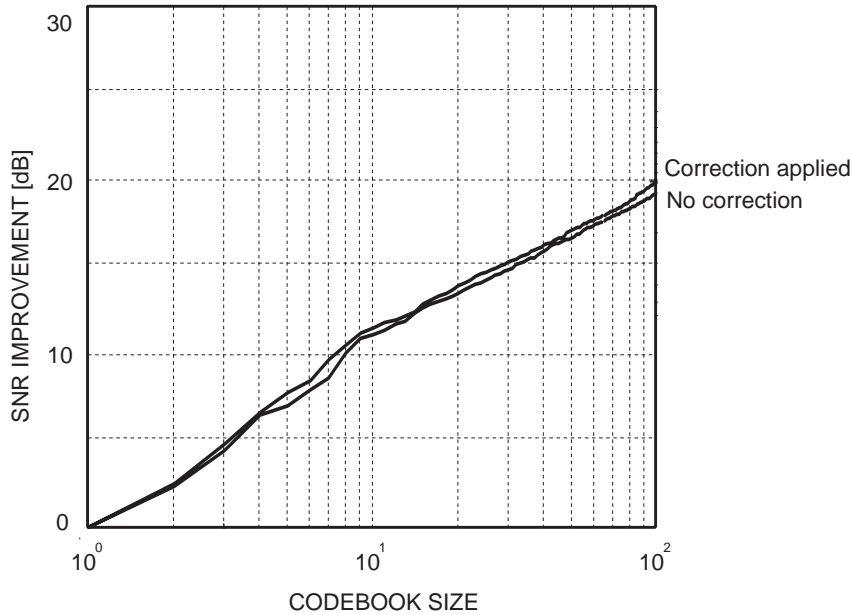


Figure 4.10: An example experiment showing the relative improvement of the quality of quantized data set after repositioning of the splitting border in each step of the binary split algorithm. Here,  $K = 10$  and  $\sigma_2/\sigma_1 = 0.1$ .

binary split algorithm. Comparison of the plots presented in Fig. 4.10 leads to a conclusion that the improvement of SNR is considerable albeit not radical. Therefore for time-constrained applications this stage may be abandoned.

### 4.3.7 Experimental results.

The results of experiments with natural images and videophone sequences (Bartkowiak and Domański, 1996b, 1999a) acknowledge, that application of the algorithm based on the binary splitting principle to chrominance vector quantization results in quantized images of high quality (cf Fig. 4.11 and Fig. 4.12) even for very low number of codebook elements. Careful analysis of the plots presented here reveals that a slight breakpoint in the PSNR curve, similar to one observed in abstract simulations (Figs 4.8 and 4.9) is characteristic also for natural images. The location of this breakpoint (usually between 10 and 30 codebook entries) suggests the number of distinct regions of color concentration, and consequently it suggests a good choice of the codebook size. As seen in the Tables 4.11 and 4.2, these figures very well coincide with high subjective evaluation of resulting quantized images (compare also Photos 9–14).

Quantized images exhibit subtle impairments, mostly within details of scarce

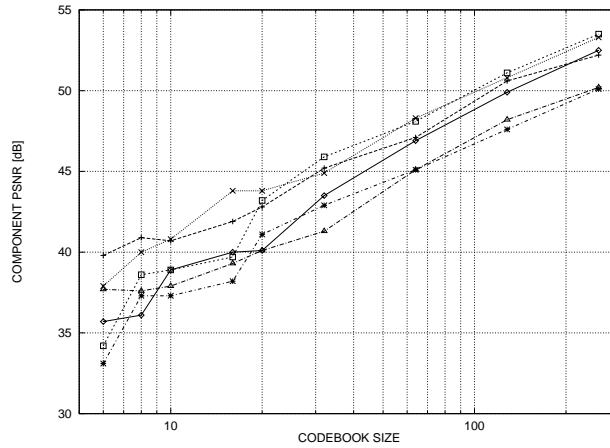


Figure 4.11: Objective quality measure (PSNR for  $C_R$ ,  $C_B$  components) versus the codebook size for test images CLAIRE, SALESMAN, and MISSA in CIF format.

and highly saturated colors (particularly visible in Photos 11–14). This quality deterioration (compare respective subjective assessments in Tables 4.1 and 4.2) is fully acceptable considering the compression achieved through quantization.

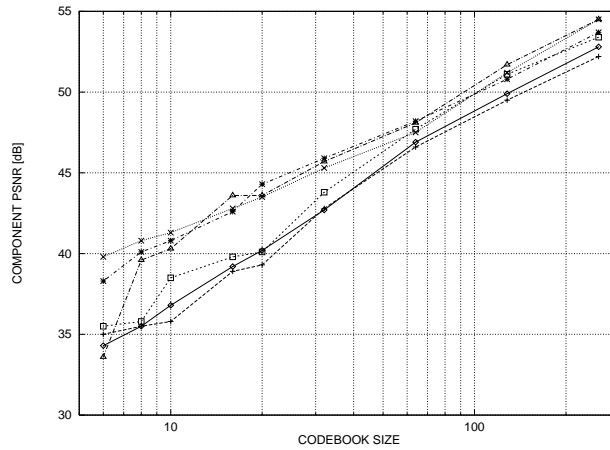


Figure 4.12: Objective quality measure (PSNR for  $C_R$ ,  $C_B$  components) versus the codebook size for test images CLAIRE, SALESMAN and AKIYO in QCIF format.

Table 4.1: Subjective evaluation of test images in CIF resolution with quantized chrominance: mean opinion score of 6 expert subjects (scale 1–5).

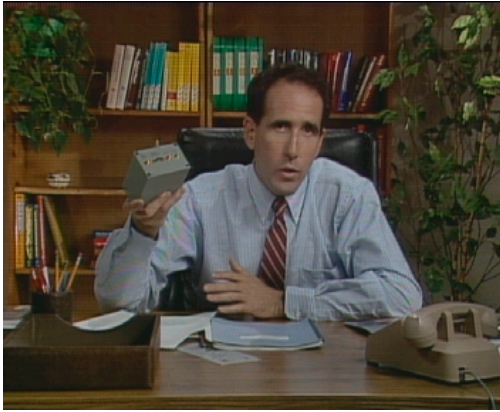
Codebook size	CLAIRE	SALESMAN	MISSA
256	5	5	5
128	5	5	5
64	5	5	5
32	5	4.5	5
20	4.5	4.5	4.5
16	4.5	4.5	4
10	4	4	4
8	4	3.5	3.5
6	4	3	3

Table 4.2: Subjective evaluation of test images in QCIF resolution with quantized chrominance: mean opinion score of 6 expert subjects.

Codebook size	CLAIRE	SALESMAN	MISSA
256	5	5	5
128	5	5	5
64	5	5	5
32	4.5	4.5	4
20	4.5	4	4
16	4	4	3.5
10	3.5	3.5	3.5
8	3	3.5	3
6	2.5	2.5	2.5

The observed results are dependent not only on the color content of the images being quantized (the “colorfulness”, or the number of distinct colors present in the scene as well as the volume spanned in the color space by those colors). For images representing the same scene at different spatial resolutions it may be easily demonstrated that the color gamut shrinks as the resolution decreases which is a phenomenon related to averaging properties of the lowpass filtering necessary before proper image downsampling. As averaging of several colors of neighboring pixels results in an intermediate value, the result is often biased towards “mean color”. This process explains the impression of lower saturation and lower contrast observed in low resolution images.

## Color Plate 2: Vector Quantization of Chrominance



**Photo 7 and 8:** Original first frames drawn from the standard videophone sequences: SALESMAN (CIF resolution) (left) and AKIYO (QCIF resolution) (right).

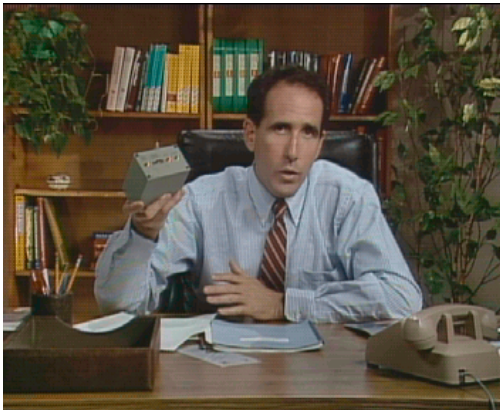


**Photo 9 and 10:** Vector quantized chrominance to 32 chrominance pairs



**Photo 11 and 12:** Vector quantized chrominance to 16 chrominance pairs.



**Photo 13 and 14:** Vector quantized chrominance to 8 chrominance pairs.

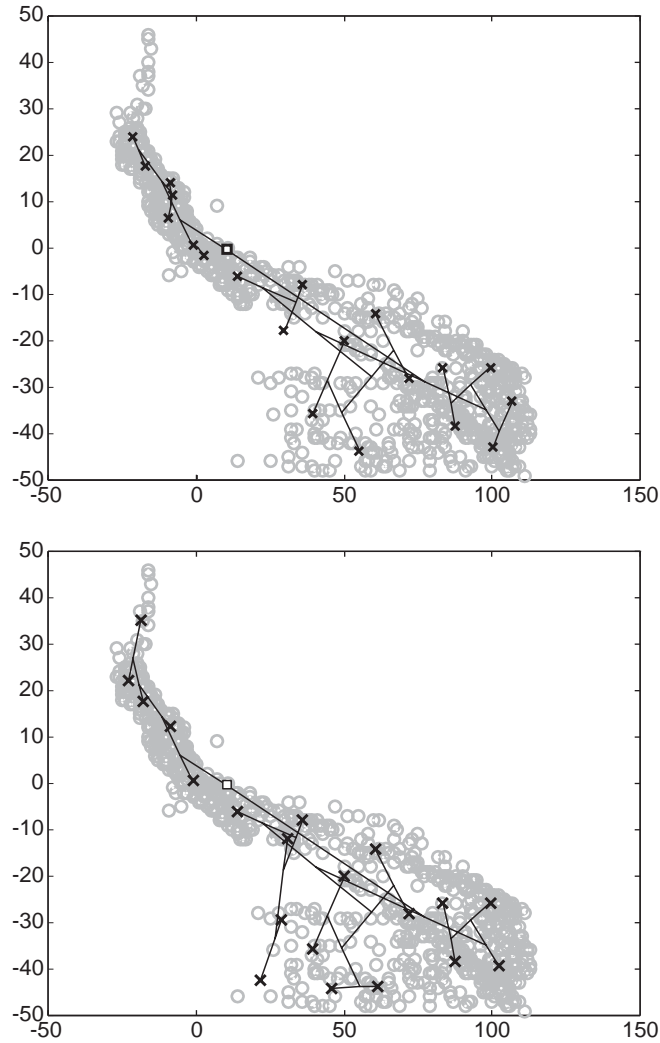


Figure 4.13: Tree structured codebook design process shown on the background of chrominance data of test image AKIYO. Application of different error criteria: upper plot - total squared error calculated over all pixels, lower plot - total squared error calculated over all distinct chrominance vectors.

As discussed in section 4.3.2, the binary splitting technique subsequently partitions the chrominance plane according to a greedy rule. In other words, chrominance sets representing pixels with largest quantization error are splitted in first order to obtain finer quantization of these pixels which results in possibly greatest decrease of the global error. Here, the term *quantization error* may be referred to as a total squared error calculated over all pixels in the image or over all colors presented in the image (in the latter case, pixels of identical chrominance are counted only once for the data clusters being formed). Both approaches result in slightly different codebooks and quantized images (compare Fig. 4.13 and Photos 11 and 12 vs Photos

15 and 16), since the second approach slightly favors less frequent colors. However first approach results in obviously lower PSNR rating, it is not evident which one should be chosen on the basis of visual comparison.

Application of alternative color spaces to vector quantization of chrominance has also been studied. Perceptual uniform spaces seem to be attractive here, since they offer a better correspondence between Euclidean distance and perceived color difference, as compared to  $YC_B C_R$  space. Consequently, a vector quantizer that minimizes the mean squared error in the chrominance plane of perceptually uniform space should produce quantized images of higher visual quality. Experiments show however, that application of  $L^*a^*b^*$  color space does not bring a significant improvement of the visual quality, yet the PSNR ratings of reconstructed  $C_B$  and  $C_R$  components are apparently lower. Therefore, regarding higher computational costs related to the additional color transformation, this approach has been abandoned.

For very low number of codebook entries quantization error manifests in form of false contours (banding) and vanishing details of scarce and highly saturated colors. Nevertheless, since images in CIF and especially QCIF resolution are very well representable with 20–30 codebook entries this range of codebook sizes has been chosen for lossy image compression at low and very low bit rates. The compression techniques described in next sections usually operate on such quantized images and video sequences.

## 4.4 Images of scalar chrominance and their properties.

The codebook obtained through the design process is a set of representative chrominance pairs. A unique number from the finite set  $\mathcal{S}$  labels each pair, and an order in the codebook entries is defined in this way. As a result of vector quantization, a respective label of codebook entry represents chrominance of each pixel in the output image. The signal formed of codebook indices constitutes the *scalar chrominance image* and will be denoted as

$$\mathbf{S} = [S_{i,j}]_{N_1 \times N_2} \text{ ,} \tag{4.16}$$

where  $N_1$  and  $N_2$  are the image dimensions.

The transformation of chrominance vectors into respective scalar chrominance values can be thought of as an instance of dimensionality reducing mapping, as defined in 4.1. Since each value of the scalar chrominance represents uniquely one

chrominance pair from the codebook, the color changes within the original image are reflected by corresponding changes in the scalar chrominance domain. The mapping defined by the codebook ordering,  $\Omega : \{\underline{X}_i\} \mapsto \{\$i\}$ , deeply influences the statistical and spectral properties of the scalar chrominance image. The latter are strongly dependent on the codebook size and the order its entries are sorted and labeled in. If the scalar chrominance image is intended for further processing, the codebook order should be optimized in order to retain those properties which are vital to this processing. For example, since most image compression techniques rely on high correlation between neighboring pixels, their efficiency is potentially decreased by high frequency artifacts which may be introduced into the scalar chrominance image within areas where its color counterpart is visually smooth.

For compression purposes, it is difficult to define a strict criterion of optimum

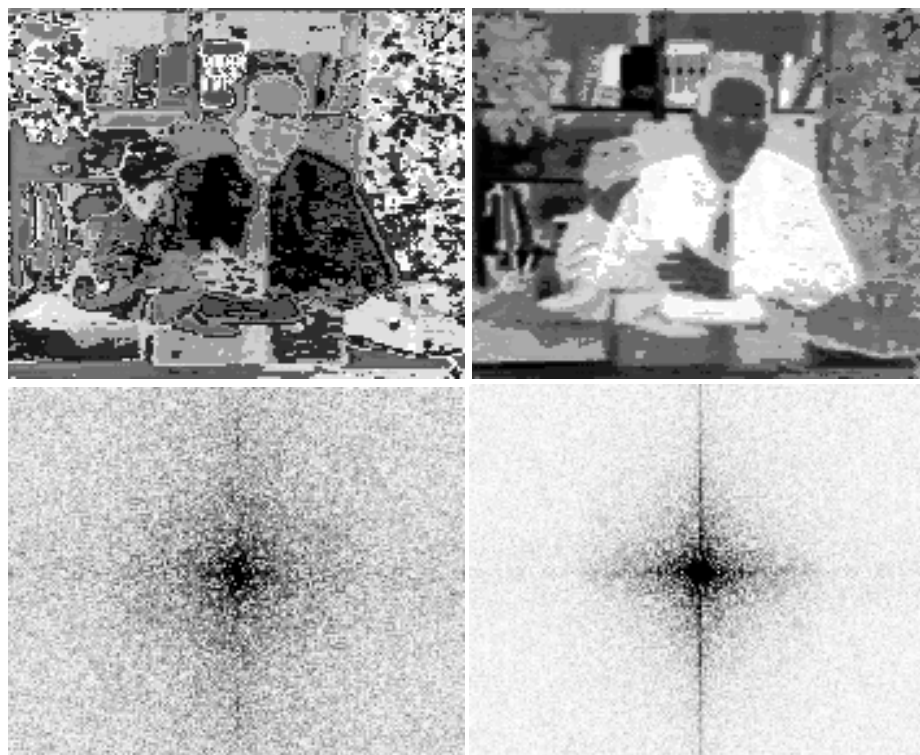


Figure 4.14: Scalar chrominance signal obtained with a codebook of size 30 for a test image SALESMAN (upper row) and its power spectra (below). Left column: codebook ordered randomly. Right column: codebook order optimized for signal smoothness.

codebook ordering. Here it is assumed, that the pixel values of scalar chrominance image are highly correlated with the adjacent pixels if consecutive labels in the codebook are assigned to chrominance pairs in such a way that most frequent changes occur between similar values. In practice, optimization algorithms can be employed

to minimize a cost function defined with the above statement in mind which corresponds to finding a shortest path in a weighted graph spanned over the codebook entries. The edges of the graph can be weighted either by the Euclidean distances between respective chrominance vectors in the chrominance plane, or by the frequency of co-occurrence of respective labels in the direct spatial neighborhood within the image.

The later strategy has been already proposed by Bartkowiak and Domański (1994) together with a simple suboptimum path searching algorithm which consists of combining closest pairs of graph vertices, and subsequently joining obtained segments into longer ones taking into account their accumulated length as long as all segments are joined. Codebook order obtained from this algorithm results in greatly increased first-order statistical relationships between neighboring pixels. Unfortunately, higher-order correlation cannot be optimized in the same way. Therefore, instead of relying on particular differences between scalar chrominance values of neighboring pixels, it is assumed that the original color image is visually smooth and this smoothness can be retained by assigning similar labels to codebook entries which are closest in the chrominance plane. A heuristic ordering postulated by the author (Bartkowiak, Domański and Gerken, 1997) aims at minimizing the total length of the chain of ordered codebook entries:

$$\Omega_{\text{opt}} = \min_{\Omega} \sum_{i=1}^{|\mathbb{S}|-1} \|\overline{X}_{S_i} - \overline{X}_{S_{i+1}}\| \quad (4.17)$$

Apart from simple application of a classic algorithm to solve the traveling salesperson problem (TSP) on a graph discussed above (as proposed by Zaccarin and Liu, 1991), an approach that exploits the structuring and ordering properties of the binary split algorithm is proposed here. The ordering procedure is performed hierarchically during the codebook design process and is defined inductively:

- Before each step of the binary split algorithm the gradually growing codebook is assumed to be already ordered (which is trivial for the first and the second step, when codebook consists only of one and two entries, respectively).

$$\overline{X}^{(k)} = \{\overline{X}_{S_1}, \overline{X}_{S_2}, \dots, \overline{X}_{S_i}, \dots, \overline{X}_{S_k}\} \quad (4.18a)$$

- Each replacement of the codebook entry  $\overline{X}_{S_i}$  with two new entries, denoted here as  $\overline{X}_{S'_i}$  and  $\overline{X}_{S''_i}$ , is associated with inserting these two new entries into the existing chain in the place of the old entry. One out of the two possible

cases that results in lower the total chain length is chosen:

$$\begin{aligned} \|\bar{\mathbf{X}}_{S_{i-1}} - \bar{\mathbf{X}}_{S'_i}\| + \|\bar{\mathbf{X}}_{S''_i} - \bar{\mathbf{X}}_{S_{i+1}}\| &< \|\bar{\mathbf{X}}_{S_{i-1}} - \bar{\mathbf{X}}_{S''_i}\| + \|\bar{\mathbf{X}}_{S'_i} - \bar{\mathbf{X}}_{S_{i+1}}\| \\ \implies \bar{\mathbf{X}}^{(k+1)} &= \{\bar{\mathbf{X}}_{S_1}, \dots, \bar{\mathbf{X}}_{S'_i}, \bar{\mathbf{X}}_{S''_i}, \dots, \bar{\mathbf{X}}_{S_k}\} \end{aligned}$$

or

$$\begin{aligned} \|\bar{\mathbf{X}}_{S_{i-1}} - \bar{\mathbf{X}}_{S'_i}\| + \|\bar{\mathbf{X}}_{S''_i} - \bar{\mathbf{X}}_{S_{i+1}}\| &> \|\bar{\mathbf{X}}_{S_{i-1}} - \bar{\mathbf{X}}_{S''_i}\| + \|\bar{\mathbf{X}}_{S'_i} - \bar{\mathbf{X}}_{S_{i+1}}\| \\ \implies \bar{\mathbf{X}}^{(k+1)} &= \{\bar{\mathbf{X}}_{S_1}, \dots, \bar{\mathbf{X}}_{S''_i}, \bar{\mathbf{X}}_{S'_i}, \dots, \bar{\mathbf{X}}_{S_k}\} \end{aligned}$$

(4.18b)

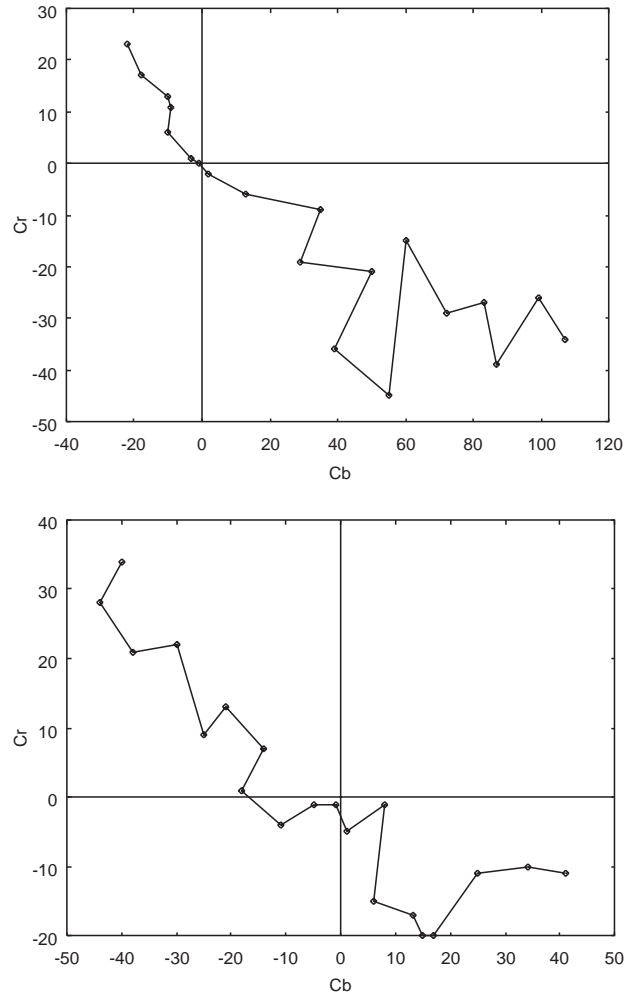


Figure 4.15: Chrominance codebooks designed and simultaneously ordered for test images in QCIF format: AKIYO (upper plot) and CLAIRE (lower plot).

Figure 4.15 shows example orders obtained for typical images.

As shown in Fig. 4.14, proposed ordering of the codebook entries leads to very smooth the image of scalar chrominance. The bandwidth is also narrower.

## 4.5 Lossless compression of the scalar chrominance.

### 4.5.1 Introduction.

As a result of vector quantization of the chrominance components of an image, their already low entropy is reduced even further, which is naturally reflected by low entropy of the corresponding scalar chrominance.



Figure 4.16: The chrominance of two test images: CLAIRE (upper row) and SALESMAN (lower row) obtained from vector quantization using codebooks of 16 entries (left side) and 32 entries (right side). Here, borders between constant-valued areas have been artificially enhanced.

Thanks to reduced number of levels (equal to the number of chrominance codebook entries) as well as to low bandwidth of the original chrominance the obtained

image of scalar chrominance consists of numerous “flat” areas of constant value with sharp discontinuities between them (cf. Fig. 4.16). Signals with such morphological properties are particularly well suitable for efficient differential coding, where at each point the actual signal value is estimated on the basis of its already transmitted neighbors and only the difference between the estimate and the actual value is transmitted. In case of an image with flat areas of a constant value the probability of a zero-valued difference is very high. Therefore the variable length code (for example the Huffman code) applied here benefits from this nonuniform distribution of transmitted values. For images with low number of levels (as in case of scalar chrominance), application of first-order prediction (*i.e.* prediction based on one neighboring pixel) has an advantage over higher-order predictors such that it generally increases the probability of zero-valued prediction error and simultaneously decreases the entropy of the prediction error.



Figure 4.17: The luminance component versus the scalar chrominance (30 codebook entries) of the test image CLAIRE.

As discussed in section 2.5.3, in natural scene images the significant changes in chrominance and luminance are highly correlated. Bartkowiak and Domański (1998a, 1998b) demonstrated, that similarly, in images with vector quantized chrominance, the locations of borders between regions of constant valued chrominance often correspond to locations of edges and object borders in the luminance component (cf. Fig. 4.17). This observations suggest that additional information extracted from the luminance component may be exploited to support efficient differential coding of scalar chrominance. For example, by utilizing the information about the edges in luminance, the scalar chrominance of arbitrary-shaped color regions may be encoded with most of the shape information being omitted.

## 4.5.2 Proposed compression scheme and its implementation.

In the proposed technique, a simple differential coding with first-order prediction has been applied to the scalar chrominance image. The operation of the predictor is controlled by the use of the luminance component, in order to exploit the mutual dependencies between luminance and scalar chrominance. An arbitrary lossy or lossless compression scheme is applied for luminance coding. Scalar chrominance encoder and decoder both use the same reconstructed luminance signal (Fig. 4.18). Edge detectors are employed as the luminance activity estimators in order to

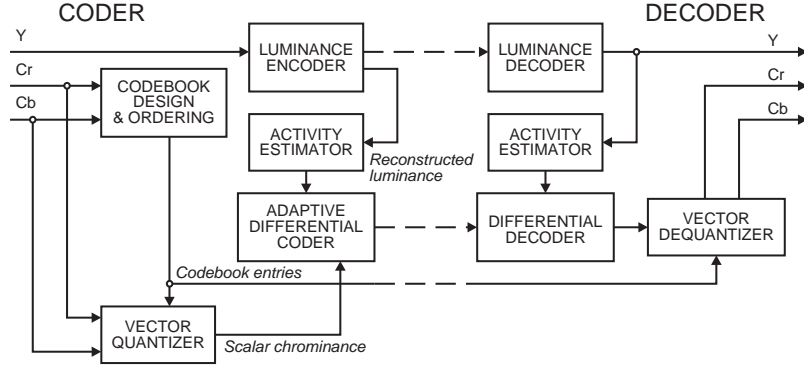


Figure 4.18: The proposed compression scheme using differential coding of scalar chrominance and exploiting the mutual correlation between scalar chrominance and luminance.

identify locations, where significant luminance changes are encountered. Since this activity map is determined on the basis of the reconstructed luminance image, it is also available at the decoder side without any need of additional information to be transmitted. Separate estimation of vertical and horizontal luminance activity allows to select the best prediction direction, *i.e.* the direction in which neighboring scalar chrominance label has most likely identical value.

The image is analyzed line by line. Apart from the border pixels, the actual value of the scalar chrominance  $S_{i,j}$  is estimated using a value of one of the neighboring points  $S_{i-1,j}$  and  $S_{i,j-1}$  (cf Fig 4.19). The direction is chosen by comparing two luminance activity measures,  $\nabla_i Y_{i,j}$  and  $\nabla_j Y_{i,j}$ ,

$$\hat{S}_{i,j} = \begin{cases} S_{i,j-1} & \text{if } |\nabla_i Y_{i,j}| > |\nabla_j Y_{i,j}| \quad \text{and} \quad |\nabla_i Y_{i,j}| > \text{threshold} \\ S_{i-1,j} & \text{if } |\nabla_i Y_{i,j}| < |\nabla_j Y_{i,j}| \quad \text{and} \quad |\nabla_j Y_{i,j}| > \text{threshold} \end{cases}, \quad (4.19)$$

where the values  $\nabla_i Y_{i,j}$  and  $\nabla_j Y_{i,j}$  express the discrete estimate of the horizontal and vertical gradient in reconstructed luminance. In the simplest case and equal spatial resolution of luminance and scalar chrominance, these may be defined as

$$\begin{aligned} \nabla_i Y_{i,j} &= Y_{i,j} - Y_{i-1,j} \\ \nabla_j Y_{i,j} &= Y_{i,j} - Y_{i,j-1}. \end{aligned} \quad (4.20)$$

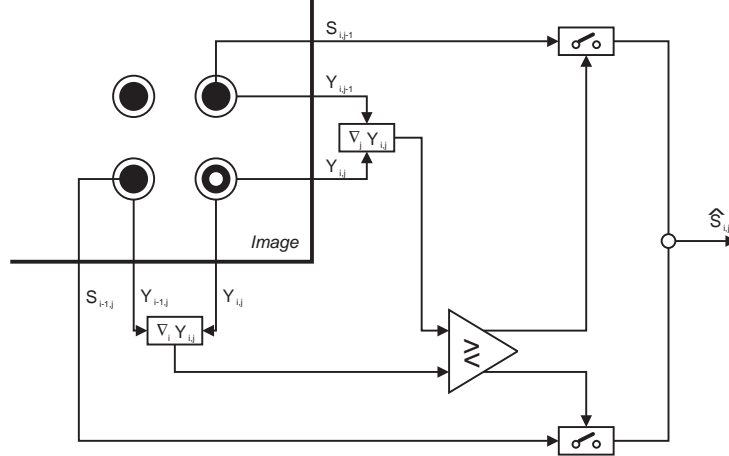


Figure 4.19: An implementation of the scalar chrominance prediction scheme controlled by luminance. Here, “○” denotes a reconstructed luminance sample, “●” denotes a scalar chrominance sample already encoded and “○” denotes the current scalar chrominance sample to be encoded.

In the case of identical values of  $\nabla_i Y_{i,j}$  and  $\nabla_j Y_{i,j}$  the chosen direction depends on the comparison of previously transmitted neighboring scalar chrominance values,  $S_{i-1,j-1}$ ,  $S_{i-1,j}$  and  $S_{i,j-1}$  :

$$\hat{S}_{i,j} = \begin{cases} S_{i,j-1} & \text{if } |S_{i,j-1} - S_{i-1,j-1}| > |S_{i-1,j} - S_{i-1,j-1}| \\ S_{i-1,j} & \text{if } |S_{i,j-1} - S_{i-1,j-1}| \leq |S_{i-1,j} - S_{i-1,j-1}| \end{cases}, \quad (4.21)$$

The prediction error  $\Delta S_{i,j} = \hat{S}_{i,j} - S_{i,j}$  is encoded using Huffman codes and transmitted to the decoder. Additional information must be transmitted in case of  $\nabla_i Y_{i,j} < \text{threshold}$  and  $\nabla_j Y_{i,j} < \text{threshold}$ , and  $\Delta S_{i,j} \neq 0$ . The latter corresponds to a situation where the scalar chrominance change is not associated with a change of luminance that is significant enough to be detected by the activity estimators (cf 4.3). Nothing is transmitted at location  $(i, j)$  if  $\nabla_i Y_{i,j} < \text{threshold}$  and  $\nabla_j Y_{i,j} < \text{threshold}$ , and  $\Delta S_{i,j} = 0$ . Therefore, unnecessary transmission of zero-valued  $\Delta S_{i,j}$  is avoided. The codebook entries are losslessly encoded and transmitted as a side information.

### 4.5.3 Experimental results.

The above described lossless compression scheme for scalar chrominance has been tested experimentally (Bartkowiak and Domański, 1998b, 1998c, 1998d) using a standard H.263 codec operating in intraframe mode as a luminance codec as well as the reference system for performance comparison. The luminance component of the interframe coded image is decoded either at the encoder and the decoder side and its horizontal and vertical activity is estimated, similarly as discussed in 4.5.2



Figure 4.20: An example of experimental results for the test image AKIYO (20 codebook entries). Upper row: scalar chrominance image (left), magnitude of the prediction error  $\Delta S_{i,j}$  (right). Lower row: Luminance activity map (left) and locations of non-zero values of  $\Delta S_{i,j}$  while luminance activity has not been detected (right).

(taking into account the different spatial resolution of luminance and chrominance components) with the value of *threshold* optimized manually.

The results of such experiments reveal that the number of locations with non-zero prediction error heavily depends on the image complexity. Moreover, it is very important to set properly the value of *threshold* in the condition 4.19, in order to minimize the number of locations, where  $\nabla_i Y_{i,j} < \textit{threshold}$  and  $\nabla_j Y_{i,j} < \textit{threshold}$  and  $\Delta S_{i,j} = 0$ , and on the other hand, to minimize the probability of unnecessary transmission of zero-valued prediction errors.

The statistical properties of the prediction error allow a very efficient encoding using appropriately designed Huffman codes (cf. Fig. 4.21).

A comparison of the obtained results with the results obtained from a standard H.263 codec (cf Table4.4) shows that similar PSNR ratings are achieved at similar bit

### Color Plate 3: Standard codec artifacts



**Photo 15 and 16:** Application of an alternative error criterion to vector quantization (16 chrominance pairs) - total squared error calculated over all distinct chrominance vectors. Cf Photo 11 and 12.



**Photo 17 and 18:** H.263 intraframe mode coding artifacts: SALESMAN (2246 bits allocated to chrominance, PSNR  $C_B$ =38.1 dB, PSNR  $C_R$ =38.7 dB) and AKIYO (3951 bits allocated to chrominance, PSNR  $C_B$ =37.3 dB, PSNR  $C_R$ =39.2 dB).



**Photo 19 and 20:** H.263 interframe coding artifacts: SALESMAN (18 b/average frame, PSNR  $C_B$ =37.5 dB, PSNR  $C_R$ =37.2 dB) and AKIYO, frame 83 (20 b/avg. fr., PSNR  $C_B$ =36.4 dB, PSNR  $C_R$ =38.9 dB)



**Photo 21 and 22:** Frames reconstructed after smoothing of scalar chrominance using median filter.

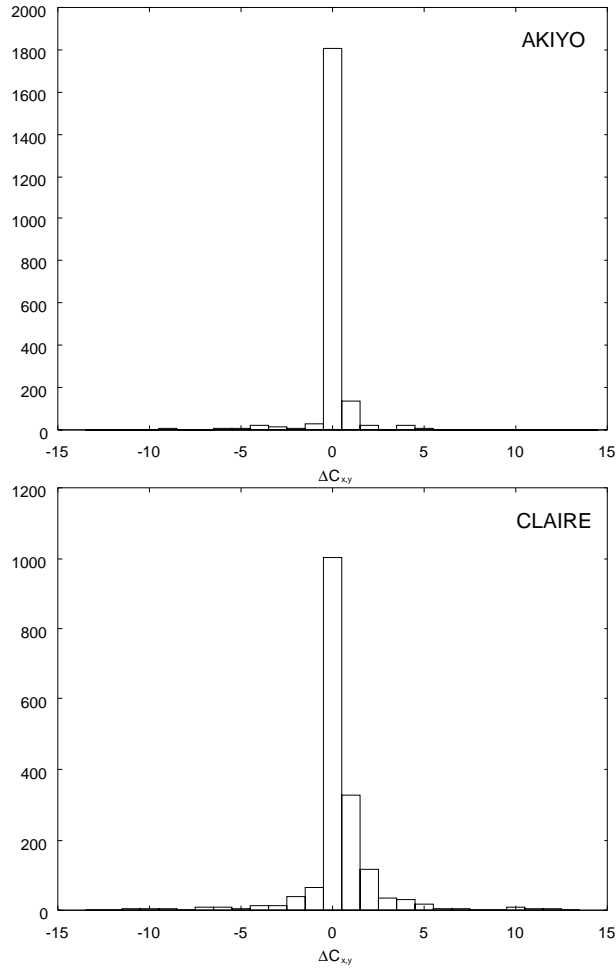


Figure 4.21: The histograms of the transmitted prediction errors  $\Delta S_{i,j}$  for test images AKIYO (upper plot) and CLAIRE (lower plot).

rates. It is important to stress the different visual appearance of the errors produced by the H.263 transform codec as compared to the vector quantization artifacts, which are the only errors introduced here by the proposed compression scheme, due to the lossless compression applied to scalar chrominance. H.263 artifacts (cf Photo 17 and 18) are concentrated spatially and manifest themselves as unnatural coloration of some image portions. These false colors are particularly annoying at the image portions representing human skin. On the other hand, in order to achieve very low bit rate in the scheme proposed, the codebooks applied here have to be significantly small, which is reflected by visible banding.

Table 4.3: Exemplary statistics obtained for standard test images in CIF format.

Test image	CLAIRE	AKIYO	AKIYO
Number of codebook entries	30	30	20
Number of zero-valued prediction errors	1002	1607	1809
Number of non-zero valued prediction errors	914	1160	480
Number of locations, where chrominance changes, but no luminance change has been detected	438	663	185

Table 4.4: Experimental comparison of the proposed scheme (denoted as CVQ) with standard H.263 codec operating in intraframe mode.

Test image	CLAIRE	CLAIRE	AKIYO	AKIYO
Compression method	H.263	CVQ	H.263	CVQ
Total number of bits for chrominance in one frame	3107	about 4500	4038	about 5500
PSNR for $C_B$ [dB]	37.2	38.4	37.4	35.0
PSNR for $C_R$ [dB]	39.9	43.3	39.5	40.3

## 4.6 Lossy compression of images with vector quantized chrominance.

### 4.6.1 Introduction.

The experiments with lossless coding show that it is possible to achieve reasonable compression of color images represented by scalar chrominance even using a very simple scheme.

In general, any lossy compression technique developed primarily for monochrome images may be adopted here for scalar chrominance coding, provided the transformation  $\mathcal{S}$  (related to vector quantization and mapping to the set of labels) does not destroy those properties of the original image, the coding technique relies on. Further considerations are focused on transform-based techniques which have been commonly employed in image and video coding standards.

Transform-based coding exploits first-order and higher-order correlation between spatially neighboring pixels. Particularly shaped quantization tables determine the importance of lowest frequency components in the signal spectrum. The

spectral properties of the scalar chrominance signal, even with properly ordered codebook, are different than typical properties of the chrominance components of natural images. In particular, its wider bandwidth results from sharp discontinuities between constant-valued areas apparent in Fig. 4.16. This property suggests potential decrease of coding efficiency as compared to natural images, which has been acknowledged experimentally (Bartkowiak and Domański, 1997). Therefore two modifications of the whole coding system have been proposed in order to increase the compression efficiency:

- In order to obtain the scalar chrominance smoother, a finer quantization is needed. To achieve this without increasing the codebook which would require transmitting more side information bits and would also involve codebook ordering being more difficult a task, a codebook interpolation is performed. For this purpose, the extreme labels,  $S_1$  and  $S_k$  are assigned values from much wider a range than  $\langle 1 \dots k \rangle$ . Moreover, the set of labels  $\{S_i\}$  is chosen in such a way, that the difference of each consecutive pair of labels  $|S_i - S_{i+1}|$  corresponds to the distance in the chrominance plane between respective codebook entries,  $\|\overline{X}_{S_i} - \overline{X}_{S_{i+1}}\|$ . Additional codebook entries are generated according to some arbitrary rule. For example, using linear interpolation involves simple generation of additional entries distributed along straight lines drawn in the chrominance plane between neighboring entries of the initial codebook (cf Fig. 4.22). This rule is known at the the decoder side, therefore there is no need to transmit the information about the interpolated entries.

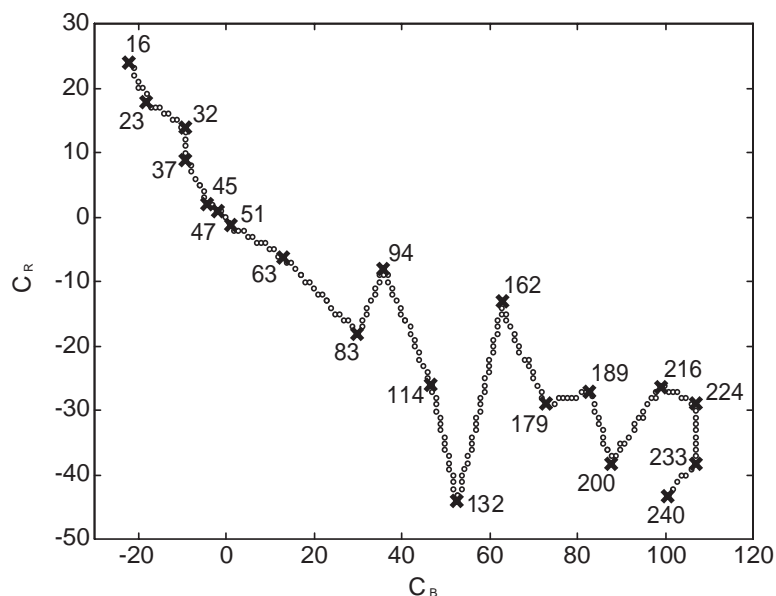


Figure 4.22: Initial codebook obtained for a test image AKIYO ( $\times$ ) with the assigned label values shown, and the codebook resulted from insertion of interpolated entries ( $\circ$ ).

- The scalar chrominance obtained by vector quantization with interpolated codebook contains a significant amount of high-frequency impulses resulting from the strong nonlinearity of the transformation  $S$ . Often, slight change in the color of neighboring image pixels corresponds to significant jump within the chain of ordered codebook entries. Because these impulses correspond to unimportant details which are exaggerated by nonlinear mapping, they can be smoothed out without introducing visible degradation (cf Fig. 4.23). A two-dimensional median filter is applied here due to its ability to remove distinct impulses from smooth signals without blurring edges.

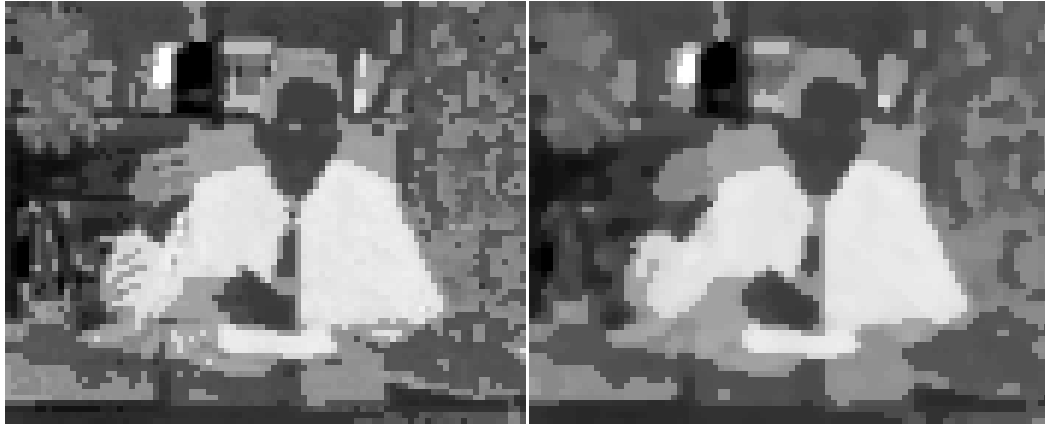


Figure 4.23: Application of median filter for smoothing of scalar chrominance for test image SALESMAN: scalar chrominance obtained with interpolated codebook of 30 entries (left plot) and the same signal after median filtering (right plot). Full color images reconstructed from smoothed scalar chrominance are shown in Photos 21 and 22.

As a result of lossy compression applied to the scalar chrominance, coding artifacts are observed in reconstructed color image. Similarly to many other compression schemes, transform coding can be modeled as adaptive lowpass filtering. Such process blurs the edges in the original image by changing the pixel values to some values intermediate between those on both sides of an edge. Unfortunately, a value of scalar chrominance which is intermediate between two other values may not correspond to an intermediate color. Moreover, it may be assigned to a chrominance pair very different from the intermediate one (cf Fig. 4.22). This phenomenon leads to very strong distortions, which while not apparent in the reconstructed scalar chrominance, become visible after vector dequantization. Since their genesis is similar to the impulses in scalar chrominance just discussed, median filtering is similarly applied to reduce these distortions. In practice, vector median filter (Astola *et al*, 1990) operating simultaneously on the three color components at the decoder side is able to take the maximum advantage of local smoothness of reconstructed luminance to support the efficient restoration of chrominance components corrupted by impulse

distortions (cf Photos 23 and 24).

#### 4.6.2 Application to existing image compression standard.

A modification of the standard JPEG technique (cf Fig. 4.24) has been proposed by Bartkowiak and Domański (1996a) by application of chrominance vector quantization together with the enhancements discussed above. As digital images are often represented using  $R'G'B'$  color space, a conversion to the  $YC_B C_R$  luminance–chrominance system which is required prior to the vector quantization of chrominance is usually implemented as a part of the typical JPEG–complaint software (IJG, 1995).

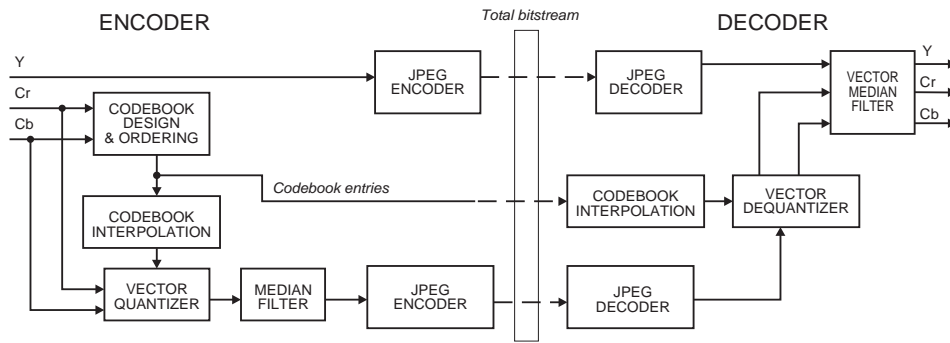


Figure 4.24: Modifications of the JPEG coding system by the use of chrominance vector quantization.

Depending on the image complexity, codebooks of 20–30 entries are applied at the chrominance vector quantization stage. Codebook entries are labeled using integer values from the range  $S_i \in \{S_{\min} = 16 \dots S_{\max} = 240\}$ , which is equal to the allowed dynamic range of digital chrominance signals (Poynton, 1996; IJG, 1995). Each intermediate integer value of the scalar chrominance corresponds to an entry in the chrominance codebook. A median filter with a square mask of the size  $3 \times 3$  is applied for scalar chrominance smoothing (cf Fig. 4.24). Similarly, a vector median filter with a square  $3 \times 3$  mask removes eventual distortions in reconstructed chrominance in the decoder.

While the luminance component of the color image is encoded by the standard JPEG coder with default quantization tables, as proposed in the ITU-T Recommendation (1992), the scalar chrominance signal requires careful matching of the quantization tables to respect its characteristic spectrum. The quantization scheme used in the experiments is expressed as

$$\forall_{m,n=0..7} L_{m,n} = \left\lceil \frac{C_{m,n}}{m+n+\text{offset}} \right\rceil, \quad (4.22)$$

where  $L_{m,n}$  denotes the value of quantized  $(m,n)$ -th DCT coefficient,  $C_{m,n}$ , and  $\lceil \cdot \rceil$  denotes rounding to the nearest integer towards zero. The parameter “offset” is optimized experimentally. Its value depends on the smoothness of the scalar chrominance image, which is also related to the perceived “colorfulness” of the original image.

Experimental results show that energy compaction for the scalar chrominance in the cosine transform domain is apparently not as big as for the original chrominance components, however for sufficiently high compression ratios the proposed modified JPEG codec produces reconstructed images with better quality both in the sense of PSNR (cf Fig. 4.25) and subjective quality (cf Photo 27).

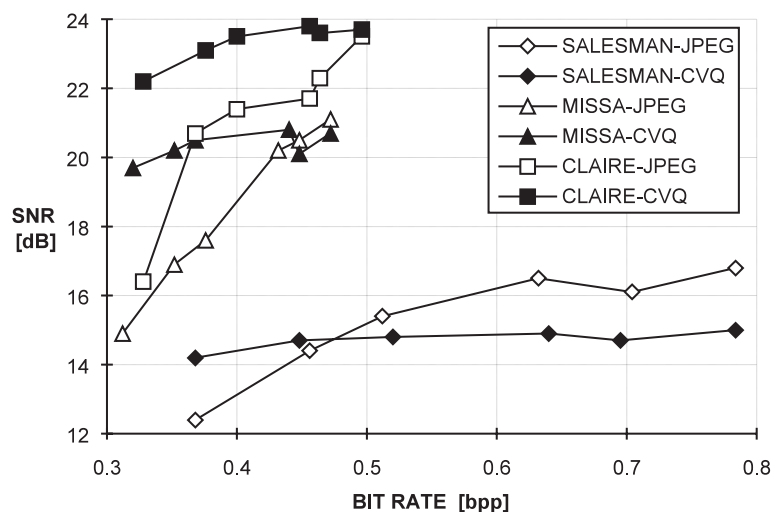


Figure 4.25: Experimental results for the test images in QCIF resolution.

The proposed chrominance coding scheme is more efficient as compared to standard JPEG, if the compression ratio exceeds some critical value. This value corresponds to significant breakdown in the JPEG performance, whereas coding based on scalar chrominance still offers reasonable quality. The location of the breakdown point depends on the contents of the image and its resolution - for QCIF images proposed codec offers higher PSNR values below 0.45 – 0.50 bpp, while for pictures with  $512 \times 512$  pixels this critical value falls even under 0.3 bpp.

Experiments confirm also, that application of vector median filter after vector dequantization brings a significant improvement both in the PSNR ratings (1–3dB gain) and the visual quality of reconstructed frames.

## Color Plate 4: Image Coding.



**Photo 23 and 24:** Example coding artifacts related to DCT blurring of scalar chrominance (cf Fig. 5.6). Reconstructed frame before (left) and after smoothing (right) by vector median filter.



**Photo 25 and 26:** Example coding artifacts resulting from DWT-related distortions of scalar chrominance (cf Fig. 5.6). Reconstructed frame before (left) and after smoothing (right) by vector median filter.



**Photo 27:** Application of chrominance vector quantization to JPEG coding: reconstructed image BOATS compressed to a bitstream of 0.36 bpp (14155 bits allocated to scalar chrominance). PSNR = 22.3 dB.

# Chapter 5

## Color video compression by the use of scalar chrominance.

### 5.1 Introduction.

In this chapter, the original techniques exploiting vector quantization of chrominance and compression of the image of scalar chrominance which have been developed in chapter 4 are extended to video sequences. The main focus here is compression for applications in very low bit rate coding. In low bit rate coding, intended for visual communications through telephone networks, motion compensated hybrid coding is commonly applied which is implemented in industrial standard codecs, namely H.261 (ITU-T, 1993b), and H.263 (ITU-T, 1996). Such component-wise codecs (cf Fig. 5.1) operate in switched *intraframe/interframe* mode, whereby *intra* frames are encoded similarly to block-based transform coding of static images, and *inter* frames are encoded differentially using motion compensated previous frame as the prediction reference.

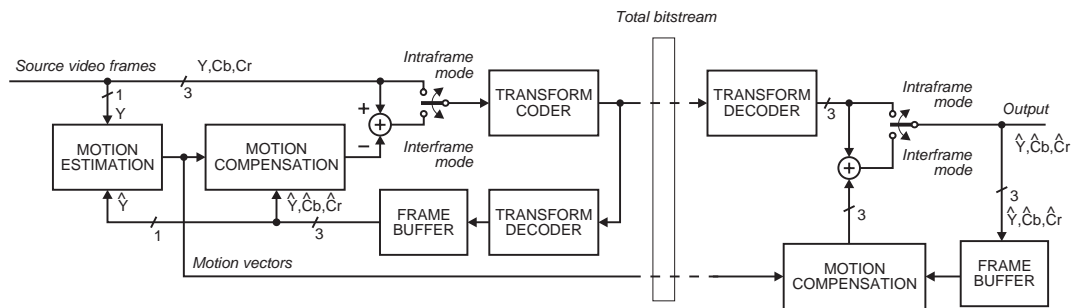


Figure 5.1: General structure of hybrid motion compensated transform coding and decoding.

High compression required for very low bit rate channels is usually achieved by processing of video sequences with spatio-temporal resolution being strongly reduced as well as by very lossy coding with most bits being allocated to the luminance component and much less to the chrominance components (Łuczak and Domański, 1998). As the luminance and both chrominance components are coded independently (*i.e.* independent scalar quantization is applied to the DCT coefficients of each component), allocation of a small number of bits to the chrominance results in poor quality of color in the reconstructed images.

Extension of the image coding techniques based on the concept of scalar chrominance processing to coding of video sequences based on hybrid motion compensated scheme requires several problems to be addressed:

- Color content in video scene changes from frame to frame. The adaptive chrominance vector quantization procedure needs to take these changes into account to ensure the quantization artifacts being acceptably small.
- Whereas the operation in *intraframe* mode involves direct lossy encoding of the image of scalar chrominance (typically by the use of transform coding) which has been covered in the section 4.6, the *interframe* mode involves motion compensation and encoding of the prediction error. These may be performed either in the domain of natural chrominance components (after dequantization of the scalar chrominance reconstructed from the frame just transmitted) or in scalar chrominance domain, in various combinations.

The main assumption here is not only to retain the basic structure of hybrid scheme shown in Fig. 5.1, but also to interfere into the existing structure of the existing standard codecs as little as possible. Therefore proposed technique has a form of some preprocessing of the video signal fed to the encoder and a respective postprocessing of the decoder output.

## 5.2 Chrominance vector quantization of video sequences.

Vector quantization of chrominance is applied to color video. Preliminary experiments (discussed in section 2.5.2) show, that it is not reasonable to design a new chrominance codebook for each frame. Changing the codebook from frame to frame would increase the probability of similarly colored pixels at the same spatial location being quantized to different chrominance representatives. The later corresponds to increased the differences between consecutive frames, which negatively impacts the efficiency of *interframe* mode. On the other hand, since the statistical distribution

of chrominance data in videophone sequences changes between consecutive frames only slightly (as shown in section 2.5.2), a codebook which has been designed for the first frame may be sustained through several frames. Only if there is a dramatic change in the scene content, design of a new codebook is necessary. Therefore in the

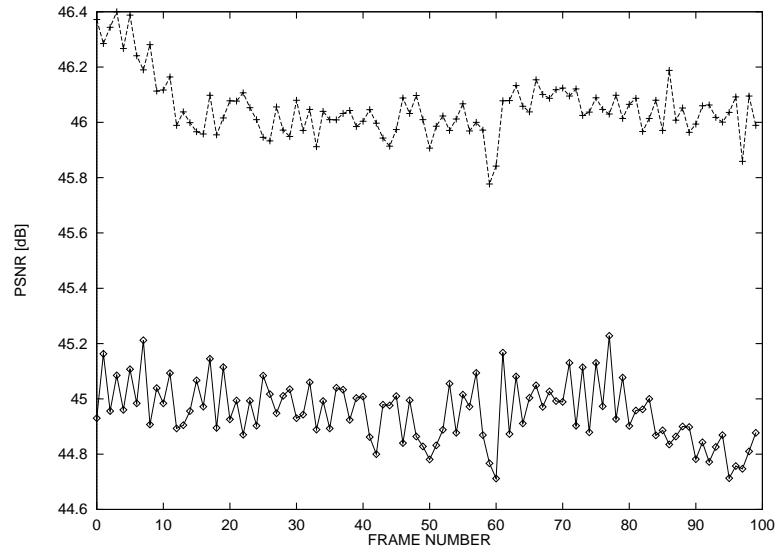


Figure 5.2: Quantization error of the chrominance components  $C_B$  ( $\diamond$ ) and  $C_R$  (+) for consecutive frames from the test sequence SALESMAN. Here, a constant chrominance codebook consisting of 30 entries which has been designed for the first frame is applied to the whole sequence.

approach proposed here and practically implemented, the chrominance codebook is determined for each *intraframe* encoded picture. It can be demonstrated (cf Fig 5.2), that even in case of video sequences of significant amount of motion the quantization error related to application of this codebook to following frames is almost constant.

## 5.3 Intraframe transform coding of scalar chrominance.

### 5.3.1 Introduction.

Typically, a frame entirely encoded in *intraframe* mode occurs very rarely in the bitstream produced by very low bit rate codecs. In practice, even streams of several hundreds of *interframe* encoded pictures are observable, since a switching to *interframe* mode for whole frame is performed only if a scene cut occurs. This is because the number of bits required for moderate quality *intra* frame is much higher than the number of bits needed in *interframe* mode.

Intraframe coding must be used at least for the so called *very first frame*, at the beginning of the session. As transmission of the *intra* frame requires a significant number of bits to be sent to the decoder, it is related to a serious delay in realtime applications. The requirements for high coding efficiency make *intraframe* mode the most demanding one. For example, H.263 very low bit rates coder operating with default quantization parameters allocates 150–200 bits to an average luminance macroblock and only 10–20 bits to a corresponding  $C_B$  or  $C_R$  block. By application of vector quantization of chrominance, the same 20–40 are available for an average block of scalar chrominance signal.

### 5.3.2 DCT-based coding.

A transform-based compression scheme of the scalar chrominance representation has been proposed for intraframe coding at very low bit rates. This scheme is very similar to image coding discussed in section 4.6. The encoding scheme involves codebook design, ordering and interpolation for each *intra* frame (cf Fig. 5.3).

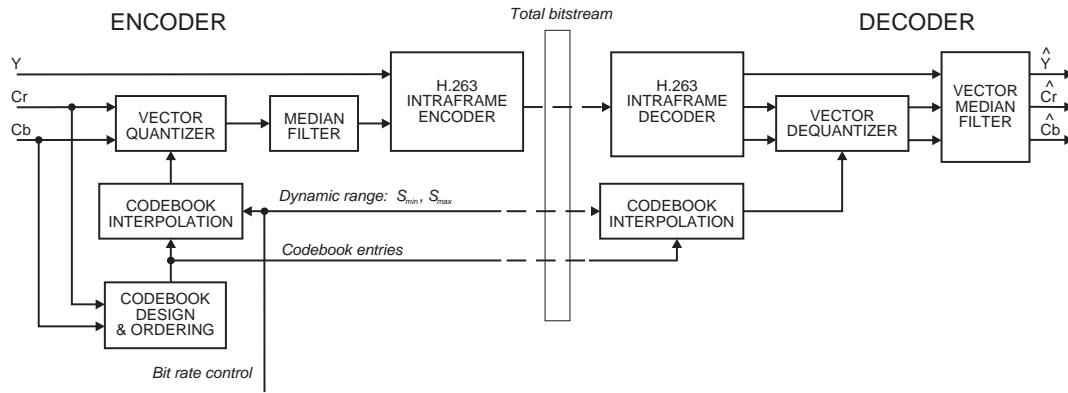


Figure 5.3: Proposed modification of the *intraframe* mode of the H.263 codec with chrominance vector quantization.

One of the most important difficulties in low bit rate coding is an effective way to control the bitstream (Łuczak and Domański, 1998). In order to achieve the target bit rate, standard codecs operating on the color video signal change the quantization factor  $QP$  in the formula 5.1 which affects quantization of all DCT coefficients, except the DC coefficient (H.263, 1997).

$$\forall_{\substack{m,n=0..7 \\ \text{except } m=n=0}} L_{m,n} = \lceil \frac{C_{m,n}}{2^{QP}} \rceil \quad (5.1)$$

Experiments (Bartkowiak and Domański, 1997a) show that due to wider the bandwidth of scalar chrominance signal its energy is spread over more DCT coefficients

which consequently exhibit lower values. Moreover, the trade-off between compression and quality is not straightforward in the scalar chrominance domain. In fact, application of the flat quantization tables as implemented by the standard H.263 codec results in very poor control of the bitstream, whereby the smallest increase of the quantization factor results in all DCT coefficients being zeroed.

In the proposed compression scheme, an alternative method has been applied to control the bitstream without affecting the quantization algorithm implemented in H.263 codec:

- The quantization factor of the H.263 codec operating on the scalar chrominance is set to a constant moderate value, *e.g.* the default value.

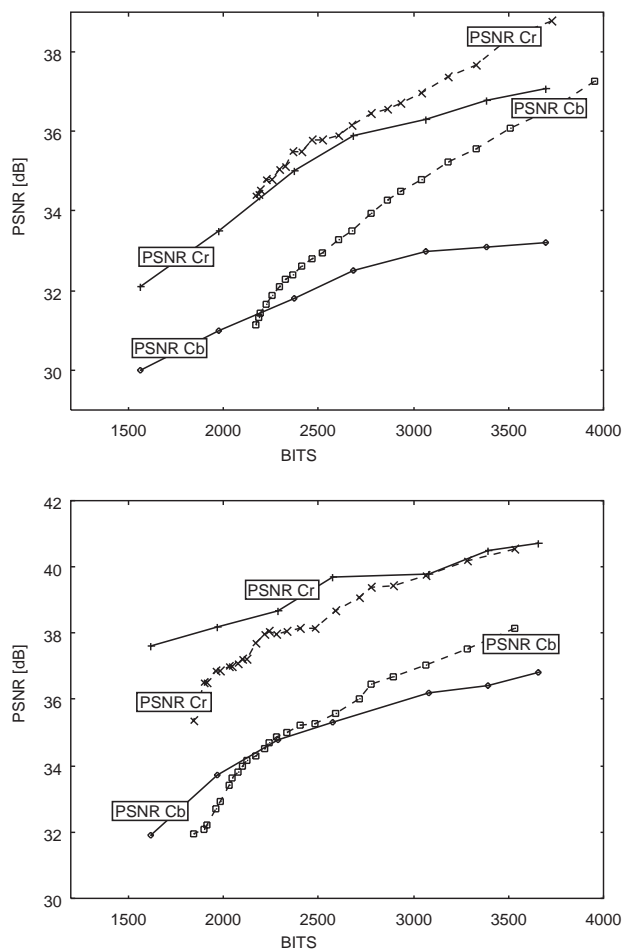


Figure 5.4: PSNR for the reconstructed chrominance components versus the total number of bits allocated to chrominance for the first frame from the test sequence CLAIRE (upper plot) and AKIYO (below). Dashed line: H.263 codec, solid line: DCT-based coding of scalar chrominance.

- The dynamic range of the scalar chrominance is controlled by changing the

extreme values  $S_{\min}$  and  $S_{\max}$  in the codebook interpolation in order to achieve desired compression ratio.

The proposed compression scheme has been tested experimentally (Bartkowiak, Domański and Gerken, 1997) using a codec compliant with the H.263 standard with default quantization factor, 20 codebook entries and dynamic range  $S_{\max} - S_{\min}$  varying from 20 to 200. For comparison purposes, the first frames from standard video sequences in QCIF format were compressed using H.263 operating on the scalar chrominance signal as well as on the  $YC_B C_R$  components. Presented plots (cf Fig. 5.4) show that the PSNR ratings achieved using chrominance vector quantization are similar (*i.e.* slightly better or slightly worse, depending on case) to these of the standard H.263 technique. In general, however, the proposed compression technique outperforms the H.263 standard in terms of PSNR values at extremely low bit rates.

The subjective evaluation of reconstructed frames (compare Photos 17 and 18 to Photos 28 and 29) leads to the conclusion that application of chrominance vector quantization to H.263 intraframe coding results in better visual quality. Particularly, the annoying color artifacts, like unnatural face coloration and abrupt hue variations in the background are visibly reduced. On the other hand, some decrease of the overall saturation may be observed, which is an artifact common in very low bit rate coding.

### 5.3.3 Coding based on discrete Walsh transform.

The immanent drawback of the compression schemes related to reducing high frequency spectral components (as in case of DCT-based coding) is the blurring phenomenon, which is very undesirable in scalar chrominance processing (as already discussed in section 4.6.1). In this section, an alternative orthogonal function basis is proposed for block-based transform coding scheme.

As discussed in sections 4.4 and 4.5.1, and shown in Fig. 4.16, the image of scalar chrominance obtained using relatively small codebook (*i.e.* codebook containing 20–30 chrominance pairs) consists of numerous irregular areas of constant value. It is well known (*e.g.* Clarke, 1985) that piecewise constant signals can be easily approximated by a small set of flat functions, as in case of Walsh functions, therefore two-dimensional discrete Walsh transform is proposed to be applied instead of DCT which is based on continuous cosine functions. Due to the character of Walsh functions, codebook interpolation is not required, since the compression relies on low complexity of the signal rather than its smoothness. Thanks to existing fast Walsh transform algorithm which does not require multiplications, the coding task is even less computationally intensive compared to DCT-based coding.

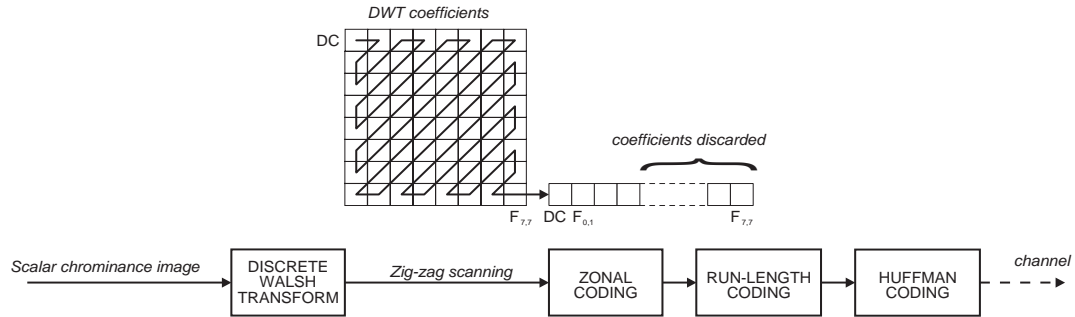


Figure 5.5: Scalar chrominance compression based on discrete Walsh transform and zonal coding.

Various quantization schemes may be applied to the blocks of DWT coefficients. For example, a scheme related to the concept of zonal coding (Clarke, 1985) is proposed. The DWT coefficients are linearly ordered using classic “zig-zag” scan. The lossy compression is achieved through discarding the transform coefficients related to highest sequences (the Walsh functions of highest order), as shown in Fig. 5.5. The number of coefficients being discarded is automatically controlled and depends on the target bit rate.

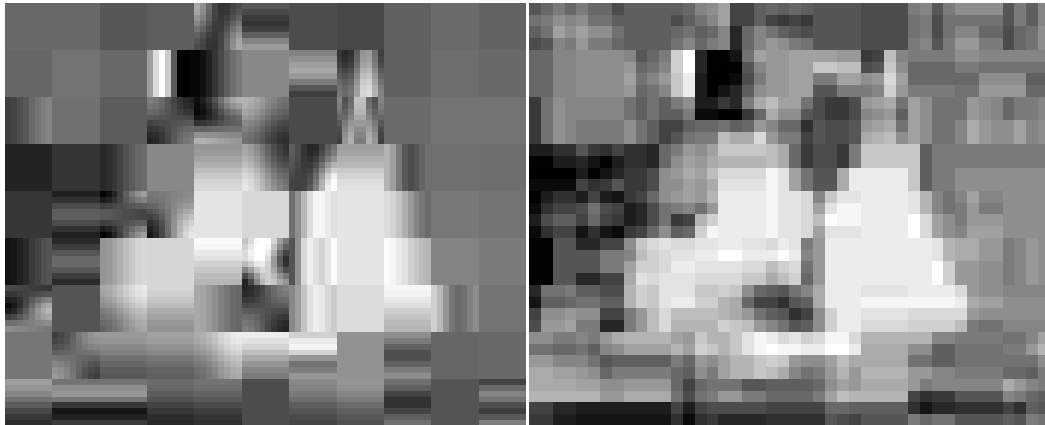


Figure 5.6: Comparison of distortions introduced to the scalar chrominance by lossy DCT-based coding (left image) and DWT-based coding (right). Here, scalar chrominance for the first frame from the test sequence SALESMAN obtained using a codebook of 30 entries is compressed to a bitstream of approximately 2200 bits. Reconstructed color images are shown on the color plate (Photos 23–26).

Experimental results (Bartkowiak, Domański and Gerken, 1997, 1998d) demonstrate interesting properties of this technique. First of all, application of discrete Walsh transform results in quite different the distortions introduced to the scalar chrominance (cf Fig. 5.6) as compared to cosine transform. No blurring characteristic to DCT is observed. Unfortunately, the energy compaction properties of

DWT are poorer than DCT, therefore most coefficients must be discarded in order to achieve a reasonable compression ratio. Consequently, the reconstructed scalar chrominance is approximated very roughly using small blocks corresponding to two-dimensional Walsh functions of low order (cf Photos 30 and 31). Similarly as in case of DCT-based coding, these approximation errors correspond to color artifacts in the reconstructed color images, which are partially removed by the vector median filter.

## 5.4 Interframe coding.

The objective of *interframe* coding is to efficiently update the content of reconstructed frames according to changes observed between consecutive frames at the input of the encoder. Motion compensated hybrid codec (cf Fig. 5.1) performs this task by estimating the grid of *motion vectors* which define local displacements of spatial details between the previously encoded frame and a current one. Motion compensation algorithm applies these vectors to previously encoded frame in order to estimate the current frame. The frame prediction error (the difference between the input frame and its estimate) is encoded by DCT-based transform coding.

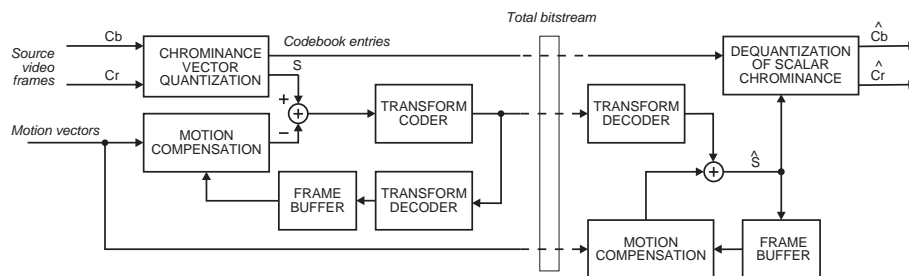


Figure 5.7: Proposed application of chrominance vector quantization to video coding in *interframe* mode. In this diagram, the luminance path has been omitted for the sake of clarity.

Chrominance vector quantization is applicable to *interframe* coding (cf Fig. 5.7). Whereas motion estimation is usually performed on the basis of the luminance component alone, so it is not affected by chrominance processing, motion compensation may be applied directly to the scalar chrominance. Moreover, the prediction error may also be calculated in the domain of scalar chrominance and subsequently lossy encoded. An efficient operation of such codec is possible under several assumptions:

1. Similarities between consecutive frames observed in color components are reflected by similarities in their scalar chrominance representation.
2. Magnitude of the frame prediction error expressed in scalar chrominance corresponds to the difference of respective chrominance values.

3. Statistical and spectral properties of the frame prediction error are suitable for efficient lossy coding.

Due to the chrominance codebook being constant over number of frames, similarly colored pixels within static portions of the scene are represented by the same value of the scalar chrominance signal. Therefore the frame prediction error exhibits large “flat” zero-valued areas, corresponding to static background (cf Fig. 5.8). On



Figure 5.8: Comparison of 100th frame prediction error in scalar chrominance (left) processed in modified coder, and the natural chrominance component  $C_B$  processed by standard H.263 coder (right). Scalar chrominance of the test video sequence AKIYO is generated using 30-element codebook. Both images are enhanced in the same way.

the other hand, often higher dynamic range and wider bandwidth make this prediction error harder to compress efficiently.

Propagation of quantization error within motion compensation loop in the standard H.263 scheme leads to strong colorful artifacts. Application of chrominance vector quantization restricts the output set of colors to the colors present in the original image, therefore the probability of “alien color” effect is strongly reduced.

Experimental results show, that *interframe* compression of scalar chrominance is very efficient even using a standard block-based transform coder with default quantization scheme and default Huffman code tables (without optimization). Obtained PSNR ratings are apparently lower for scalar chrominance-based codec as compared to standard H.263 codec at the same compression ratio (cf Fig 5.9), however the objective error measure decreases more slowly with growing compression.

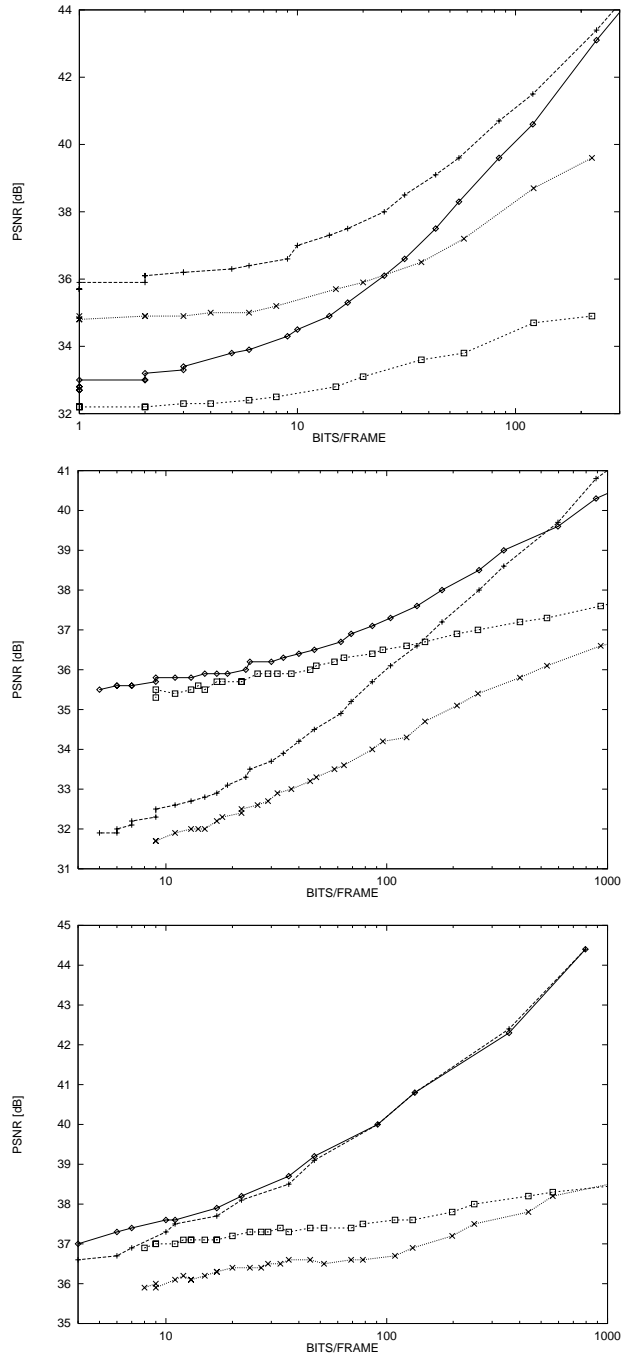


Figure 5.9: PSNR of the reconstructed chrominance components versus the number of bits allocated to one *inter* frame averaged over 100 frames of the video sequences AKIYO (upper plot), MISSA (middle plot), SALESMAN (lower plot). Here,  $C_B$  ( $\diamond$ ) and  $C_R$  (+) components obtained from the standard H.263 codec are compared to  $C_B$  ( $\square$ ) and  $C_R$  ( $\times$ ) components obtained by the application of scalar chrominance.

## Color Plate 5: Video coding.



**Photo 28 and 29:** Application of chrominance vector quantization to DCT-based video coding in intraframe mode: reconstructed first frames of sequence SALESMAN (left), whereby 2252 bits are allocated to scalar chrominance and  $\text{PSNR } C_B = 37.7$  dB,  $\text{PSNR } C_R = 37.8$  dB, and AKIYO (right), whereby 3761 bits are allocated to scalar chrominance and  $\text{PSNR } C_B = 33.3$  dB,  $\text{PSNR } C_R = 38.4$  dB.



**Photo 30 and 31:** Application of chrominance vector quantization to DWT-based video coding in intraframe mode: reconstructed first frames of sequence SALESMAN (left), whereby 2456 bits are allocated to scalar chrominance and  $\text{PSNR } C_B = 37.5$  dB,  $\text{PSNR } C_R = 35.4$  dB, and AKIYO (right), whereby 3948 bits are allocated to scalar chrominance and  $\text{PSNR } C_B = 30.8$  dB,  $\text{PSNR } C_R = 35.9$  dB.



**Photo 32 and 33:** Application of chrominance vector quantization to video coding in interframe mode: Reconstructed 99th frames from sequences SALESMAN (left), whereby 26 bits are allocated to an average frame and  $\text{PSNR } C_B = 37.2$  dB,  $\text{PSNR } C_R = 36.0$  dB, and AKIYO (right), whereby 20 bits are allocated to an average frame and  $\text{PSNR } C_B = 33.6$  dB,  $\text{PSNR } C_R = 36.3$  dB.

Reconstructed frames shown in color plates (cf Photos 32 and 33) prove that these lower PSNR values do not necessarily correspond to lower visual quality. This is because the type of distortions introduced by coding in scalar chrominance domain is apparently different from those observed in H.263 coder, even though similar framework of motion compensated DCT-based coding is employed.

The general observation is that video sequences coded using proposed scheme often achieve higher notes in subjective evaluation than those coded using H.263. Whereas the hue variation and colorful spots are replaced by another color artifacts specific to chrominance vector quantization, these appear to be more tolerable by an average observer.

# Chapter 6

## Conclusions.

### 6.1 Recapitulation.

The research presented in this dissertation is focused on compression of color images and video, especially at very low bit rates, where very high compression ratios are necessary. In order to deal with the color signal efficiently, vector-oriented approach is proposed. Therefore the work is devoted to vector-oriented methods for image and video compression. These methods are defined by the author as methods which exploit the dependencies between color components used to represent the color signal in various color spaces. This exploitation may be approached by joint processing of the color components or by vector-oriented control of separate component-wise processing, as discussed in the examples known from literature. Another possibility is to perform a dimensionality reducing mapping of the vector values representing color of image pixels. It is proposed to achieve such mapping through vector quantization in the chrominance plane, whereby the two chrominance components of color image represented in a luminance-chrominance system are quantized to a set of representatives.

The thesis of this dissertation is that it is possible to achieve efficient compression of color images and video by the use of two-dimensional vector quantization of the chrominance-components. Several examples of such coding techniques are given in the dissertation to prove the above claim.

Application of chrominance vector quantization is motivated by the statistical and spectral properties of natural color images and videophone sequences. New compression methods are proposed for color images and video. These vector-oriented methods exploit mutual dependencies between color components in order to achieve high coding efficiency. This exploitation is done in several ways:

- Statistical co-occurrence of certain combinations of color components, which

is responsible for sparseness of color histograms, is exploited in vector quantization of chrominance, whereby the chrominance pairs of each image sample are approximated using a representative pair from a very limited set.

- Further dependence between luminance and quantized chrominance is exploited in differential coding controlled by the luminance.
- Vector median filtering exploits the correlation between luminance and chrominance in order to remove impulse coding artifacts in chrominance relying on luminance smoothness.
- In interframe video coding, luminance and chrominance correlation is exploited in frame prediction, whereby motion vectors determined for luminance are used for motion compensation of vector quantized chrominance.

Thanks to using an efficient representation of the chrominance components of color signal, satisfactory coding results are achieved, which is proved by a competitive comparison to standard very low bit rate coding techniques. Presented examples show that it is possible to achieve very high compression while preserving acceptable quality of color in reconstructed images and video.

## 6.2 Summary of developments and achievements.

The dissertation presents new methods developed by the author for compression of color images and video. These methods are particularly efficient at very low bit rates, where severe distortions are introduced by standard component-wise coding methods.

Studies on statistical properties of natural scene images and videophone sequences reveal sparseness of the color data distribution. This sparseness is especially demonstrated in the chrominance plane by the use of two-dimensional histograms of the chrominance data. Moreover, relative stability of the chrominance distribution over consecutive frames is concluded from the temporal analysis of the histogram peaks. Respective implications to efficient image and video compression are formulated.

A new class of original compression methods based on vector quantization of chrominance is proposed. These methods map quantized chrominance vectors onto a set of scalar numbers and further processing is done in the domain of such scalar representation. Such representation is referred to as scalar chrominance.

For good quality quantized images vector quantization algorithms are studied. Application of classic binary splitting technique to chrominance codebook design is proposed. A computationally efficient algorithm is developed. The performance of this algorithm is experimentally verified using artificial data sets generated in such a way to mimic the statistical distribution of chrominance data in natural scene images. Proposed vector quantization algorithm is also tested using single frames drawn from standard videophone sequences. Obtained results prove that such images can be quantized to very few chrominance representatives without significant degradation of the visual quality.

Statistical and spectral properties of the scalar chrominance representation are studied. Since these properties are deeply influenced by the way the chrominance codebook entries are mapped onto the set of scalar values, these mappings are studied also. A simple heuristic algorithm is proposed that leads to beneficial properties of the scalar chrominance.

Two compression techniques are proposed to encode the images with vector quantized chrominance. Lossless compression using predictive coding is proposed first. An original coding technique is developed, whereby the prediction direction is controlled by the orientation of edges detected in luminance component. Experimental results of this technique reveal that high compression is achievable. Lossy compression of the scalar chrominance using block-based transform coding is proposed. As DCT-based coding benefits from signal smoothness, codebook interpolation technique is proposed in order to obtain finer quantization. This technique is applied to the JPEG image coding standard and compared to the baseline JPEG. Obtained results show that higher quality of reconstructed images than those reconstructed from standard JPEG coding is achievable at very high compression ratios.

The concept of chrominance vector quantization is extended to videophone sequences. Application of constant chrominance codebook to sequences of frames between consecutive scene cuts is proposed due to the stability observed in chrominance histograms. An intraframe coding technique is proposed that uses discrete cosine transform as well as discrete Walsh transform. Experimental verification of both proposed approaches is performed. The obtained results prove high efficiency of the technique. Interframe coding of scalar chrominance is proposed using typical H.263 motion-compensated scheme and motion vectors calculated for the luminance component. Experimental comparison of this coding technique to H.263 interframe coding is performed. The obtained results prove that similar or higher visual quality of reconstructed sequences is achievable as compared to those reconstructed from standard H.263 coding.

All the compression techniques developed exhibit at least comparable efficiency to standard coding techniques. Whereas the PSNR ratings are sometimes lower than those achieved for standard JPEG or H.263 coding, the visual quality of decoded images and video sequences are often higher. The efficiency of these techniques can be improved even further by optimization of the respective quantization schemes and entropy coding tables. It is important to stress that such elements of standard codecs are highly optimized. Therefore the experimental comparison of the proposed vector-oriented methods to the standard techniques is biased and favors the latter. Even under these circumstances, proposed methods prove to be competitive to the coding techniques being standardized. Therefore the thesis should be considered as being proved.

### 6.3 Possible extensions and further work.

Proposed compression methods can be further improved through several optimizations. First of all, Huffman code tables optimized for a class of images may be applied. Such tables are usually fixed in very low bit rate codecs and therefore transmission of optimal tables for a given image or video sequence is avoided. Universal Huffman code should be determined using a large pool of images or video sequences which unfortunately was not available to the author.

Secondly, quantization schemes proposed for transform coding both in intraframe and in interframe modes are only crudely matched to the signal spectral properties using some heuristics. In fact, it is very difficult to determine an optimal quantization strategy of transform coefficients due to highly nonlinear mapping from the chrominance vectors to scalar chrominance domain which is employed in the techniques proposed. Since the nature of this nonlinearity heavily depends on the codebook content and the latter is image dependent, the choice of the quantization strategy should also be optimized for a given image or video sequence.

The smoothness of the scalar chrominance signal is heavily dependent on the order in which the entries of the chrominance codebook are mapped onto the set of scalar values. On the other hand, the artifacts observed in reconstructed chrominance components after lossy coding of scalar chrominance signal are often exaggerated by the nonlinear mapping. An advanced algorithm may be developed which would attempt to optimize the codebook order taking into account the above phenomena.

General improvements of the compression methods related to vector quantization of chrominance are possible. Whereas chrominance codebook design algorithm

proposed in this dissertation attempts to minimize the mean squared error of the quantized image, it is not equivalent to visually optimal quantization. For example, in order to minimize the artifacts related to gamut shrinking, a vector quantizer that minimizes the maximum error should be used. On the other hand, it is desirable that the locations of borders between areas of constant chrominance correspond to locations of edges in the original image. Such quantization may be achieved using techniques that combine the codebook design with segmentation. As it has been already demonstrated by Bartkowiak and Domański (1999b), such approach allows to achieve very efficient coding that significantly outperforms the H.263 codec.

# Bibliography.

1. Abel J.,S., Bhaskaran V., Lee H. J., (1992) “Color image coding using and orthogonal decomposition”, *Image Processing Algorithms and Techniques III*, SPIE, 1992, vol. 1657, 58–67.
2. ANSI Working Group (1995) report no. T1A1.5/95-107R1.
3. Ashdown I. (1994), “Octree color quantization”, *Radiosity: A Programmer’s Perspective*, John Wiley.
4. Astola J., Haavisto P., Neuvo Y. (1990), “Vector median filters”, *Proceedings of the IEEE*, vol. 78, no. 4, pp. 678–689.
5. Balasubramanian R., Allebach J. P., Bouman C. (1994), “Color–image quantization with use of a fast binary splitting technique”, *Journal of the Optical Society of America A*, vol. 11, no. 11, pp. 2777–2786.
6. Balasubramanian R., Bouman C., Allebach J. P. (1994), “Sequential scalar quantization of color images”, *Journal of Electronic Imaging*, vol. 3, no. 1, pp. 45–59.
7. Balasubramanian R., Bouman C., Allebach J. P. (1995), “Sequential scalar quantization of vectors: An Analysis”, *IEEE Trans. on Image Processing*, vol. 4, No. 9, pp. 1282–1295.
8. Barrilleaux J., Hinkle R., Wells S. (1987), “Efficient vector quantization for color image encoding”, *Proceedings of Int. Conference on Acoustics, Speech and Signal Processing ICASSP’87*, vol. 2, pp. 740–743.
9. Bartkowiak M., Domański (1994), “Color image archivisation for medical purposes”, *Journal on Communications, Proc. Int. Workshop on Image Processing: Theories, Methodology, Systems and Applications*, Budapest, pp. 66–68.
10. Bartkowiak M. (1995), “Badania eksperymentalne własności statystycznych kolorowych sekwencji video”, Raport naukowy PR-87/9/1995/P Instytutu Elektroniki i Telekomunikacji Politechniki Poznańskiej, Poznań.

11. Bartkowiak M., Domański (1995a), “Vector median filters for processing of color images in various color spaces”, *Proceedings 5th Int. Conference on Image Processing and its Applications*, IEE, Edinburgh, UK, pp. 833–836.
12. Bartkowiak M., Domański (1995b), “Color statistics in image sequences and their implications for VLBC”, *Proceedings 2nd International Workshop on Image and Signal Processing: Theory, Methodology, Systems and Applications*, Budapest, pp. 63–72.
13. Bartkowiak M., Domański M. (1996a), “JPEG technique improvement using chrominance vector quantization”, *Proceedings XIXth National Conference Circuit Theory and Electronic Networks*, Kraków–Krynica, vol. II, pp. 543–548.
14. Bartkowiak M., Domański M. (1996b), “Vector representation of chrominance for very low bit rate coding of video”, *Signal Processing VIII, Theories and Applications, Proceedings Eight European Signal Processing Conference EUSIPCO’96*, Trieste, pp. 1351–1354.
15. Bartkowiak M., Domański M., Gerken P. (1997), “Intraframe compression scheme with better color quality”, *Proceedings IInd Erlangen Symposium: Advances in Digital Image Communication*, Erlangen, pp. 35–40.
16. Bartkowiak M., Domański M. (1998a), “Compression”, *The Color Image Processing Handbook*, Sangwine S. (ed), Chapman and Hall.
17. Bartkowiak M., Domański M. (1998b), “An efficient Technique for high-compression of chrominance data”, *International Journal on Machine Graphics and Vision: Proceedings 5th Conference on Computer Graphics and Image Processing, GKPO’98*, Borki, vol. 7, no. 1/2, pp. 87–97.
18. Bartkowiak M., Domański M. (1998c), “Efficient representation of chrominance for very low bit rate coding”, *Lecture Notes in Computer Science: Proceedings European Conference on Multimedia Applications, Services and Techniques ECMAST’98*, Berlin, pp. 415–424.
19. Bartkowiak M., Domański M. (1998d), “High compression of chrominance exploiting its correlation with luminance”, *Signal Processing IX, Theories and Applications, Proceedings European Signal Processing Conference EUSIPCO’98*, Rhodos, pp. 2321–2324.
20. Bartkowiak M., Domański M. (1999a), “Color representation by the use of scalar chrominance”, *Color Imaging: Device-Independent Color, Color Hardcopy, and Graphic Arts IV*, SPIE, vol. 3648, pp. 312–319.

21. Bartkowiak M., Domański M. (1999b), “High compression of chrominance by use of information from luminance”, presented on *SPIE Symposium on Electronic Imaging: Science and Technology*, San Jose, 1999.
22. Boucher P., Goldberg M. (1984), “Color image compression by adaptive vector quantization”, *Proceedings International Conference on Acoustics, Speech and Signal Processing ICASSP’84*, pp. 29.6.1–29.6.4.
23. Van den Branden Lambrecht C. J., Farrel J. E. (1996), “Perceptual quality metric for digitally coded color images”, *Proceedings of the European Signal Processing Conference EUSIPCO’96*, Trieste, pp. 885–888.
24. Braudaway G. W. (1987), “A procedure for optimum choice of a small number of colors from a large palette for color imaging”, *Proceedings Electronic Imaging Conference*, San Francisco, pp. 75–79.
25. Braquelaire J.-P., Brun L. (1997), “Comparison and optimization of methods of color image quantization”, *IEEE Transactions on Image Processing*, vol. 6, no. 7, pp. 1048–1052.
26. Brelstaff G., Troscianko T. (1992), “Information content of natural scenes: implications for neural coding of color and luminance”, *Human Vision, Visual Processing and Digital Display III*, SPIE, vol. 1666, pp. 302–309.
27. Burton G. J., Moorhead I. R. (1987), “Color and Spatial Structure in Natural Scenes”, *Applied Optics*, vol. 29, pp. 157–170.
28. Carbrey, R. L. (1960), “Video transmission over telephone cable by pulse code modulation”, *Proceedings IRE*, vol. 48, pp. 1546–1561.
29. Chaddha N., Tan W.-C., Meng T. H. Y. (1994), “Color quantization of images based on human vision perception”, *Proceedings International Conference on Acoustics, Speech and Signal Processing ICASSP’94*, vol. 5, pp. 89–92.
30. Chen Y., Petersen H., Bender W. (1993), “Lossy compression of palettized images”, *Proceedings International Conference on Acoustics, Speech and Signal Processing ICASSP’93*, vol. 5, pp. 325–328.
31. Chiang S. W., Po L. M. (1997), “Adaptive lossy LZW algorithm for palettised image compression”, *Electronics Letters*, vol. 30, no. 10, pp. 852–854.
32. Chan C. K., Ma C. K. (1991), “Maximum descent method for image vector quantization”, *Electronics Letters*, vol. 27, pp. 1772–1773.

33. Chan C. K., Ma C. K. (1994), "A fast method of designing better codebooks for image vector quantization", *IEEE Transactions on Communications*, vol. 42, no. 2/3/4, 237–242.
34. Charrier Ch., Knoblauch K, Cherifi H. (1997), "VQ-coded image quality optimized by color space selection", *Proc. of the Picture Coding Symposium PCS'97*, Berlin, pp. 195–200.
35. Clarke R. J. (1985), *Transform Coding of images*, Academic Press, London.
36. Clarke R. J. (1995), *Digital Compression of Still Images and Video*, Academic Press, London.
37. Davis L. (1991), *Handbook of Genetic Algorithms*, Van Nostrand Reinhold, New York.
38. Delp E. J., Mitchell O. R. (1979), "Image compression using block truncation coding", *IEEE Transactions on Communications*, vol. 27, pp. 1335–1342.
39. De Valois K. K., Switkes E. (1983), "Simultaneous masking interactions between chromatic and luminance gratings", *Journal of the Optical Society of America*, vol. 73, no. 1, pp. 11–18.
40. Domański M., *Zaawansowane techniki kompresji obrazów i sekwencji wizyjnych*, Wydawnictwo Politechniki Poznańskiej, Poznań, 1998.
41. Equitz W. H. (1989), "A new vector quantization clustering algorithm", *IEEE Transactions on Acoustics, Speech and Signal Processing*, vol. 37, no. 10, pp. 1568–1575.
42. Eskielioglu A. M., Fisher P. S. (1994), "The variance of the difference image: an alternative quality measure", *Proceedings of the International Picture Coding Symposium PCS'94*, California, USA, pp. 88–91.
43. Fairchild M. D. (1998), *Color Appearance Models*, Adison–Wesley, Reading, MA.
44. Feng Y., Nasrabadi N. M. (1988), "A new vector quantization technique: address–vector quantization", *Proceedings IEEE Global Telecommunication*, Institute of Electrical and Electronic Engineers, pp. 755–759.
45. Feng Y., Nasrabadi N. M. (1989), "A dynamic–address vector quantization algorithm based on inter–block and inter–color correlation for color image coding", *Proceedings International Conference on Acoustics, Speech and Signal Processing, ICASSP'89*, vol. III, pp. 1755–1758.

46. Freisleben B., Schrader A. (1997), "Color quantization with a hybrid genetic algorithm", *Proceedings International Conference on Image Processing and Its Applications, IPA '97*, pp. 86–90.
47. Gan Q., Kotani K., Miyahara M. (1991), "Geometry of Digital Colors in Munsell Color Space", *Proceedings of the Picture Coding Symposium PCS'91*, pp. 63–66.
48. Gentile R. S., Allebach J. P., Walowit E. (1990), "Quantization of color images based on uniform color spaces", *Journal of Imaging Technology*, vol. 16, no. 1.
49. Gentile R. S., Walowit E., Allebach J. P. (1990), "Quantization and multilevel halftoning of color images for near–original image quality", *Journal of the Optical Society of America*, vol. 7, no. 6, pp. 1019–1026.
50. Gersho A., Gray R. M. (1991), *Vector Quantization and Signal Compression*, Kluwer Academic Publishers, Boston.
51. Gervautz M., Purgathofer W. (1990), "A simple method for color quantization: octree quantization", Glassner A. S. (ed), *Graphics Gems*, Academic Press, San Diego, CA, pp. 287–293.
52. Godlove I. H. (1951), "Improved color difference formula with applications to the perceptibility and acceptability of fadings", *Journal of the Optical Society of America*, vol. 41, pp. 760–772.
53. Goldberg D. E. (1989), *Genetic Algorithms in Search, Optimization and Machine Learning*, Addison–Wesley, Reading, MA.
54. Gormish M. J. (1995), "Compression of palettized images by color", *Proceedings International Conference on Image Processing ICIP'95*, pp. 274–277.
55. Hamilton W. R. (1866), *Elements of Quaternions*, Longmans, Green and Co., London.
56. Heckbert P. (1982), "Color image quantization for frame buffer display", *Computer Graphics*, vol. 16, no. 3, pp. 297–307.
57. Horita Y., Miyahara M. (1991), "Image coding based on uniform color space", *Proceeding of the Picture Coding Symposium PCS'91*, pp. 337–340.
58. Huang C.-M., Harris R. W. (1993), "A comparison of several vector quantization codebook generation approaches", *IEEE Transactions on Image Processing*, vol. 2, no. 1, pp. 108–112.

59. Huffman D. A. (1952), "A method for the construction of minimum redundancy codes", *Proceedings of the IEEE*, vol. 40, pp. 1098–1101.
60. IJG (1995), Independent JPEG Software Group, JPEG public software library available on-line at <ftp://ftp.uu.net/graphics/jpeg>
61. ITU-R (1994a) Recommendation BT.601-4, *Encoding Parameters of Digital Television for Studios*, ITU, Geneva.
62. ITU-R (1994b) Recommendation BT.709-1, *Basic Parameter Values for the HDTV Standard for the Studio and for International Programme Exchange*, ITU, Geneva.
63. ITU-T(CCITT) (1992) Recommendation T.81 (ISO/IEC 10918-1), *Information Technology – Digital Compression and Coding of Continuous-Tone Still Images*, ITU, Geneva.
64. ITU-T(CCITT) (1993a) Recommendation T.82 (ISO/IEC 11544), *Information Technology – Progressive Bi-Level Image Compression*, ITU, Geneva.
65. ITU-T (1993b) Recommendation H.261, *Video Codec for Audiovisual Services at  $p \times 64$  kbit/s*, ITU, Geneva.
66. ITU-T (1996) Recommendation H.263, *Video Coding for Narrow Telecommunication Channels at  $< 64$  kbit/s*, ITU, Geneva.
67. Iverson V. S., Riskin E. A. (1993), "A fast method for combining palettes of color quantized images", *Proceedings International Conference on Acoustics, Speech and Signal Processing ASSP'93*, vol. 5, pp. 317–320.
68. Jacquin A. E. (1992), "Image coding based on a fractal theory of iterated contractive image transformations", *IEEE Transactions on Image Processing*, vol. 1, no. 1, pp. 18–30.
69. Jain A. K., Pratt W. K. (1972), "Color image quantization", *Proceedings National Telecommunications Conference*, IEEE publication no. CHO 601-5-NTC.
70. Jayant N., Noll P. (1984), *Digital Coding of Waveforms*, Englewood Cliffs NJ, Prentice Hall.
71. Kalouptsidis N., Manolakis D, Karayannis G. (1983), "A family of computationally efficient algorithms for multichannel signal processing - A tutorial review", *Signal Processing*, vol. 5, pp. 5–19.

72. Kim K. M., Lee C. S., Lee E. J., Ha Y. H. (1996), "Color image quantization using weighted distortion measure of HVS color activity", *Proceedings International Conference on Image Processing ICIP '96*.
73. Kohonen T. (1982), "Self-organized formation of topological correct feature maps", *Biological Cybernetics*, vol. 43, no. 1, pp. 59-69.
74. Kohonen T. (1988), *Self-Organization and Associative Memory*, Springer-Verlag, Berlin.
75. Kolpatzik B. W., Bouman C. A. (1995), "Optimized universal palette design for error diffusion", *Journal of Electronic Imaging*, vol. 4, no. 2, 131-143.
76. Kok C. W., Chan S. C., Leung S. H. (1993), "Color quantization by fuzzy quantizer", *Nonlinear Image Processing*, SPIE, vol. 1920, pp. 235-242.
77. Kotani K., Gan Q., Miyahara M. (1991), "Objective picture quality scale for optimum image coding", *Proceedings of the Picture Coding Symposium PCS'91*, pp. 341-344.
78. Kotani K., Gan Q., Horita Y., Miyahara M., Algazi V. R. (1993), "Objective picture quality scale for color image coding", *Proceedings of the Picture Coding Symposium PCS'93*, Lausanne, pp. 20.1-20.2.
79. Kunt M., Ikonomopoulos A., Kocher M. (1958), "Second generation image coding techniques", *Proceedings of the IEEE*, vol. 73, pp. 549-574.
80. Lawler E. L. (ed) (1985), *The Travelling Salesman Problem: A Guided Tour of Combinatorial Optimization*, Interscience Series in Discrete Mathematics, John Wiley, New York.
81. Legge G. E., Foley J. M. (1980), "Contrast masking in human vision", *Journal of the Optical Society of America*, vol. 70, no. 12, pp. 1458-1471.
82. Li H. D., Jain V. K. (1996), "Color image coding by vector subbands/ECVQ and activity map", *Proceedings International Conference on Acoustics, Speech and Signal Processing ICASSP'96*, vol. IV, pp. 2044-2047.
83. Limb J. O., Rubinstein C. B. (1972), "Statistical dependence between components of a differentially quantized color signal", *IEEE Transactions on Communication Technology*, vol. 20, pp. 890-899.
84. Limb J. O., Rubinstein Ch. B. (1974), "Plateau coding of the chrominance components of color picture signals", *IEEE Transactions on Communications*, vol. 22, no. 6, pp. 812-820.

85. Limb J. O., Rubinstein Ch. B., Thompson J. E. (1977), "Digital coding of color video signals - a review", *IEEE Transactions on Communications*, vol. 25, no. 11, pp. 1349–1384.
86. Linde Y., Buzo A., Gray R. M. (1980), "An algorithm for vector quantizer design", *IEEE Transactions on Communications*, pp. 84–89.
87. Liu T.–S., Chang L.–W. (1994), "Greedy tree growing for color image quantization", *Proceedings International Conference on Acoustics, Speech and Signal Processing ICASSP'94*, vol. 5, pp. 97–100.
88. Liu T.–S., Chang L.–W. (1995), "Fast color image quantization with error diffusion and morphological operations", *Signal Processing*, vol. 43, pp. 293–303.
89. Lloyd S. P. (1982), "Least squares quantization in PCM", *Institute of Mathematical Statistics Meeting*, Atlantic City, pp. 129–136.
90. Łuczak A., Domański M. (1998), "Badania eksperymentalne kodeka H.263 dla kanałów o przepływnościach 16-64 kbit/s", *Krajowe Sympozjum Telekomunikacji*, Bydgoszcz, pp. 248–254.
91. Machuca R., Philips K. (1983), "Applications of vector fields to image processing", *IEEE Transactions on Pattern Analysis and Machine Intelligence*, vol. 5, pp. 316–329.
92. MacQueen J. B. (1967), "Some methods for classification and analysis of multivariate observations", *Proceedings 5th Berkeley Symposium Mathematical Statistics and Probability I*, pp. 281–297.
93. Maragos P. A., Mersereau R. M., Schafer R. W. (1984), "Multichannel predictive coding of color images", *Proceeding International Conference on Acoustics, Speech and Signal Processing , 1984 CASSP'84*, pp. 29.6.1–29.6.4.
94. Max J. (1960), "Quantizing for minimum distortion", *IRE Transactions on Communication Theory*, March 1960, pp. 7-12.
95. Meyr H., Rosdolsky H. G., Huang T. S. (1974), "Optimum runlength codes", *IEEE Transactions on Communications*, vol. 22, pp. 826–835.
96. Mersereau R. M., Dudgeon D. E. (1984), *Multidimensional digital signal processing*, Prentice–Hall, Englewood Cliffs NJ.
97. McFall J. D., Mitchell J. L., Pennebaker W. B. (1989), "A default color palette for restricted palette displays", *Proc. SPIE Digital Image Processing Applications*, vol. 1075, pp. 179–184.

98. Miyahara M. (1988), “Quality assessments for visual service”, *IEEE Communications Magazine*, October 1988, pp. 51–60.
99. Miyahara M., Yoshida Y. (1988), “Mathematical transform of RGB color data to Munsell HVC color data”, *Proceedings SPIE Visual Communication and Image Processing*, Cambridge.
100. Miyahara M., Gan Q., Kotani K. (1994), “Mathematical transform of (R,G,B) data to the munsell color system (MTM) – a precise transformation based on visual perception”, *Proceedings International Picture Coding Symposium PCS’94*, California, USA, pp. 146–148.
101. Mullen K. T. (1985), “The contrast sensitivity of human color vision to red–green and blue–yellow chromatic gratings”, *Journal on Physiology*, 1985, 381–400.
102. Musmann H. G., Hötter M., Ostermann J. (1989), “Object oriented analysis–synthesis coding of moving images”, *Signal Processing: Image Communication*, vol. 1, pp. 117–138.
103. Musmann H. G. (1998), “Very low bit rate coding of video”, *Przetwarzanie Obrazów i Multimedia*, seminar of the Institute of Electronics and Telecommunications, Poznań University of Technology.
104. Murching A. M., Woods J. W. (1994), “Adaptive subsampling of color images”, *Proceeding of the International Conference on Image Processing ICIP’94*, vol. 3, pp. 963–965.
105. Netravali A. N., Haskell B. G. (1988), *Digital Pictures. Representation and Compression*, Plenum Press, New York.
106. Nibblack W. (1986), *An Introduction to Digital Image Processing*, Prentice Hall.
107. Oehler K. L., Riskin E. A., Gray R. M. (1991), “Unbalanced tree–growing algorithms for practical image compression”, *Proceedings International Conference on Acoustics, Speech and Signal Proc. ICASSP’91*, pp. 2293–2296.
108. Orchard M., Bouman C. (1991), “Color quantization of images”, *IEEE Transactions on Signal Processing*, vol. 39, no. 12, pp. 2677–2690.
109. Overloop J. V., Philips W., Torfs D., Lemahieu I. (1997), “Segmented image coding of palettized images”, *Proceedings International Conference on Acoustics, Speech and Signal Processing ICASSP’97*, vol. IV, pp. 2937–2939.

110. Parkkinen J., Jaaskelainen T. (1989), “Color vision: machine and human”, *Visual Communications and Image Processing*, SPIE, vol. 1199, pp. 1184–1192.
111. Pasco R. (1976), “Source coding algorithms for fast data compression”, PhD thesis, Stanford University.
112. Pei S.-C., Cheng C.-M. (1995), “Dependent scalar quantization of color images”, *IEEE Transactions on Circuits and Systems for Video Technology*, vol. 5, no. 2, pp. 124–139.
113. Pennebaker W. P., Mitchell J. L. (1993), *JPEG Still Image Data Compression Standard*, van Nostrand Reinhold, New York.
114. Pirsh P., Stenger L., “Statistical analysis and coding of color video signal”, *Acta Electronica*, vol. 19, no. 4, pp. 277–287.
115. PNG (1996), *Portable Network Graphics Specification*, W3C Technical Report.
116. Poirson A. B., Wandel B. A. (1993), “Appearance of colored patterns: pattern–color separability”, *Journal of the Optical Society of America*, vol. 10, no. 12, pp. 2458–2470.
117. Poynton Ch. A. (1996), *A Technical Introduction to Digital Video*, John Wiley & Sons, New York.
118. Pratt W. K. (1971), “Spatial transform coding of color pictures”, *IEEE Transactions on Communications*, vol. 19, pp. 980–992.
119. Pratt W. K. (1991), *Digital image processing* (2nd ed), John Wiley, New York.
120. Przelaskowski A., “Miary jakości”, *Multimedia. Algorytmy i standardy kompresji*, Skarbek W. (ed), Akademska Oficyna Wydawnicza PLJ, Warszawa, 1998.
121. Réndon E, Salgado L., Menéndez J. M., Garcia N. (1997), “Adaptive color quantization through self–organization neural networks”, *Proceedings 4th International Workshop on Systems, Signals and Image Processing*, Poznań, pp. 195–198.
122. Riskin E. A., Gray R. M. (1991), “A greedy tree growing algorithm for the design of variable rate vector quantizers”, *IEEE Transactions on Signal Processing*, vol. 39, no. 11, pp. 2500–2507.
123. Rissanen J., “Generalized kraft inequality for arithmetic coding”, *IBM Journal of Research and Development*, vol. 20, pp. 198–203

124. Sangwine S. J. (1996), "Fourier transforms of color images using quaternion, or hypercomplex numbers", *Electronics Letters*, vol. 32, no. 21, pp. 1979–1980.
125. Sangwine S. J. (1997), "Fourier transforms of color images: the quaternion FFT", *Proceedings of 4th International Workshop on Systems, Signals and Image Processing*, Poznań, pp. 207–210.
126. Sharma G., Trussel H. J. (1997), "Digital color imaging", *IEEE Transactions on Image Processing*, vol. 6, no. 7, pp. 901–932.
127. Sharma G., Vrhel M. J., Trussel H. J. (1998), "Color imaging for multimedia", *Proceeding of the IEEE*, vol. 86, no. 6, pp. 1088–1108.
128. Scheunders P., (1996), "A genetic approach towards optimal color image quantization", *Proceedings International Conference on Image Processing ICIP'96*.
129. Senoo T., Girod B. (1992), "Vector quantization for entropy coding of image subbands", *IEEE Transactions on Image Processing*, vol. 1, no. 4, pp. 526–532.
130. Skarbek W. (1993), *Metody reprezentacji obrazów cyfrowych*, Akademicka Oficyna Wydawnicza PLJ, Warszawa.
131. Skarbek W. (1998), "Kompresja obrazów - rozwój metod", *Multimedia. Algoritmy i standardy kompresji*, Skarbek W. (ed), Akademicka Oficyna Wydawnicza PLJ, Warszawa, 1998.
132. Tremblay M. P., Zaccarin A. (1994), "Transmission of the color information using quad-trees and segmentation-based approaches for the compression of color images with limited palette", *Proceedings International Conference on Image Processing ICIP'94*, pp. 967–971.
133. Tremeau A., Calonnier M., Laget B. (1994), "Color quantization error in terms of perceived image quality", *Proceedings International Conference on Acoustics, Speech and Signal Processing ICASSP'94*, vol. 5, pp. 93–96.
134. Trussel H.J., Kulkarni M. S. (1996), "Sampling and processing of color signals", *IEEE Transactions on Image Processing*, vol. 5, no. 4, pp. 677–681.
135. Van Dyck R. E., Rajala S. A. (1991), "Sensitivity to color errors introduced by processing in different color spaces", *Proceedings IEEE Workshop on Visual Signal Processing and Communications*, Taiwan, vol. 1, pp. 192–195.
136. Van Nes F. I., Bouman M. A. (1967), "Spatial modulation transfer in the human eye", *Journal of the Optical Society of America*, vol. 57, no. 3, pp. 401–406.

137. Venable D., Stinehour J., Roetling P. (1990), "Selection and use of small color sets for pictorial display", *Proceedings SPSE 43rd Annual Meeting*, Rochester, New York, pp. 90–92.
138. Verevka O., Buchanan J. W. (1995), "Local K-means algorithm for color image quantization", *Proceedings Graphics/Vision Interface Conference*, pp. 128–134.
139. Vetterli M., Kovačević J. (1995), *Wavelets and Subband Coding*, Prentice Hall, Englewood Cliffs, NJ.
140. Waldemar P., Ramstad T. A. (1994), "Subband coding of color images with limited palette size", *Proceeding International Conference on Acoustics, Speech and Signal Processing ICASSP'94*, vol. V, pp. 353–356.
141. Wan S., Wong S., Prusinkiewicz P. (1988), "An algorithm for multidimensional data clustering", *ACM Transactions on Mathematical Software*, vol. 14, no. 2, pp. 153–162.
142. Wan X., Jay Kuo C.-C. (1996), "Color distribution analysis and quantization for image retrieval", *SPIE Conference on Storage and Retrieval for Still Image and Video Databases*, San Jose.
143. Wang C. Y., Chang L. W. (1992), "Color image coding using variable vector quantization in (R, G, B) domain", *Proceedings SPIE Visual Communications and Image Processing*, vol. 1818, pp. 512–523.
144. Watson A. B. (1994), "Perceptual optimization of DCT color quantization matrices", *Proc. International Conference on Image Processing ICIP'94*, 1994, pp. 100–104.
145. Welch T. A. (1984), "A technique for high performance data compression", *IEEE Computer* vol. 17, no. 6, pp. 8–19.
146. Witten I. H., Neal R. M., Cleary J. G. (1987), "Arithmetic coding for data compression", *Communications of the ACM*, vol. 30, no. 6, pp. 520–540.
147. Woods J., O'Neil S. (1986), "Subband Coding of Images", *IEEE Transactions on Acoustics, Speech and Signal Processing*, vol. 34, no. 5, pp. 1278–1288.
148. Wu X. (1992), "Color quantization by dynamic programming and principal analysis", *ACM Transactions on Graphics*, vol. 11, no. 4, pp. 348–372.
149. Wyszecki G., Stiles W. S. (1982), *Color Science: Concepts and Methods, Quantitative Data and Formulae*, John Wiley, New York.

150. Xiang Z., Joy G. (1994), "Color image quantization by agglomerative clustering", *IEEE Computer Graphics and Applications*, vol 14, no. 3, pp. 44-48.
151. Yamaguchi H. (1984), "Efficient encoding of colored pictures in R, G, B components", *IEEE Transactions on Communications*, vol. 32, no. 11, pp. 1201-1209.
152. Yang C.-K., Lin J.-C., Tsai W.-H. (1994), "Color image compression by moment-preserving block truncation coding", *Proceedings International Conference on Image Processing ICIP'94*, pp. 972-976.
153. Yovanof G. S., Sullivan J. R. (1992), "Lossless predictive coding of color graphics", *SPIE Proceedings Image Processing and Techniques III*, vol. 1657, pp. 68-82.
154. Zaccarin A., Liu B. (1991), "Transform coding of color images with limited palette size", *Proceeding International Conference on Acoustics, Speech and Signal Proc. ICASSP'91*, pp. 2625-2628.
155. Zaccarin A., Liu B. (1993), "A novel approach for coding color quantized images", *IEEE Transactions on Image Processing*, vol. 2, no. 4, pp. 442-453.
156. Zhang Y., Po L.-M. (1995), "Fractal color image compression using vector distortion measure", *Proceedings International Conference on Image Processing ICIP'95*, pp. 276-279.
157. Ziv J., Lempel A. (1977), "An universal algorithm for sequential data compression", *IEEE Transactions on Information Theory*, vol. 23, no. 3, pp. 337-343.
158. Ziv J., Lempel A. (1978), "Compression of individual sequences via variable-rate coding", *IEEE Transactions on Information Theory*, vol. 24, no. 5, pp. 53-60.